ABSTRACT

Title of thesis: CONCEPTUAL DESIGN STUDIES OF A MONO TILTROTOR

Robin Preator, Master of Science, 2005

Thesis directed by: Professor J. Gordon Leishman
Department of Aerospace Engineering

The Mono Tiltrotor (MTR) has been proposed by the Baldwin Technology Company as an innovative VTOL concept that integrates a tilting coaxial rotor, an aerodynamically deployed folding wing, and an efficient cargo handling system. The MTR has been targeted to meet heavy-lift, long-range mission objectives for which there is growing demand from military planners. This thesis describes a series of conceptual design studies aimed at determining the potential value that the MTR concept would possess, if it were to be technically realized. A versatile rotorcraft sizing analysis was developed to perform sizing and weight predictions for conventional single rotor and coaxial helicopters, as well as the MTR concept, based on key input mission and design requirements. This analysis was partly based on historical trends used in the rotorcraft and fixed-wing aircraft industries. These methods were expanded upon to include the capability for sizing the unique MTR concept. As presented, the results of this design analysis include a detailed weight budget of any number of potential aircraft point designs. The sizing methodology was validated against legacy helicopter sizing and component weights data, with

good overall agreement. Comparisons, in terms of sizing and potential performance, between the MTR concept and conventional and coaxial helicopters sized to perform the same heavy-lift, long range mission are then presented. Key mission and design trade studies are also detailed, which were performed to study and refine the design concept and analytical methodology. The optimization of two key design points is also presented. These design points include a heavy-lift, long-range (20 ton payload, 1,000 nm range) MTR, and an MTR Scaled Demonstrator (2 ton payload, 700 nm range). Detailed performance studies are reported for each optimized point design. Overall, it was found that the MTR concept, if technically realized, offers unprecedented performance capability in terms of payload, range, and mission versatility. This comes in a very compact package relative to the size of a helicopter that would be required to complete the same mission.

CONCEPTUAL DESIGN STUDIES OF A MONO TILTROTOR

by

Robin Preator

Thesis submitted to the Faculty of the Graduate School of the
University of Maryland, College Park in partial fulfillment
of the requirements for the degree of
Master of Science
2005

Advisory Committee:

Professor J. Gordon Leishman, Chair/Advisor
Professor Inderjit Chopra
Professor Roberto Celi

DEDICATION

To my mother, whose love and determination helped to set me on this path, and to Lesley, who has been by my side and supported me every step of the way.

ACKNOWLEDGMENTS

Funding for this work was provided by the Office of Naval Research and the Army Aviation Applied Technology Directorate. I would like to thank Doug Baldwin of the Baldwin Technology Company for his innovation and drive that created the opportunity for a fascinating design study. I would like to thank Professor Tishchenko and VT Nagaraj for taking time to sit with me and teach me some of the nuances of rotorcraft design and sizing. I would also like to thank Professors Chopra and Celi for all of their input and for taking part in my thesis committee. Many thanks go out to all of my professors at the University of Maryland as I have learned more than I thought possible in the last two years, and to all of the staff members at the Department of Aerospace Engineering, who keep life running smoothly. Most of all, I would like to thank Professor Leishman for giving me this great opportunity and for giving me the support, guidance and wisdom to help see it through.

TABLE OF CONTENTS

LIST OF TABLES

LIST OF FIGURES

NOMENCLATURE

LIST OF PRINCIPAL SYMBOLS

A	Area
AR	Aspect ratio
b	Span
c	Chord
C_{e}	Specific fuel consumption coefficients
C	Tail volume coefficient
C_{d_0}	Profile drag coefficient of blade sections
C_{D_0}	Profile drag coefficient of aircraft component
$C_{D_{\mathrm{i}}}$	Induced drag coefficient
C_L	Lift coefficient of wing
$C_{L_{\max}}$	Maximum lift coefficient of wing
C_T	Rotor thrust coefficient, $T/(\rho A(\Omega R)^2)$
C_P	Rotor power coefficient, $P/(\rho A(\Omega R)^3)$
C_{pow}	Power conversion factor
C_T/σ	Blade loading coefficient
D	Rotor diameter
D_{TAIL}	Diameter of tail boom
DL	Disk loading, T/A
e_{w}	Oswald's wing span efficiency factor
E	Energy efficiency parameter
f_{eq}	Equivalent flat plate area
F	Fuel flow rate
F_{CF}	Centrifugal force
FM	Figure of merit
f_{SH}	Transmission shaft torque overload factor
g	Acceleration due to gravity
H_{p}	Pressure Altitude
H_ρ	Density altitude
k	Component weight correlation coefficient
k_{alt}	Engine lapse factor
k_{EW}	Empty weight fraction
k_{WE}	Weight efficiency coefficient
l_{sep}	Separation distance from wing to tail
l_{SS}	Length of suspension strut
L	Flight range of vehicle
l/d	length to diameter ratio
L/D	Lift-to-drag ratio
N_{B}	Number of rotor blades
N_{ENG}	Number of engines
P	Power required

Q	Torque required
R	Rotor radius
S	Wing or tail area
SFC	Specific fuel consumption
t	Time
t_{MR}	Main rotor thrust recovery factor
t_{TR}	Tail rotor thrust recovery factor
t/c	thickness-to-chord ratio
T	Temperature
T	Rotor thrust
V_{C}	Climb velocity
V_{hel}	Cruise speed in helicopter mode
V_{air}	Cruise speed in airplane mode
W_{crew}	Crew weight
W_{DG}	Design gross weight for airplane mode
W_{EW}	Empty weight
W_{fuel}	Fuel weight
W_{LG}	Landing gear weight
W_{MEP}	Mission equipment package weight
W_{PL}	Payload weight
V_{stall}	Stall speed of wing
W_{TAIL}	Tail boom weight
W_{TB}	Tilt boom weight
W_{TO}	Takeoff weight
α_{TPP}	Tip path plane angle of attack
η_{pr}	Propulsive efficiency in helicopter mode
η_{coax}	Coaxial rotor efficiency
η_{prop}	Propulsive efficiency in airplane mode
ρ	Ambient air density
ρ_0	Air density at sea-level
ΩR	rotor tip speed
κ	Rotor induced power factor
Λ	Wing sweep angle
μ	Advance ratio
σ	Solidity, $N_B c/\pi R$
σ_p	Density ratio, σ/σ_0
ζ	Mechanical efficiency factor

ABBREVIATIONS & SUBSCRIPTS

air	Airplane mode
APU	Auxiliary power unit
CF	Centrifugal force
CHS	Container handling system
cr	Cruise condition

CREW	Crew
EMP	Empennage
ENG	Engine
ES	Electrical system
FS	Fuel system
fuel	Fuel
FUS	Fuselage
GB	Gear box
GHE	Ground handling equipment
hel	Helicopter mode
hov	Hovering flight condition
HT	Horizontal tail
HOGE	Hover out of ground effect
HUB	Rotor hub
IGB	Intermediate gear box
INST	Cockpit instruments, avionics & sensors
MEP	Mission equipment package
MR	Main rotor
MSL	Mean sea level
MTR	Mono Tiltrotor
MTR-SD	Mono Tiltrotor Scaled Demonstrator
nom	Nominal value
PIS	Power plant installation system
ref	Reference value
RES	Reserve
ROA	Radius of action
SH	Shaft
SP	Swashplate
SS	Suspension structure
TAIL	Tail boom
TB	Tilt boom
TM	Tilt mechanism
TR	Tail rotor
VT	Vertical tail
VTOL	Vertical takeoff and landing
w	Wing
WFM	Wing folding mechanism

Chapter 1

Introduction

The Mono Tiltrotor (MTR) is a proposed innovative vertical takeoff and landing (VTOL) concept featuring a tilting coaxial proprotor, an aerodynamically actuated folding wing and a suspended and streamlined cargo handling system. Proposed by Baldwin Technology Company [1, 2], the MTR has been focused towards heavy-lift, long-range, VTOL applications, for which there is a growing need in the modern military. In fact, the interest in developing heavy-lift rotorcraft concepts has spanned several decades [3, 4, 5, 6, 7].

Recently, the US Army proposed requirements for a Future Transport Rotorcraft (FTR) that would have the capability of carrying a 20 ton payload over a mission radius of 500 km (270 nm) under "hot and high" (95°F, 4,000 ft) conditions [8]. An aircraft with these capabilities would greatly increase the tactical ability of any military group. However, the FTR mission requirements far exceed the capability of any current rotorcraft in production as shown in Figure 1.1. To meet these FTR goals, a design that is either much greater in size than legacy rotorcraft or that features breakthrough innovations would be required using current technology. Because of its compact structural design and the ability to morph between a vertical lifting helicopter and an efficient cruising airplane flight mode, the MTR concept presents a possible unique solution to meet these stringent requirements.

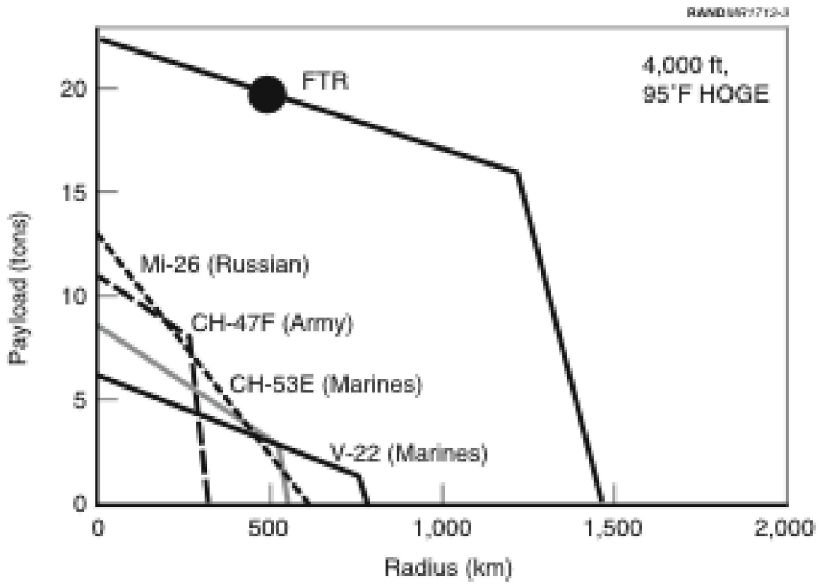

Figure 1.1: Payload-range capabilities of current rotorcraft technology versus FTR requirements at "hot and high" conditions [8].

The MTR in helicopter mode (Figure 1.2) is an efficient lifting platform, which essentially resembles a large, coaxial rotor, crane-like helicopter. The MTR is capable of vertical takeoff, hover and low speed cruise in this flight mode. In hovering flight, the wing panels are folded, with the wing tips pointing down toward the ground, to minimize the aerodynamic download in hovering flight. This is a key advantage that the MTR possesses over current tiltrotor concepts, which are penalized by large downloads. Large download penalties lead to increased engine power requirements and/or decreased payload capability for a fixed engine. The MTR also features a rotor disk loading comparable to that of a conventional, heavy-lift helicopter, which allows for efficient hovering capability. A relatively low disk loading also leads to lower downwash velocities felt on the ground during takeoff and landing, which increases operational capability in austere environments and overall mission versatility for a VTOL aircraft.

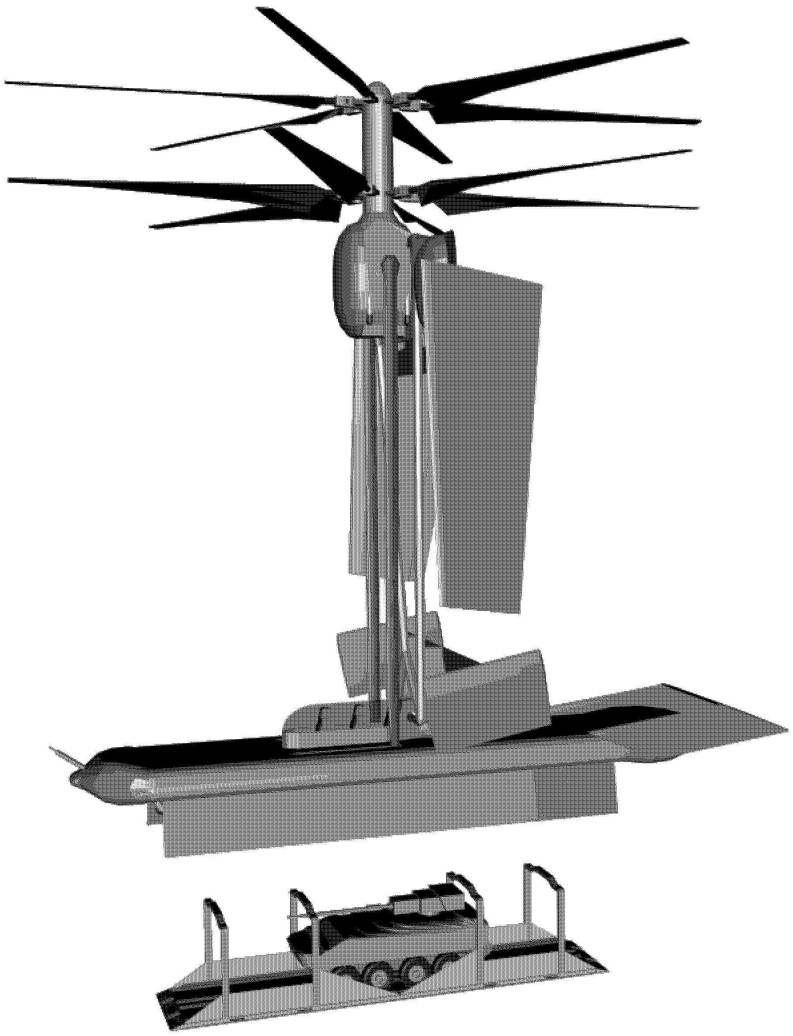

Figure 1.2: MTR concept in vertical-lift helicopter mode (BTC).

The tail structure of the MTR remains folded down during hovering flight and is locked to the cargo handling system. The tail of the MTR features a twin tail boom and a load bearing tilt boom, which is optimized for supporting compression loads. The two trapeze struts, which support the suspended cargo handling system, are optimized for supporting tensile loads. In helicopter mode, these members act in combination to absorb any loads that might be experienced during takeoff and landing. Because the tail boom is folded down in hovering flight, the roll, pitch and yaw control must be controlled by the rotor system by using cyclic pitch and differential collective blade pitch. The flight crew is housed in a cockpit which sits atop the cargo handling system. While this arrangement could have potential advantages in deploying and acquiring payload units, the crew compartment location could lead to serious handling qualities issues, as the flight crew would experience significant response lag times relative to their control inputs.

In airplane mode (Figure 1.3), the tail structure is folded up and locked into position to provide the aircraft with pitch and yaw control capability. The wings are folded up and locked into position to provide aerodynamic lift and to offload the rotor system. Roll control is provided by flaperons on the wings. The proper orientation of the payload unit is maintained through the use of control surfaces, which are on the aft end of the cargo handling system. The nacelle, which houses the power plant, transmission, fuel and coaxial rotor system, is tilted forward 90° such that the rotor system is able to act as a large, coaxial propeller. Additional fuel is carried in fuel pods located on the folding wing panels. The ability to cruise in such an airplane mode is where the speed and range advantages of any tiltrotor

concept materialize.

Airplanes are much more efficient cruising vehicles, possessing higher lift-to-drag ratios (L/D), than helicopters for several reasons. Helicopters tend to have more drag, with much of it being produced by the rotor hub and shaft. In addition helicopters usually do not have lifting wings, which means that the rotor system provides powered lift and thrust, where in an airplane configuration only powered thrust is required. For these reasons, airplanes tend to fly faster and over longer ranges than is possible using helicopters. However, the problem with conventional airplanes is that they usually lack VTOL capability. In the instances when a fixed-wing aircraft can takeoff vertically through thrust vectoring, they tend to burn a great deal of fuel in the process, and lack the ability to hover for any significant period of time. Thus, having the capability to convert from a helicopter to an airplane mode allows a tiltrotor aircraft to cruise at higher speeds and over longer distances than conventional helicopters, while still retaining efficient VTOL and hovering capability.

The takeoff and conversion history of the MTR concept is shown in Figure 1.4. The MTR is first shown at rest with the cargo handling structure and engine nacelle with landing gear on the ground. In takeoff mode, the rotor system lifts itself pulling along the wing, tail structure and cargo handling system. The MTR then is shown hovering in helicopter mode to capturing some payload unit. An advantage of the suspended cargo handling system of the MTR is that it can be tailored to handle a wide range of payload types. Pictured in Figures 1.2 and 1.4 is a payload unit designed to carry a military vehicles such as a Stryker. Standard MILVAN

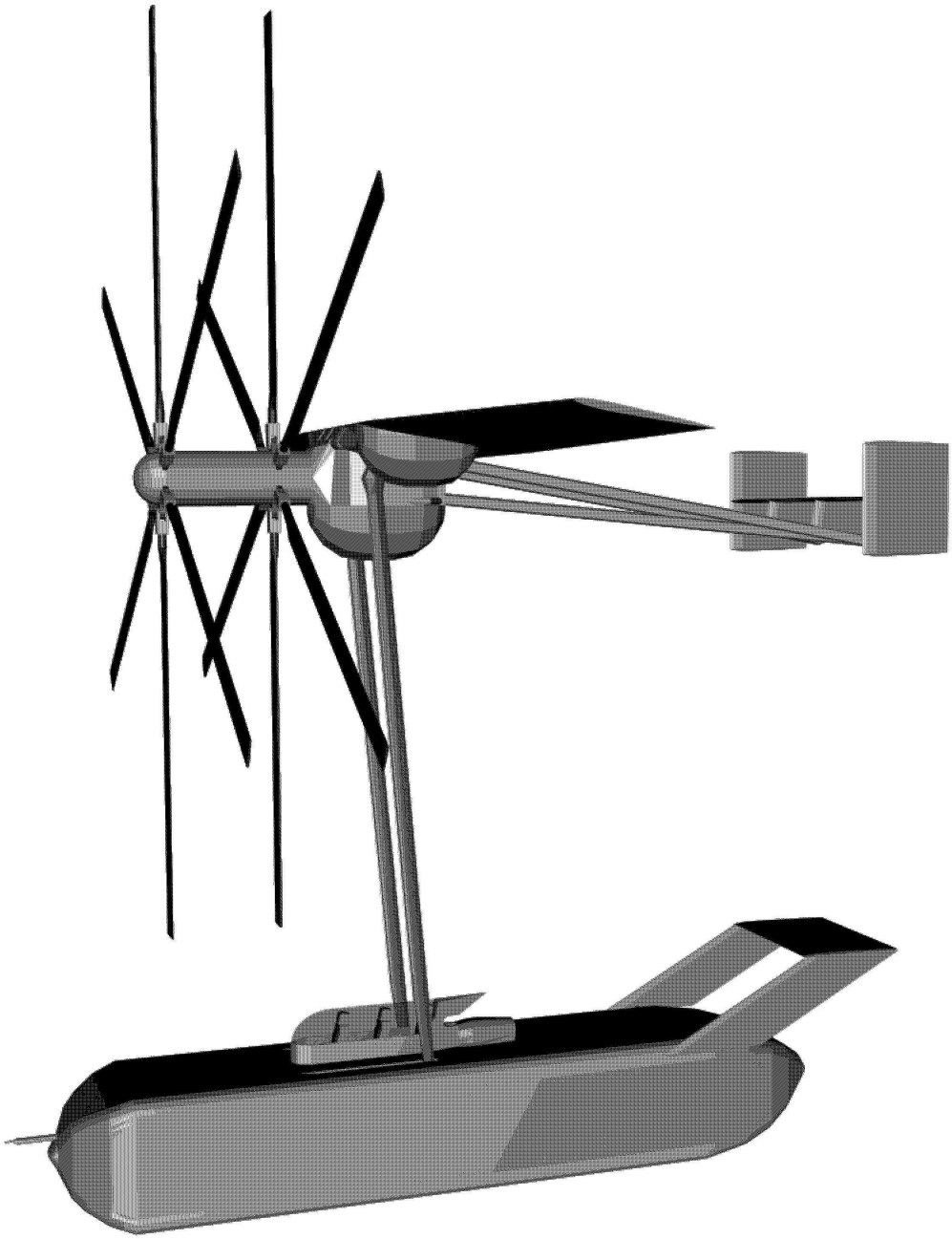

Figure 1.3: MTR concept in airplane cruise mode (BTC).

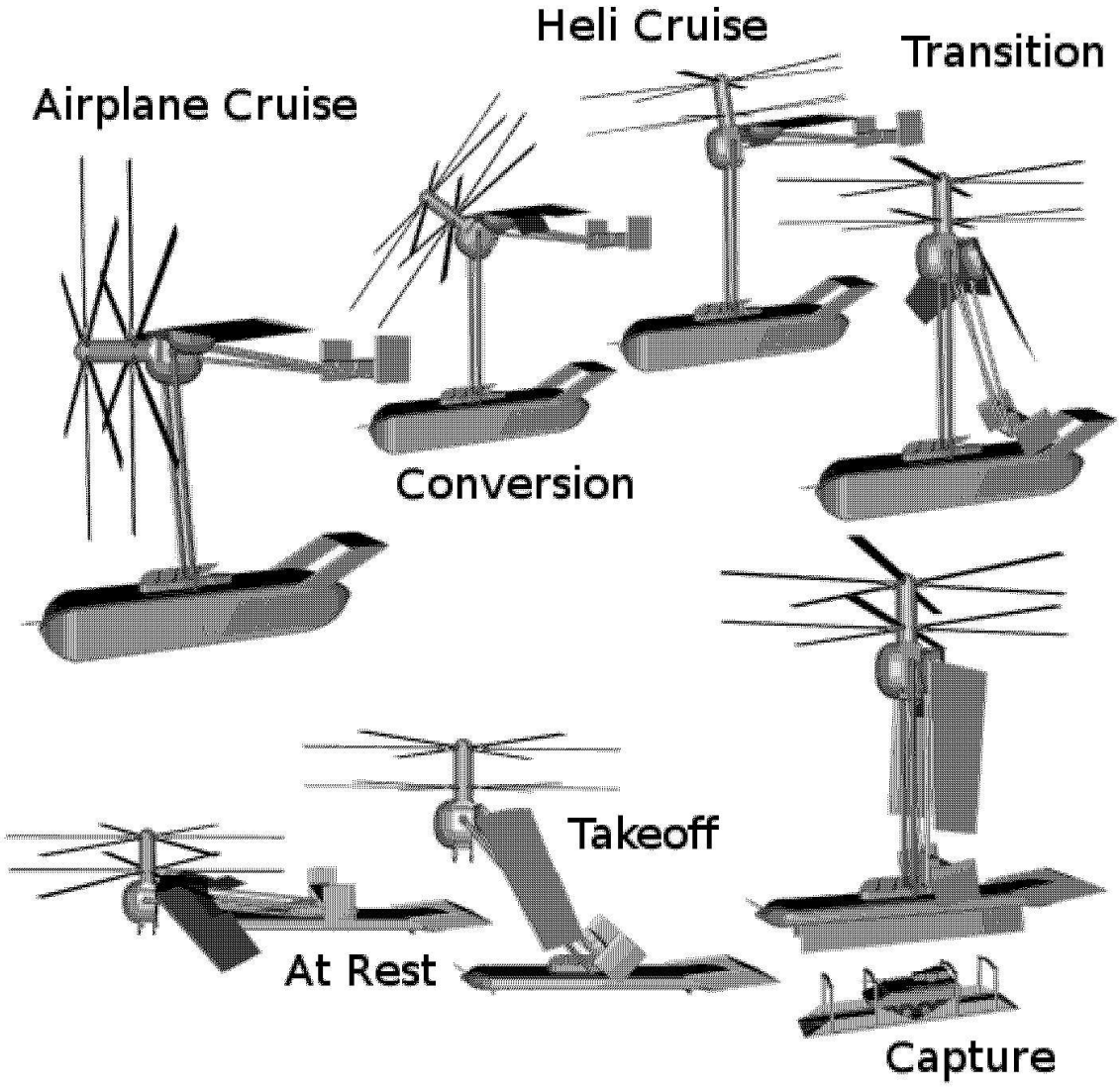

Figure 1.4: MTR concept starting at rest, taking off, and converting to airplane cruise mode (BTC).

containers, used by the military to transport supplies and munitions, can also be accommodated. After the payload unit is acquired, it is enveloped and streamlined to minimize aerodynamic drag in cruising flight. Transition flight begins, as the MTR begins to gain forward speed in helicopter mode. The wing and tail begin to fold upward, actuated by aerodynamic forces to achieve helicopter cruise mode. Once the wing and tail groups are locked-in and sufficient forward speed is attained, the engine nacelle tilts forward 90° to convert to airplane cruise mode.

The original goal of this work was to make an objective assessment of the MTR concept through a series of conceptual design studies. Certainly, there are many technological issues that need to be addressed with the MTR, such as the ability to tilt a large coaxial rotor 90° without blade strikes or other failures related to aeroelastics. Another key technical issue with the MTR include the ability to deploy the wings and tail from a folded position solely through aerodynamic forces, which is the focus of future analytical studies and wind tunnel tests. There are also concerns related to handling qualities and aircraft maneuverability with the suspended load and in building the suspensions struts with sufficient strength to compensate for the large moments that would be created through the motion of the suspended load.

However, these particular studies were focused primarily on judging the potential value of the MTR concept and, therefore, carried the assumption that the many hurdles facing the MTR concept could be overcome and that the MTR would be technically realized. Once this assumption is made, the question becomes – what might this aircraft look like, how much would it weigh and how would it perform

given a certain set of requirements? This idea forms the overall framework for the MTR conceptual studies. To determine the potential value of the MTR concept, a comprehensive sizing analysis was developed and validated, and the MTR was compared with legacy helicopter designs. Numerous design trade studies and performance analyses were completed, as discussed in the following chapters, including sizing and performance studies of both a long-range, heavy-lift MTR and an MTR Scaled Demonstrator.

Chapter 2

Design Methodology

The present method of analysis follows, in part, a conceptual rotorcraft design analysis developed over several years at the University of Maryland. The analysis was originally based on the work of Tishchenko [9, 10, 11]. The parametric equations and algorithmic procedures have been used successfully by the University of Maryland over the past seven years in the AHS's Student Design Competition [12, 13, 14, 15, 16, 17, 18]. This analysis has been revised and updated to examine coaxial rotorcraft configurations, especially that of the unique coaxial MTR configuration. The methodology of the design analysis takes key mission requirements and design inputs, and iteratively estimates the overall vehicle size, weight, fuel requirements and a detailed component weight breakdown for each design output. The elements of the design are based on a series of nonlinear equations describing both the performance and component weights of candidate rotorcraft designs.

Because the MTR is a hybrid aircraft concept combining some of the attributes of a dual rotor coaxial helicopter and a fixed-wing aircraft, sets of parametric equations describing the operation of the MTR both in helicopter and airplane mode have been developed. These equations are seamlessly integrated together in the design algorithms. Because the design proceeds as a highly nonlinear iterative process, these equations must be robust, but also highly representative of the underlying

performance of the vehicle in each of its operational flight conditions.

There are many sizing tools that have been developed in the rotorcraft and fixed-wing industries. Particularly for rotorcraft, there are codes available for sizing helicopters and tiltrotors such as HESCOMP and VASCOMP, developed by the Boeing Company [19]. VASCOMP was developed particularly to size tiltrotors of the XV-15 or V-22 configuration, which is fundamentally different from the MTR conceptual design. Therefore, it would not be accurate to size the MTR concept using a code such as VASCOMP, although such stock codes were valuable as a reference for some weight trends of interest in this study.

The component weight calculations for the MTR concept were based, in part, on the use of historical data for both helicopters and fixed-wing aircraft, and also on a detailed weights analysis for the MTR originally proposed by BTC. This initial design had an notional 80 ft diameter coaxial rotor [1, 2]. Mission requirements, such as payload weight, range (or mission radius of action), atmospheric conditions and hover times, are used along with rotor and engine design inputs to perform initial aircraft sizing estimates. These initial estimates are fed into the equations that calculate power requirements and fuel efficiencies in all flight modes, and sum the fuel burn required at each mission leg, depending on the selected mission profile.

Several mission profiles, which are discussed later in this chapter, were carefully designed to study the potential capabilities of the MTR design. A key in the determination of the fuel requirements in cruise flight is the estimation of the aerodynamic efficiency, or lift-to-drag ratio (L/D), of the overall aircraft. The estimation of this parameter is discussed later in this chapter. The fuel burn routine iterates on

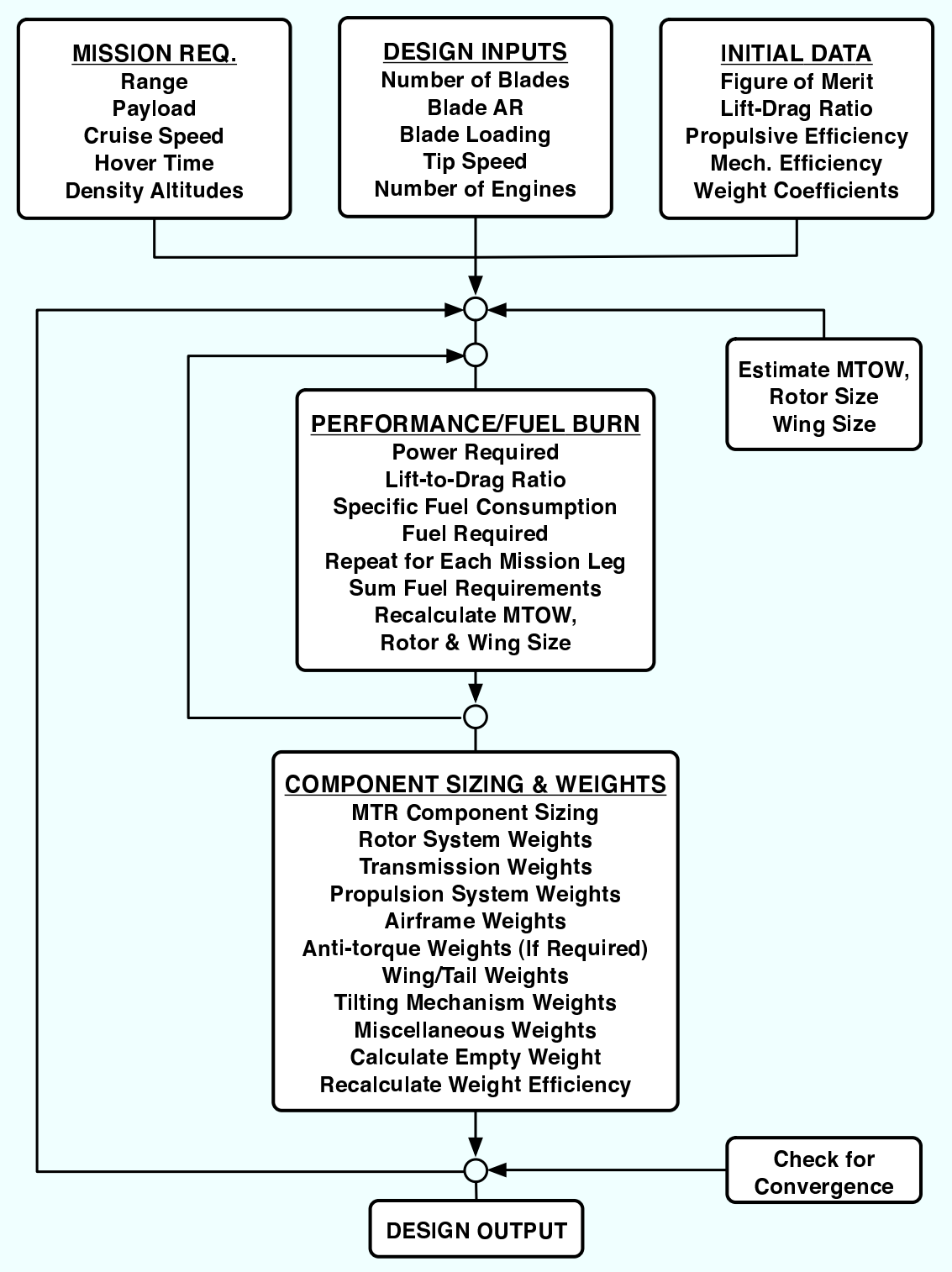

Figure 2.1: Flowchart of the conceptual rotorcraft design analysis.

the initial sizing values until an aircraft size is achieved that matches the calculated fuel requirements. A flowchart of the design process is shown in Figure 2.1.

Once the fuel burn routine reaches convergence, these initial performance and sizing results proceed to a detailed component weight breakdown, where each component of the aircraft is estimated based on some combination of volumetric properties, load requirements and empirical trends. These trends materialize in the form of specific weight equations and weight factors. When the component weight calculations are completed, the total empty weight of the vehicle is estimated along with the weight efficiency (or empty weight fraction). The entire process iterates several times (including the fuel burn routine) until converging on a weight efficiency that correctly corresponds to the overall vehicle size and weight. It is possible to make these calculations rapidly, developing a great number of design points to perform any number of trade studies, which are discussed in later chapters. Sample code, written in MATLAB, is provided in Appendix C.

2.1 MTR Mission Profiles

The MTR design methodology features a versatile mission tailoring capability. For a given design, one of three mission profiles can be selected to match the design requirements. Each mission profile is fully customized for the design by varying parameters such as hover times, density altitudes, payload weights, design cruise speed, and the flight range of each mission leg. The first of the three mission profiles is a long-range cruise mission, as shown in Figure 2.2. In this first mission profile,

the MTR takes off in helicopter mode with a payload at a given density altitude, H_{ρ_1}, hovers for some time, t_1, converts to airplane mode, and climbs to the design cruise density altitude, H_{ρ_2}. The MTR then cruises for a given range, L_2, at cruise speed, V_2. The aircraft then descends and converts back to helicopter mode, hovers for some time, t_3, at density altitude, H_{ρ_3}, and then lands at the destination.

The second mission profile is a radius of action mission, as depicted in Figure 2.3. In the radius of action mission, the MTR takes off in helicopter mode, converts to airplane mode, and cruises to a destination point, where there is some hover time, t_3, allotted for dropping the payload, W_{PL_1}, and then picking up an optional payload, W_{PL_2}. The aircraft then converts back to airplane mode, climbs to altitude, and either cruises back to the original takeoff point or to some other specified destination.

The third mission profile is a helicopter pickup mission, which is depicted in Figure 2.4. This mission profile was designed for a mission in which the payload is not at the same location as the takeoff point. The MTR would travel to the payload in helicopter cruise mode for some short distance, L_2. After collecting the payload in hover mode over some time, t_3, the aircraft converts to airplane mode and climbs to cruise some distance, L_4, until the destination is reached.

For the validation studies and the comparisons to legacy helicopters, which is made in Chapter 3, the first mission profile was used. Meanwhile, for most of the design and performance studies presented in Chapter 3, the second mission profile was used exclusively. This radius of action mission profile is a key objective for transport aircraft, simulating the deployment of assets to the battle-space and flight

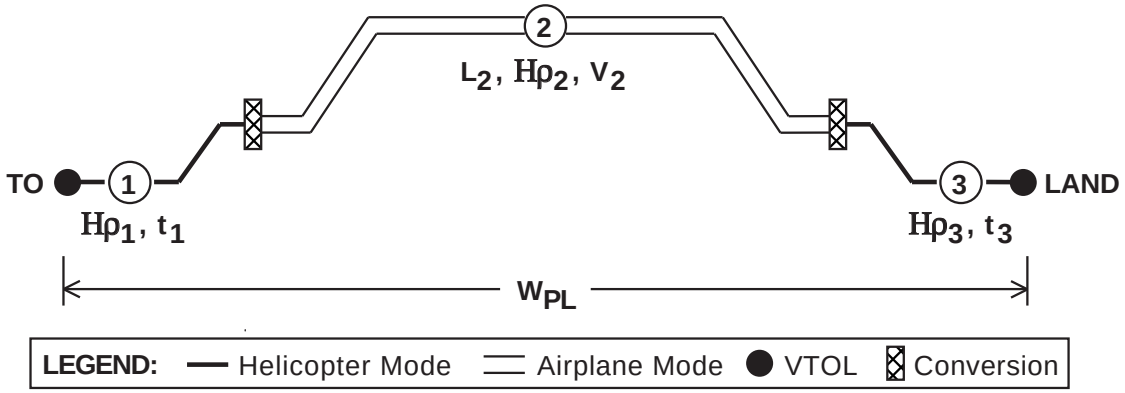

Figure 2.2: MTR long-range cruise mission profile.

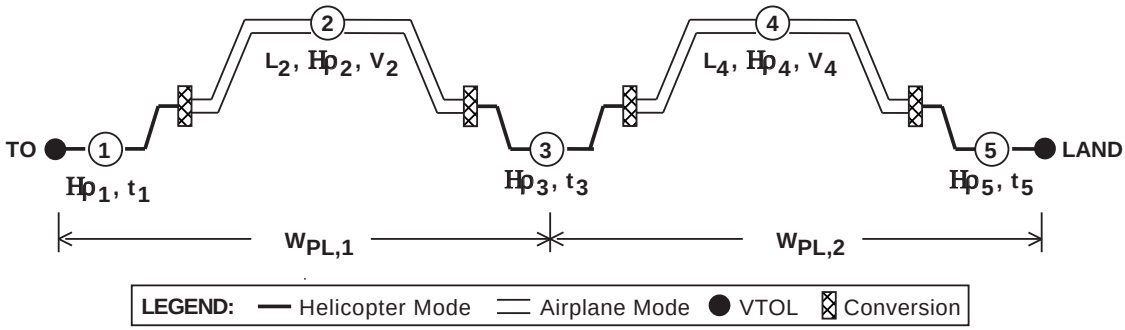

Figure 2.3: MTR radius of action mission profile.

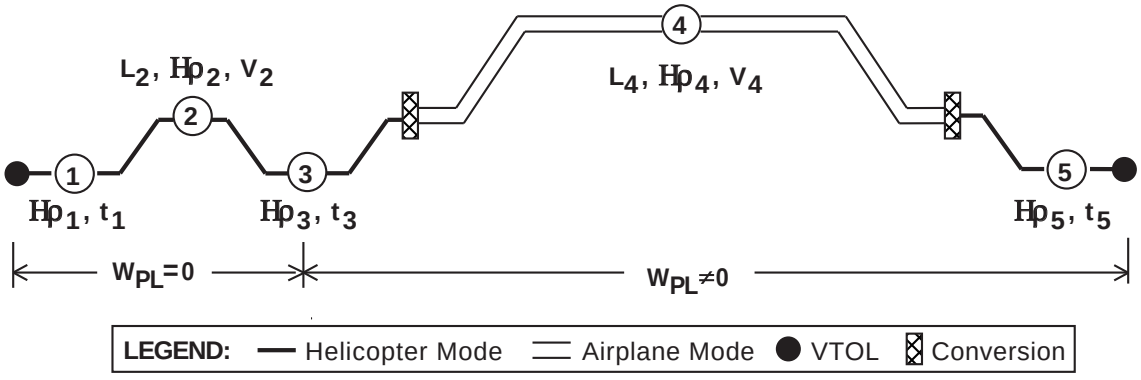

Figure 2.4: MTR helicopter pickup mission profile.

back to the departure point or to any other safe location. To implement any of these mission profiles, it is necessary to calculate the power requirements in any of the flight modes. For hovering flight this is a relatively simple task, but for cruising flight this requires good knowledge of the aerodynamic efficiency in terms of the lift-to-drag ratio of the overall aircraft.

2.2 Lift-to-Drag Ratio Analysis

Estimation of the overall lift-to-drag ratio (L/D) of the aircraft is a key calculation in the MTR design methodology. The L/D is a measure of the aerodynamic efficiency of the design configuration for a given flight condition. The fuel requirements in cruise flight are calculated directly from the aircraft L/D, creating the need for its rapid and accurate calculation within the design analysis. To calculate the L/D ratio of the MTR, it is necessary to estimate its equivalent flat plate area, f_{eq}, for each flight mode (hover and airplane). This was done by performing a component drag breakdown of the full aircraft.

2.2.1 Component Drag Breakdown

The component drag breakdown provides a good first estimate of the overall drag of an aircraft without having to perform costly wind tunnel tests, a priori. For each component of the aircraft, the drag coefficients based on frontal area were estimated based on the shape and operational Reynolds number of each component and sub-component. These drag coefficients are primarily based on empirical data

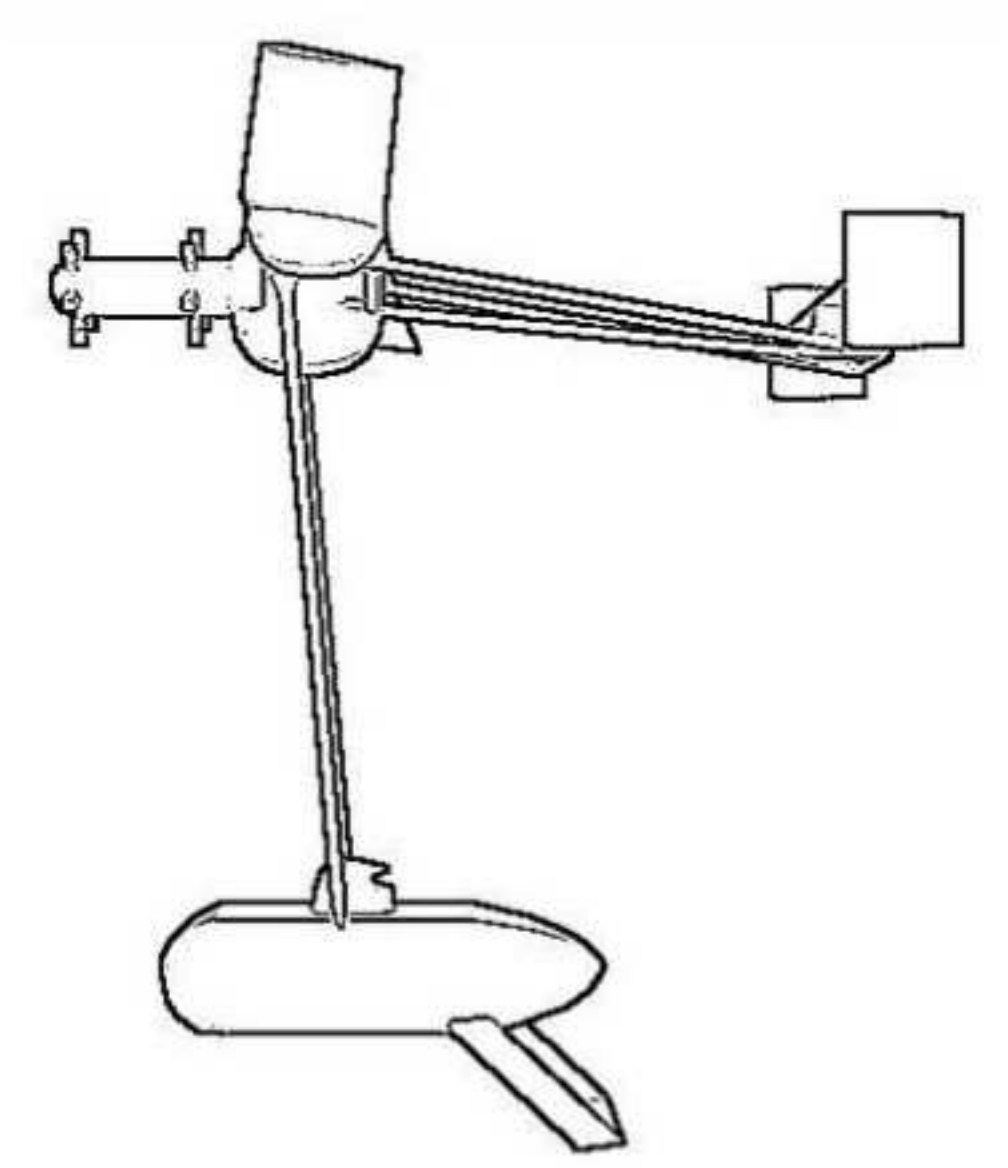

Figure 2.5: Conceptual design sketch of MTR flying in airplane mode with enveloped and streamlined MILVAN payload (BTC).

derived from wind tunnel tests on isolated components. For this analysis, the results documented in Hoerner [20] were used for the drag of basic shapes and components typical of airplanes. Results documented in Prouty [21] were used for the MTR components that were characteristic of helicopters. For example, the engine nacelle in airplane mode was modeled as an ellipsoid with length to diameter ratio, l/d, of 1.1 based on dimensioned drawings of a heavy-lift MTR, designed to carry a standard MILVAN container – see Figure 2.5. According to Hoerner, this ellipsoid combination yields a drag coefficient, C_{D_0}, of approximately 0.09. The frontal area, A_f, for each component was calculated based on dimensioned drawings of the MTR. The equivalent flat plate area, f_{eq}, was then calculated for each component and summed to find the total equivalent flat plate area for each flight mode using

$$f_{\mathrm{eq}} = \sum_{i=1}^{n} C_{\mathrm{D}_{0_{\mathrm{i}}}} \; A_{f_{\mathrm{i}}} \tag{2.1}$$

The component drag breakdowns for the MTR in airplane and helicopter mode are given in Table 2.1 and 2.2, respectively. A component interference factor was added to account for three-dimensional component interference effects and any surface irregularities. This value was assumed to be 20% of the sum of the component flat plate areas.

For airplane mode, it is shown in Table 2.1 that the components that have the most significant contributions to the vehicle drag are the engine nacelle, fuel pods, suspension struts, and cargo handling unit. The total equivalent flat plate area of this MTR configuration in airplane mode, f_{air}, was estimated to be 36.6 ft^2. The low drag of the MTR in airplane mode depends heavily on the aerodynamic design of

Component	Characteristic Length (ft)	Re	l/d	C_{D_0}	A_f (ft^2)	f (ft^2)
Wings	9.2	2.6×10^7	8.3	0.045	86.7	3.9
Nacelle	12	3.4×10^7	1.1	0.09	94.3	8.5
Fuel Pods	7	2.0×10^7	1.57	0.09	38.5	3.5
Tail Boom	33	9.4×10^7	-	0.05	4.1	0.2
Horiz Stab	6.5	1.9×10^7	8.3	0.045	20.3	0.9
Vert Stab	9	2.6×10^7	8.3	0.045	10.8	0.5
M/R Shaft	5	1.4×10^7	-	0.04	19.6	0.8
Struts	1.2	3.4×10^6	3	0.1	17.6	1.8
Cargo Handling	10	2.8×10^7	2	0.1	100	10
Crew Comp	4.5	1.3×10^7	1.6	0.06	8.0	0.5
Interference	-	-	-	-	-	6.0
Total, f_{air}						**36.6**

Table 2.1: MTR component drag breakdown in airplane mode.

Component	Characteristic Length (ft)	Re	l/d	C_{D_0}	A_f (ft^2)	f (ft^2)
Wings	9.2	1.4×10^7	8.3	0.045	86.7	3.9
Nacelle	13	1.9×10^7	0.4	0.2	122.5	24.5
Fuel Pods	7	1.0×10^7	1.57	0.09	38.5	3.5
Tail Boom	33	4.9×10^7	-	0.05	4.1	0.2
Horiz Stab	6.5	9.6×10^6	8.3	0.045	20.3	0.9
Vert Stab	9	1.3×10^7	8.3	0.045	10.8	0.5
M/R Hubs	-	-	-	0.6	40	24
M/R Shaft	5	5.6×10^5	-	0.3	90	27
Struts	1.2	1.8×10^6	3	0.1	17.6	1.8
Cargo Handling	10	1.5×10^7	2	0.1	100	10
Crew Comp	4.5	6.6×10^7	1.6	0.06	8.0	0.5
Interference	-	-	-	-	-	19.3
Total, f_{hel}						**116.1**

Table 2.2: MTR component drag breakdown in helicopter mode.

the cargo handling system. It is known that an untreated MILVAN container carried as a slung load can have an equivalent flat plate area of up to 100 ft^2. However, the current MTR design includes an enveloped, streamlined container, as shown in Figure 2.5. Through the use of fore and after bodies and a rounding edge radius, the drag can be reduced by a factor of ten, as shown by the results in Hoerner [20].

Table 2.2 shows that the MTR in helicopter mode has a much higher equivalent flat plate area. This is primarily a consequence of the vertical orientation of the main rotor shaft, which leads to large increases in the hub, shaft and engine nacelle drag. The hub was modeled as being equivalent to two CH-53 hubs, for which drag data was given by Prouty [21]. The helicopter flate plate area, f_{hel}, of 116.1ft^2 is comparable to that of a large crane helicopter design. Additionally, the rotating engine nacelle is optimized for minimal drag in axial flight and produces significantly higher drag in helicopter cruise. While this is a large amount of drag, the MTR is not designed for extended cruising flight in helicopter mode.

The values for equivalent flat plate area derived in the component drag analysis pertain only to the particular point design of a large, heavy-lift MTR. For refined analysis about this point design, these values for equivalent flat plate area must be scaled approximately with the aircraft weight. In an examination of flat plate drag data for legacy helicopters and airplanes, the equivalent flat plate area can be scaled with the square root of the aircraft gross weight [22]. Therefore, the flat plate area in the design analysis was defined using

$$f_{\text{eq}} = k_{\text{eq}}\sqrt{W_{\text{TO}}} \tag{2.2}$$

where the value of k_{eq} is calculated based on the values of flat plate area, f_{eq}, and takeoff weight, W_{TO}, of the MTR at its reference condition, or the weight of the aircraft used to perform the component drag analysis. In this case, the reference condition was an MTR sized to carry 20 tons of payload over a 500 nm radius of action.

2.2.2 Lift-to-Drag Ratio Estimation

With the equivalent flat plate area of the aircraft, it is possible to directly calculate the engine power requirements and L/D of the overall aircraft in cruise for a given airspeed and density altitude. The engine power requirements in airplane mode were estimated using the standard power equation [23]

$$P_{\text{req}_{\text{air}}} = \frac{1}{2\eta_{\text{prop}}\zeta_{\text{air}}}\rho V_{\text{air}}^3 f_{\text{air}} + \frac{1}{2\eta_{\text{prop}}\zeta_{air}}\rho V_{\text{air}}^3 S_{\text{w}} \frac{C_{\text{L}}^2}{\pi\ e_{\text{w}}\ AR_{\text{w}}} \tag{2.3}$$

where S_{w} is the wing area, C_{L} is the lift coefficient of the wing and e_{w} is Oswald's span efficiency factor. The propulsive efficiency of the proprotor system in airplane mode, η_{prop}, and the mechanical transmission efficiency, ζ_{air} are taken into account to calculate required engine power. The helicopter cruise power requirements can be calculated using [22]

$$P_{\text{req}_{\text{hel}}} = \kappa\frac{W_{\text{TO}}^2}{2\rho A_{\text{MR}} V_{\text{hel}}\eta_{\text{pr}}\zeta_{\text{hel}}} + \frac{\sigma_{\text{MR}} C_{\text{d}_0}}{8\eta_{\text{pr}}\zeta_{\text{hel}}}(1 + 4.65\mu^2)\rho A_{\text{MR}}(\Omega R)_{\text{MR}}{}^3 + \frac{1}{2\eta_{\text{pr}}\zeta_{\text{hel}}}\rho V_{\text{hel}}^3 f_{\text{hel}} \tag{2.4}$$

where μ is the edgewise advance ratio of the rotor, η_{pr} is the propulsive efficiency of the rotor system in helicopter mode and ζ_{hel} is the mechanical efficiency of the transmission in helicopter mode. The induced power requirements have been esti-

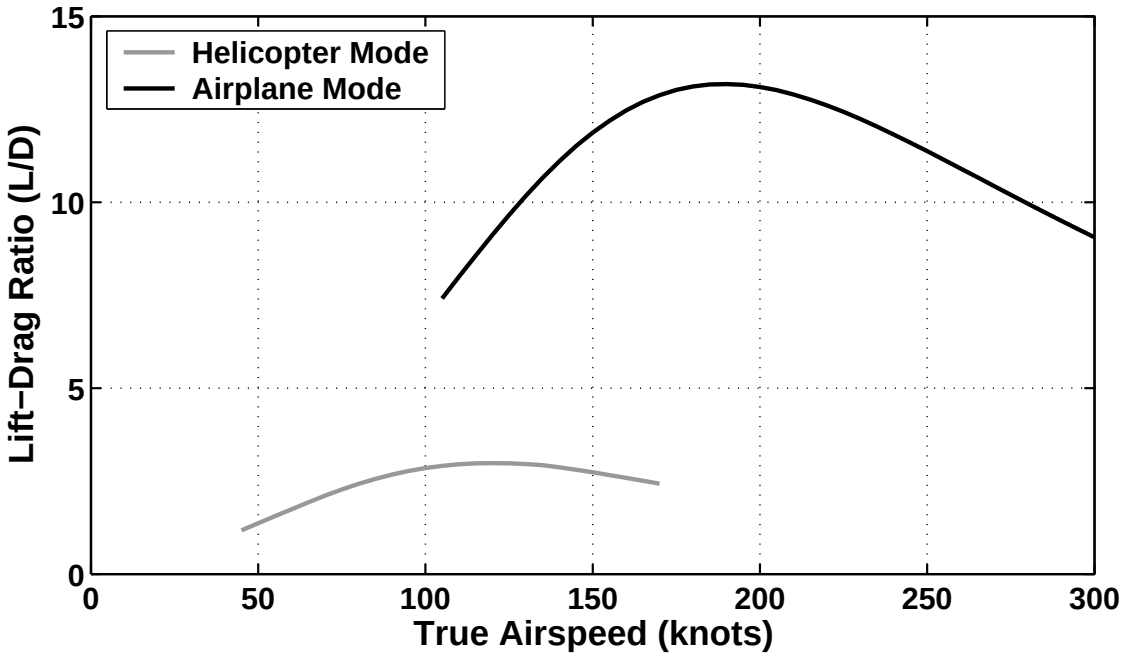

Figure 2.6: Lift-to-drag ratio of the MTR in both helicopter and airplane modes.

mated using Glauert's "high-speed" approximation to the induced velocity through the rotor [22]. Equations 2.3 and 2.4 were also used to create power required curves for the MTR point design, as described later. The L/D ratio of the MTR was then calculated using

$$\frac{L}{D} = \frac{W_{\mathrm{TO}} V_{cr}}{P_{\mathrm{req}} \eta \, \zeta} \tag{2.5}$$

These calculation steps were performed for a heavy-lift MTR configuration designed to carry 20 tons of useful payload over a 500 nm radius of action mission profile. The L/D ratio of the aircraft for both flight modes is shown in Figure 2.6 versus airspeed at MSL conditions. Notice that in helicopter mode, the MTR has a relatively low L/D ratio that is reached at a relatively low airspeed. This is comparable to conventional helicopter designs. The benefits of conversion to airplane mode can be clearly seen by the large improvement in L/D ratio, with the maximum value

being reached at nearly twice the airspeed as that in helicopter mode. Figure 2.6 also shows that the MTR design configuration is aerodynamically efficient, with L/D ratios of 14 being predicted in airplane mode based on the component drag synthesis. The following sections begin to consider the details of the performance, sizing and weight calculations featured in the MTR conceptual design analysis.

2.3 General Performance & Sizing Analysis

The sequence of performance and sizing calculations that follows has been outlined, in part, by Tishchenko et al. [11] for the conceptual design of large transport helicopters (i.e., those with payloads of over 6 tons). However, the present design analysis has been developed in a much more general form to allow trade studies to be conducted for different types of mission profiles, especially over longer ranges less typical of a conventional helicopter, and also between different vertical flight vehicle configurations. The analysis was also developed to encompass conventional helicopters (with both single and dual coaxial rotors) that would carry smaller payloads of less than 6 tons.

The analysis was further developed for the specific unique features of the MTR architecture, taking into consideration the unique morphing and external load carrying capabilities of the design, assuming these morphing capabilities could indeed be technically realized. While the analysis possesses the ability to size helicopters as well as MTR aircraft, the sequence of equations presented in the following sections details the sizing and weight calculations of only the MTR concept. Detailed lists of

calculations used in the design analysis to size conventional and coaxial helicopters are given in Appendix A. A key part of the performance analysis is the accurate determination of component weights, which as previously mentioned, was based in part on correlation studies against extensive historical data for existing helicopters. The correlation coefficients used in the performance studies are given in Appendix B. The equations and coefficients presented here are compatible with English Standard units, although they can be carefully converted to be compatible with any other unit system.

2.3.1 Takeoff Weight & Energy Efficiency

The takeoff weights of the vehicle depend depend both on their structural efficiency (empty weight fraction) and the aerodynamic efficiency. As a rule of thumb, acquisition cost is proportional to the empty weight of the aircraft, so structural efficiency is paramount for a heavy-lift rotorcraft design concept. Aerodynamic efficiency, which is a function of both hovering efficiency and cruise (forward flight) efficiency, affects the fuel weight required. Fuel weight is a major factor in determining direct operating costs.

A relatively small part of most mission time is spent in hover, therefore, the fuel weight is determined primarily by the cruise efficiency in airplane mode. The effect of hover time is considered later. Using the Bréguet range equation [23], the range L can be written as

$$L = \frac{(L/D)_{\text{air}}\ \eta_{\text{prop}}\ \zeta_{\text{air}}}{SFC_{\text{cr}}} \ln\left(\frac{W_{\text{TO}}}{W_{\text{TO}} - W_{\text{fuel}}}\right) \tag{2.6}$$

where SFC_{cr} is the specific fuel consumption of the engines in cruise and $(L/D)_{\text{air}}$ is the corresponding lift-to-drag ratio in airplane mode. The range can also be written as

$$L = E \ln\left(\frac{W_{\text{TO}}}{W_{\text{TO}} - W_{\text{fuel}}}\right) \tag{2.7}$$

where E has been referred to as an "energy efficiency" as defined by Tishchenko et al. [11] as

$$E = \frac{(L/D)_{\text{air}}\ \eta_{\text{prop}}\ \zeta_{\text{air}}}{SFC}_{\text{cr}} \tag{2.8}$$

This index is useful as a comparative metric because it is a composite of aerodynamic, mechanical and fuel efficiency. It does not, however, provide a direct measure of the efficiency of the vehicle in conveying its payload. The weight of the fuel burned is then

$$W_{\text{fuel}} = W_{\text{TO}}\,(1 - \exp(-L/E)) \tag{2.9}$$

which comes directly from the Bréguet equation. For small ranges this is equivalent to

$$W_{\text{fuel}} \approx \frac{L\ W_{\text{TO}}}{E} \tag{2.10}$$

Therefore, the determination of fuel required in cruise flight requires a determination of the cruise efficiency.

The takeoff weight of the vehicle can now be estimated according to the equation

$$W_{\text{TO}} = \frac{W_{\text{PL}} + W_{\text{crew}} + W_{\text{MEP}} + W_{\text{fuel}_{\text{hov}}}}{k_{\text{WE}} - k_{\text{FW}} - 0.005} \tag{2.11}$$

where a fuel allowance of 0.5% of the total fuel has been made in the preceding equation to account for warm-up, taxi and takeoff portions of the flight profile. The

fuel weight coefficient for short ranges can be calculated as

$$k_{\mathrm{FW}} = \frac{L + V_{\mathrm{air}}\, t_{\mathrm{res}}}{E} \tag{2.12}$$

where t_{res} is a specified reserve time in each flight mode. The reserve time depends, in part, on whether IFR or VFR flight conditions prevail. For long range vehicles the weight of fuel burned during the flight must be taken into account in the performance evaluation. The fuel weight efficiency coefficient in this case become

$$k_{\mathrm{FW}} = 1 - \exp\left(-\frac{L + V_{\mathrm{air}}\, t_{\mathrm{res}}}{E}\right) \tag{2.13}$$

It should be noted that the parameter k_{WE} in Eq. 2.11 is the net structural weight efficiency of the vehicle, which is defined by Tishchenko et al. [11] as

$$k_{\mathrm{WE}} = \frac{W_{\mathrm{TO}} - W_{\mathrm{EW}}}{W_{\mathrm{TO}}} \tag{2.14}$$

This quantity is equivalent to using an empty weight fraction that is defined as

$$k_{\mathrm{EW}} = \frac{W_{\mathrm{EW}}}{W_{\mathrm{TO}}} = 1 - k_{\mathrm{WE}} \tag{2.15}$$

While weight efficiency has been used by default throughout the present work, they are easily related for other comparative purposes by using Eq. 2.15.

The weight of fuel required for the mission, W_{fuel}, depends on that required for hovering flight plus that required in cruise flight. For the hovering portion of the flight, the fuel weight required is

$$W_{\mathrm{fuel}_{\mathrm{hov}}} = SFC_{\mathrm{hov}} N_{\mathrm{ENG}} P_{\mathrm{ENG}}\, t_{\mathrm{hov}} \tag{2.16}$$

where SFC_{hov} is the specific fuel consumption of the engines in hovering flight and $N_{\mathrm{ENG}} P_{\mathrm{ENG}}$ is the total power required. Notice that the fuel weight is also affected

by the part of the mission time that is required to hover, t_{hov}. The specific fuel consumption can be defined as

$$SFC = \left(\frac{W_{\text{fuel}}}{P_{\text{ENG}} N_{\text{ENG}}}\right) \frac{1}{t_{\text{flight}}} \tag{2.17}$$

Also, the flight time, t_{flight}, in the cruise condition is

$$t_{\text{flight}} = \frac{L + t_{\text{res}} V_{\text{air}}}{V_{\text{air}}} \tag{2.18}$$

where L is the range at the cruise speed, V_{air}, and t_{res} is the time reserve to meet various operational and/or certification requirements. This means that the total fuel weight, W_{fuel}, is given by the equation

$$W_{\text{fuel}} \;=\; W_{\text{TO}} \left(\frac{L + V_{\text{air}}\, t_{\text{RES}_{\text{air}}}}{E_{\text{air}}} + 0.005\right) + W_{\text{fuel}_{\text{hov}}} \tag{2.19}$$

2.3.2 Main Rotor Sizing Equations

For a hovering vehicle, the solidity of the main rotor(s), σ_{MR}, drives the rotor weight. It is easily shown that the rotor solidity is given by

$$\sigma_{\text{MR}} = \frac{N_{B_{\text{MR}}}}{\pi AR_{B_{\text{MR}}}} \tag{2.20}$$

where $N_{B_{\text{MR}}}$ is the number of rotor blades per rotor and $AR_{B_{\text{MR}}} = R/c$ is the aspect ratio of the blades. This leads to the effective disk loading, DL, of the rotor system as

$$DL = \left(\frac{C_T}{\sigma}\right)_{\text{MR}} \sigma_{\text{MR}}\, \rho_0\, (\Omega R)^2_{\text{MR}} \tag{2.21}$$

where ρ_0 is the ambient air density at mean sea level (MSL) conditions. Disk loading, DL, is defined as the thrust per unit disk area of the rotor system [22]. Throughout

this design study for a coaxial rotor system, the disk loading is considered to be the total thrust (or takeoff weight) of the aircraft divided by the sum of the area of the two rotor disks. This is equivalent to assuming that each rotor carries half of the net aircraft weight. Solving for the main rotor diameter D_{MR} of each rotor using the latter equation gives

$$D_{\mathrm{MR}} = \sqrt{\frac{2W_{\mathrm{TO}}}{\pi DL}} \tag{2.22}$$

The power requirements for flight can now be established. The machine is assumed to have N_{ENG} engines that each deliver a power of P_{ENG}. For the coaxial rotor system the power required is

$$N_{\mathrm{ENG}} P_{\mathrm{ENG}} = \frac{(W_{\mathrm{TO}}\, t_{\mathrm{MR}})^{3/2}}{\sqrt{\pi/2}\; FM_{\mathrm{MR}}\; \zeta_{\mathrm{MR}} D_{\mathrm{MR}}\; \eta_{\mathrm{coax}} \sqrt{\sigma_p} \sqrt{\rho_0}} \tag{2.23}$$

where FM is the figure of merit of the rotor system and t_{MR} is a thrust recovery factor that takes into account interference effects between the rotor and the airframe. The term η_{coax} represents a loss of net rotor aerodynamic efficiency because of rotor-on-rotor interference and the interacting flow fields between the two rotors. Based on NACA tests with coaxial rotors [24] it would seem that on average $\eta_{\mathrm{coax}} \approx 0.85$, which means that there is a loss of net rotor efficiency with a coaxial for rotors with the same equivalent disk loading and net solidity (or equivalent C_T/σ). This is equivalent to the use of a coaxial induced power factor, κ_{int}, which increases the induced power requirements over and above that required for two single (isolated) rotors. The interference (efficiency) coefficient also depends on the relative thrust/torque balance between the rotors, although this is a secondary effect for the

conceptual design process. The nominal installed engine power is then

$$P_{\mathrm{ENG}_{\mathrm{nom}}} = P_{\mathrm{ENG}} C_{\mathrm{pow}} \tag{2.24}$$

where C_{pow} is an installation loss factor. The torque required for the main rotor system is then

$$Q_{\mathrm{MR}} = \frac{(P_{\mathrm{ENG}} N_{\mathrm{ENG}}) R_{\mathrm{MR}}\ \zeta_{\mathrm{MR}}}{(\Omega R)_{\mathrm{MR}}} \tag{2.25}$$

The main rotor torque requirements define the transmission sizing requirements and other component weights for the aircraft. These weights are considered in the following sections.

2.3.3 Wing Sizing Calculations

Wing sizing is a key component of the overall MTR design methodology. The overall size of the wings (in terms of wing area and wing span) has a profound effect on the operational envelope and overall size of the aircraft. Two flight conditions set the requirements for wing area in the MTR design, namely: conversion between flight modes and high-altitude cruise flight. For the conversion regime, the wing area requirement is predicated on the need to have a sufficiently low stall (or conversion) speed, such that the power required during conversion can be minimized. When a mission profile requires high-altitude cruise, there needs to be sufficient wing area to cruise at this altitude and at the design cruise speed, while maintaining sufficient stall margins for maneuvers and gusts. Depending on the mission requirements for the design, the largest limiting design driver for the aircraft wing area can change. Therefore, the design analysis calculates the required wing area for each driver, and

chooses the largest value as the design solution. The wing area required for achieving a design stall (or conversion) speed is given by

$$S_{\mathrm{w_{stall}}} = \frac{W_{\mathrm{TO}}}{\frac{1}{2}\rho_{\mathrm{TO}} V_{\mathrm{stall}}^2 C_{L_{\mathrm{max}}}} \tag{2.26}$$

where $C_{L_{\mathrm{max}}}$ is the maximum lift coefficient of the wing with flaps deflected. This value was assumed to be 2.5, which consistent with conventional wings using a double-slotted flap and for wings that operate in the slipstream of a propeller. The design stall speed, V_{stall}, was established as 120 knots, which was considered to be sufficiently slow for a safe, efficient conversion corridor. Note that the wings are being sized for the stall speed at the takeoff density altitude. The wing area required for efficient cruising flight is given by

$$S_{\mathrm{w_{cr}}} = \frac{W_{\mathrm{TO}}}{\frac{1}{2}\rho_{\mathrm{cr}} V_{\mathrm{cr}}^2 C_{L_{\mathrm{cr}}}} \tag{2.27}$$

where the value $C_{L_{\mathrm{cr}}}$ is the maximum lift coefficient in cruise to maintain sufficient stall margins. This value was set to $C_{L_{\mathrm{cr}}} = 0.8$ for this analysis based on standard airfoil characteristics and vertical gust and maneuver load requirements. After the values $S_{\mathrm{w_{stall}}}$ and $S_{\mathrm{w_{cr}}}$ were calculated, the largest of these two values was selected as the wing area for the MTR design.

After the required wing area was calculated, the wing span must be determined, which is a function of the wing aspect ratio. The wing span was constrained to be no greater than 140% of the rotor diameter because of the need to allow sufficient space for wing folding in the hovering flight condition. Setting the wing span to the maximum allowed value would lead to the highest possible wing aspect ratio and, therefore, to the highest L/D ratio in cruise, and so reducing the required fuel

weight. However, a higher aspect ratio corresponds to a higher wing weight, which tends to offset this benefit. In fact, it was found that there was an optimum value for the wing aspect ratio for a given mission that will lead to a minimum takeoff weight.

Figure 2.7 shows the variation in takeoff weight with wing aspect ratio for MTR aircraft designed for a 500 nm radius of action mission with a 20 ton payload carried on both mission legs, MSL conditions at takeoff and landing, 20 minutes of destination hover time, and high altitude cruise. While an aspect ratio of nearly 10 would be feasible, the minimum takeoff weight of the MTR for this mission is achieved using a wing aspect ratio of approximately 7.5. It is also shown that there is a relatively low level of sensitivity to aircraft weight with changes in wing aspect ratio. For example, a wing aspect ratio of 10 could be selected with only a 0.5 ton penalty to the aircraft weight. This is because the increases in wing weight are almost entirely offset by decreases in fuel weight. However, the wing span of the MTR was found to be very sensitive to changes in the wing aspect ratio. The wing span was calculated based on the required wing area and the input wing aspect ratio using the equation

$$b_{\mathrm{w}} = \sqrt{S_{\mathrm{w}} AR_{\mathrm{w}}} \tag{2.28}$$

The variation in wing span with wing aspect ratio for the MTR designed to perform the same radius of action mission is shown in Figure 2.8. A wing aspect ratio of 10 will lead to a wing span that is nearly 20 ft larger than an MTR with a wing aspect ratio of 7.5, which corresponds to minimum takeoff weight and rotor

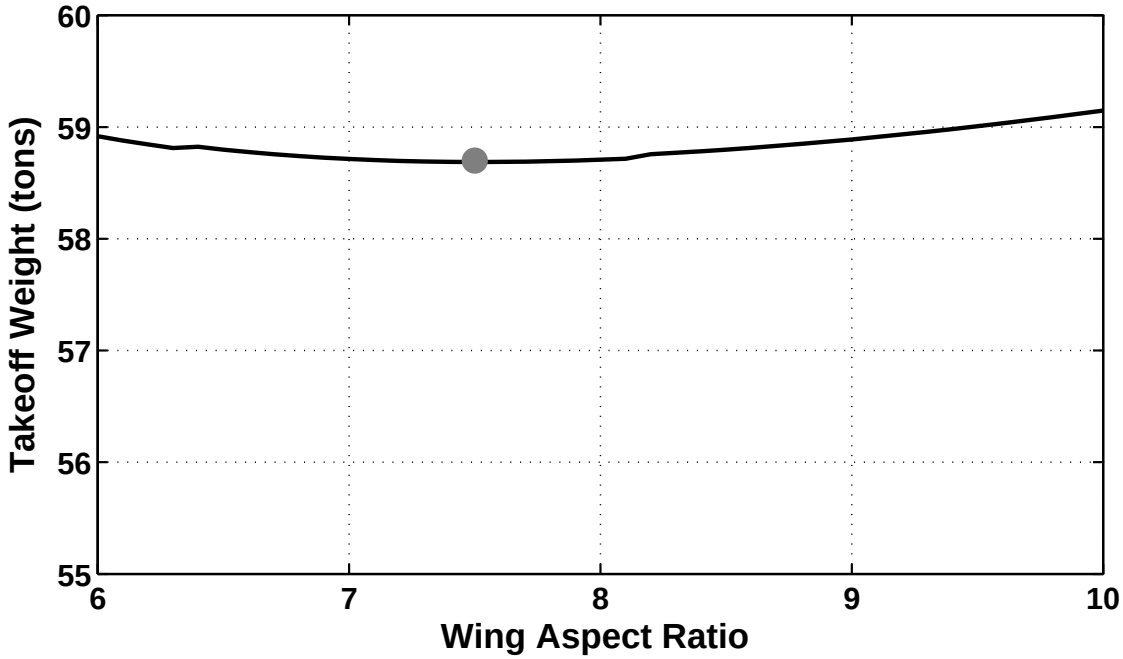

Figure 2.7: Variation in MTR takeoff weight with changes in wing aspect ratio.

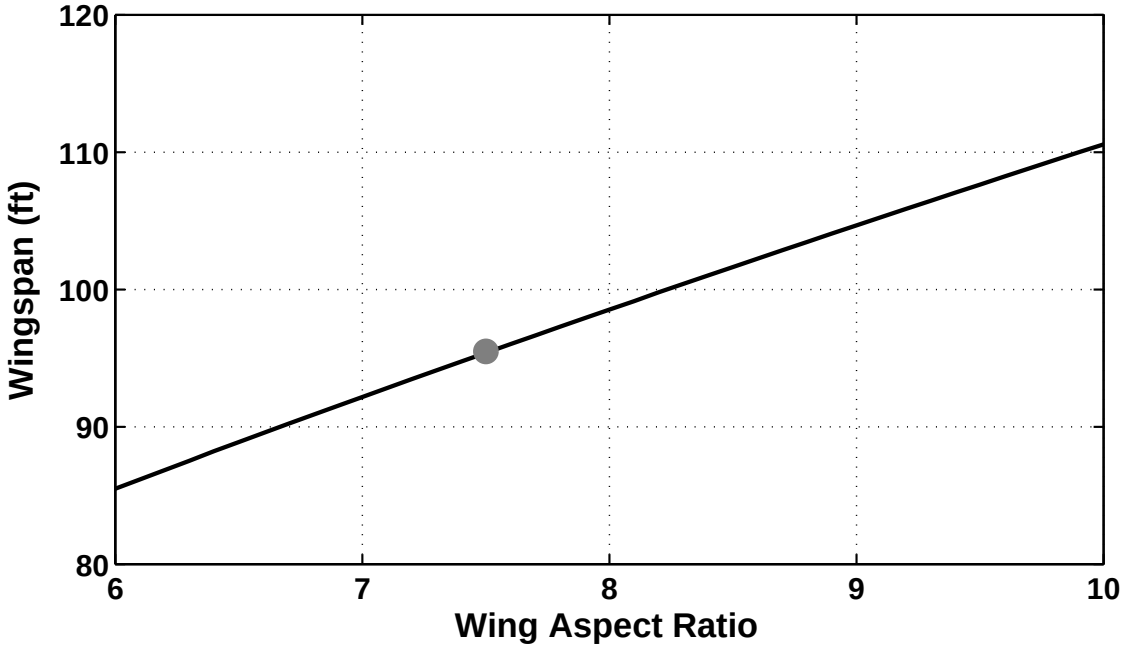

Figure 2.8: Variation in MTR wing span with changes in wing aspect ratio.

size. Therefore, to minimize takeoff weight, rotor size, and wing span a design wing aspect ratio of 7.5 was selected for heavy-lift, long-range missions with high-altitude cruise flight. When sizing another class of vehicle, this simple trade study is repeated to select optimal wing aspect ratio. With the initial estimates of the takeoff weight, rotor size and wing area, it is then possible to begin to estimate the required fuel to perform the given mission.

2.3.4 Fuel Burn Calculations

The fuel requirements were calculated in the mission specific routines based on the selected mission profile after making initial estimates for the aircraft take-off weight, rotor size, and wing size. Within this mission fuel burn routine, power requirements, L/D, specific fuel consumption and fuel requirements were calculated for each mission leg, in sequence, based on the given mission inputs. The vehicle weight was updated at each leg, thereby accounting for the fuel burned during flight. The properties of the standard atmosphere were used along with inputs of pressure altitude, H_P, and the temperature above MSL, ΔT, to calculate the air density, ρ and engine loss factor, k_{ALT}. The atmospheric density ratio can be found using

$$\sigma_{\mathrm{P}} = \frac{\rho}{\rho_0} = \left(1 - 6.873 \times 10^{-6} H_{\mathrm{P}}\right)^{5.26} \left(\frac{T_0}{T_0 + \Delta T}\right) \tag{2.29}$$

The air density is then calculated simply as

$$\rho = \rho_0 \sigma_{\mathrm{P}} \tag{2.30}$$

The engine loss factor accounts for the degradation in performance of a modern turboshaft at altitudes above MSL and temperatures above standard conditions.

The engine loss factor is based on the performance of an average modern turboshaft engine and was calculated as a function of the density altitude using

$$k_{\text{alt}} = \left(1 - 2.23 \times 10^{-4} H_\rho\right)^{-1} \tag{2.31}$$

These values were calculated for each mission leg based on the design inputs before performing the mission calculation steps. The following is a sequential list of calculations for the long range mission profile with mission legs 1–3.

Mission Leg 1

As shown in Figure 2.2, the first mission leg is hovering flight in helicopter mode just after takeoff. To calculate the fuel required to hover for a given time, the power required to hover, P_1, must be calculated using

$$P_1 = \frac{(W_{\text{TO}}\ t_{\text{MR}})^{3/2}}{\sqrt{\pi/2}\ FM_{\text{MR}}\zeta_{\text{MR}}D_{\text{MR}}\ \eta_{\text{coax}}\sqrt{\sigma_1}\sqrt{\rho_0}} \tag{2.32}$$

This also is the power required to take off, which is used to set the engine power requirements. The engine power required was calculated based on the power required to take off, P_1, the number of engines and the takeoff density altitude, which is represented by the engine loss factor, k_{alt_1}, which can be written

$$P_{\text{ENG}} = \frac{P_1\ k_{\text{alt}_1}}{N_{\text{ENG}}} \tag{2.33}$$

The engine power required will be higher if the takeoff density altitude is higher than MSL, leading to a larger engine requirement and a larger overall aircraft size. The nominal engine power was then calculated as

$$P_{\text{ENG}_{\text{nom}}} = P_{\text{ENG}} C_{\text{pow}} \tag{2.34}$$

The specific fuel consumption is calculated as a function of power required and power available using

$$SFC_1 = C_{e_1} + \frac{C_{e_2}}{P_1/(P_{\mathrm{ENG}_{\mathrm{nom}}} N_{\mathrm{ENG}})} \tag{2.35}$$

The total fuel required for the first mission leg is then calculated as a function of the power required, specific fuel consumption, and time to hover, t_1, using

$$W_{\mathrm{fuel}_1} = P_1 \; SFC_1 \; t_1 \tag{2.36}$$

Mission Leg 2

The second mission leg is a long range cruise in airplane mode, as shown schematically in Figure 2.3. The fuel requirements for this mission leg are calculated differently. The first step is to adjust the weight of the aircraft based on the fuel burned in the previous mission leg by subtracting this weight from the initial takeoff weight, i.e.,

$$W_2 = W_{\mathrm{TO}} - W_{\mathrm{fuel}_1} \tag{2.37}$$

The new aircraft gross weight, W_2, represents the weight of the aircraft at the beginning of the second mission leg and is used for the following calculations. To calculate the power requirements, and ultimately the L/D of the MTR in airplane cruise, it is necessary to calculate the wing lift coefficient. This is calculated by the definition of the lift coefficient and with the use of the mission input values for the second mission leg, giving the equation

$$C_{L_2} = \frac{2W_2}{\rho_2 V_2^2 S_{\mathrm{w}}} \tag{2.38}$$

The lift coefficient in cruise is then used to calculate the induced drag (i.e., drag due to lift), $C_{\mathrm{D_i}}$, of the MTR in cruise using the equation

$$C_{D_i} = \frac{C_{L_2}^2}{\pi AR_{\mathrm{w}}\ e_{\mathrm{w}}} \tag{2.39}$$

The induced drag is used in combination with the mission inputs and flat plate drag of the MTR in airplane mode to calculate the power requirements in cruise, as shown previously, using

$$P_2 = \frac{\rho_2 V_2^3\,(f_{\mathrm{air}} + S_{\mathrm{w}} C_{D_{\mathrm{i}}})}{2\eta_{\mathrm{prop}}\zeta_{\mathrm{air}}} \tag{2.40}$$

The power available in the second mission leg, $P_{\mathrm{av_2}}$, depends upon the total engine power and the engine lapse from increases in density altitude. This is represented in the equation

$$P_{\mathrm{av_2}} = \frac{P_{\mathrm{ENG_{nom}}} N_{\mathrm{ENG}}}{k_{\mathrm{alt_2}}} \tag{2.41}$$

Note that power available will decrease with increases in density altitude. The specific fuel consumption for this mission leg is calculated again as a function of the ratio between required and available power using

$$SFC_2 = C_{e_1} + \frac{C_{e_2}}{(P_2/P_{\mathrm{av_2}})} \tag{2.42}$$

The lift-to-drag ratio, or aerodynamic efficiency, is required to calculate the fuel burned during cruise. This is calculated using

$$\left(\frac{L}{D}\right)_2 = \frac{W_2 V_2}{P_2\ \eta_{\mathrm{prop}}\ \zeta_{\mathrm{air}}} \tag{2.43}$$

The vehicle energy efficiency, E_2, a cruise efficiency metric proposed by Tishchenko [11] is calculated as a function of the aerodynamic, propulsive, mechanical and fuel

efficiencies of the aircraft using

$$E_2 = \frac{(L/D)_2 \ \eta_{\text{prop}} \ \zeta_{\text{air}}}{SFC_2} \tag{2.44}$$

The fuel requirements for the second mission leg are then calculated as a function of the vehicle energy efficiency, aircraft gross weight and the mission input range, L_2, using

$$W_{\text{fuel}_2} = W_2 \left(1 - \exp(-L_2/E_2)\right) \tag{2.45}$$

Mission Leg 3

The third and final mission leg for this long-range haul profile is characterized by hovering flight in helicopter mode, as shown in Figure 2.4. After the previous two mission legs, the gross weight of the aircraft should be much lower than at takeoff. Therefore, the aircraft weight at the start of this final mission leg is given by

$$W_3 = W_2 - W_{\text{fuel}_2} \tag{2.46}$$

The greatly reduced gross weight in the final mission leg will lead to much lower power requirements and, therefore, the required fuel to be carried. The power requirements are calculated similarly to that of the first mission leg as

$$P_3 = \frac{(W_{\text{TO}} \ t_{\text{MR}})^{3/2}}{\sqrt{\pi/2} \ FM_{\text{MR}} \ \zeta_{\text{MR}} D_{\text{MR}} \sqrt{\sigma_3} \sqrt{\rho_0}} \tag{2.47}$$

As before, the power available in this mission leg is calculated based on the total engine power and the engine losses from changes in density altitude using

$$P_{\text{av}_3} = \frac{P_{\text{ENG}_{\text{nom}}} N_{\text{ENG}}}{k_{\text{alt}_3}} \tag{2.48}$$

The specific fuel consumption is calculated similarly using

$$SFC_3 = C_{e_1} + \frac{C_{e_2}}{(P_3/P_{\text{av}_3})} \tag{2.49}$$

Finally, the required fuel weight for the third and final mission leg is calculated as a function of the power requirements, specific fuel consumption and mission input hover time using

$$W_{\text{fuel}_3} = P_3 \; SFC_3 \; t_3 \tag{2.50}$$

Total Fuel Weight

The total fuel weight for the mission is then taken as the sum of the individual mission leg fuel requirements, with additional factors for takeoff, landing, climb, descent, conversion between flight modes and reserve fuel using

$$W_{\text{fuel}_{\text{tot}}} = (1 + k_{\text{f}}) \left(W_{\text{fuel}_1} + W_{\text{fuel}_2} + W_{\text{fuel}_3} + W_{\text{fuel}_{\text{res}}} \right) \tag{2.51}$$

where the fuel reserve, $W_{\text{fuel}_{\text{res}}}$, is calculated as a function of the power requirements in cruise, specific fuel consumption and required reserve time using

$$W_{\text{fuel}_{\text{res}}} = P_2 \; SFC_2 \; t_{\text{res}} \tag{2.52}$$

and k_{f} is a factor that takes takeoff, landing, climb and conversions into account. The latter is defined as a function of the number of conversions between modes, N_{conv}, and the number of full climbs and descents involved in the mission profile, N_{cl} using

$$k_{\text{f}} = N_{\text{conv}} k_{\text{conv}} + N_{\text{cl}} k_{\text{cl}} \tag{2.53}$$

For the long-range haul mission profile, the values of N_{conv} and N_{cl} are 2 and 1, respectively. For the radius of action mission profile, these values would be 4 and 2. After the total fuel requirements are calculated, the takeoff weight is recalculated using this newly calculated fuel weight and the current values for the empty weight, payload and crew weight using

$$W_{\text{TO}} = W_{\text{EW}} + W_{\text{PL}} + W_{\text{fuel}_{\text{tot}}} + W_{\text{crew}} \tag{2.54}$$

The rotor size, D_{MR}, and wing size, S_{w}, are then recalculated, as discussed previously. The mission subroutine is then iterated until converging on the proper fuel weight and aircraft size for the given empty weight. This procedure is a loop within the main calculation loop, which uses the component weight equations to converge on the proper combination of empty weight and size, as shown in Figure 2.1.

2.3.5 Additional MTR Component Sizing

The specific equations used in the sizing of the MTR other than the rotor system and wing must also be established. This includes the tail group as well as the payload suspension structure and container handling system. The horizontal tail area S_{HT} of the MTR is defined as

$$S_{\text{HT}} = \frac{C_{\text{HT}} \bar{c}_{\text{w}} S_{\text{w}}}{l_{\text{sep}}} \tag{2.55}$$

where C_{HT} is the horizontal tail volume coefficient. The corresponding vertical tail area S_{VT} is given by

$$S_{\text{VT}} = \frac{C_{\text{VT}} b_{\text{w}} S_{\text{w}}}{l_{\text{sep}}} \tag{2.56}$$

where C_{VT} is the vertical tail volume coefficient. The twin tail boom length (separation distance from wing to tail) of the MTR is written as a fraction of the main rotor diameter as

$$l_{\mathrm{sep}} = k_{\mathrm{HT}} R_{\mathrm{MR}} \tag{2.57}$$

where in the first instance $k_{\mathrm{HT}} = 1.2$ has been used, which again is consistent with the conceptual design suggested by Baldwin [1]. With the assumption of a defined aspect ratio then the spans of the horizontal and vertical tails on the MTR are given by

$$b_{\mathrm{HT}} = \sqrt{AR_{\mathrm{HT}} S_{\mathrm{HT}}} \tag{2.58}$$

and

$$b_{\mathrm{VT}} = \sqrt{AR_{\mathrm{VT}} S_{\mathrm{VT}}} \tag{2.59}$$

respectively. In keeping with the assumptions of geometric proportionality, the length of the suspension structure is defined as a fraction of the main rotor radius as

$$l_{\mathrm{SS}} = k_{\mathrm{SS}} R_{\mathrm{MR}} \tag{2.60}$$

where it has been assumed that $k_{\mathrm{SS}} = 1.35$.

2.4 Component Weights

The parametric weight equations for the conventional helicopter configuration were developed following the work of Tishchenko et al. [11]. These equations were appropriately modified for a coaxial rotor system based on historical data (where available) and new sets of parametric equations were also developed for the MTR

architecture. The following section details the component weight calculations for only the MTR design. The component weight equations for conventional and coaxial helicopters are listed in Appendix A. A component breakdown of the MTR architecture is shown in Figure 2.9. This is an early conceptual sketch, but it gives a representation of how the groups referred to in this section look and fit together into the overall design. The correlation coefficients used in the component weight studies are given in Appendix B.

2.4.1 Rotor Weights

The weight of the main rotor blades, $W_{\mathrm{B_{MR}}}$, is defined based on their size and average weight per unit volume as

$$W_{\mathrm{B_{MR}}} = k_{\mathrm{B_{MR}}} \left(\frac{\sigma_{\mathrm{MR}} R_{\mathrm{MR}}^{2.7}}{\bar{AR}^{0.7}} \right) \tag{2.61}$$

where

$$\bar{AR} = \frac{AR_{\mathrm{B_{MR}}}}{18} \tag{2.62}$$

For a coaxial rotor system the value of $W_{\mathrm{B_{MR}}}$ is doubled because of the two rotors, all other factors being equal.

The weight of the main rotor hub is driven by the strength requirements, mostly to react centrifugal forces acting on the blades from their rotation. The hub weight $W_{\mathrm{HUB_{MR}}}$ is defined by the equation

$$W_{\mathrm{HUB_{MR}}} = k_{\mathrm{HUB_{MR}}} N_{\mathrm{B_{MR}}} \, f_{\mathrm{Z_{MR}}} \left(10^{-4} F_{\mathrm{CF_{MR}}} \right)^{N_{\mathrm{HUB}}} \tag{2.63}$$

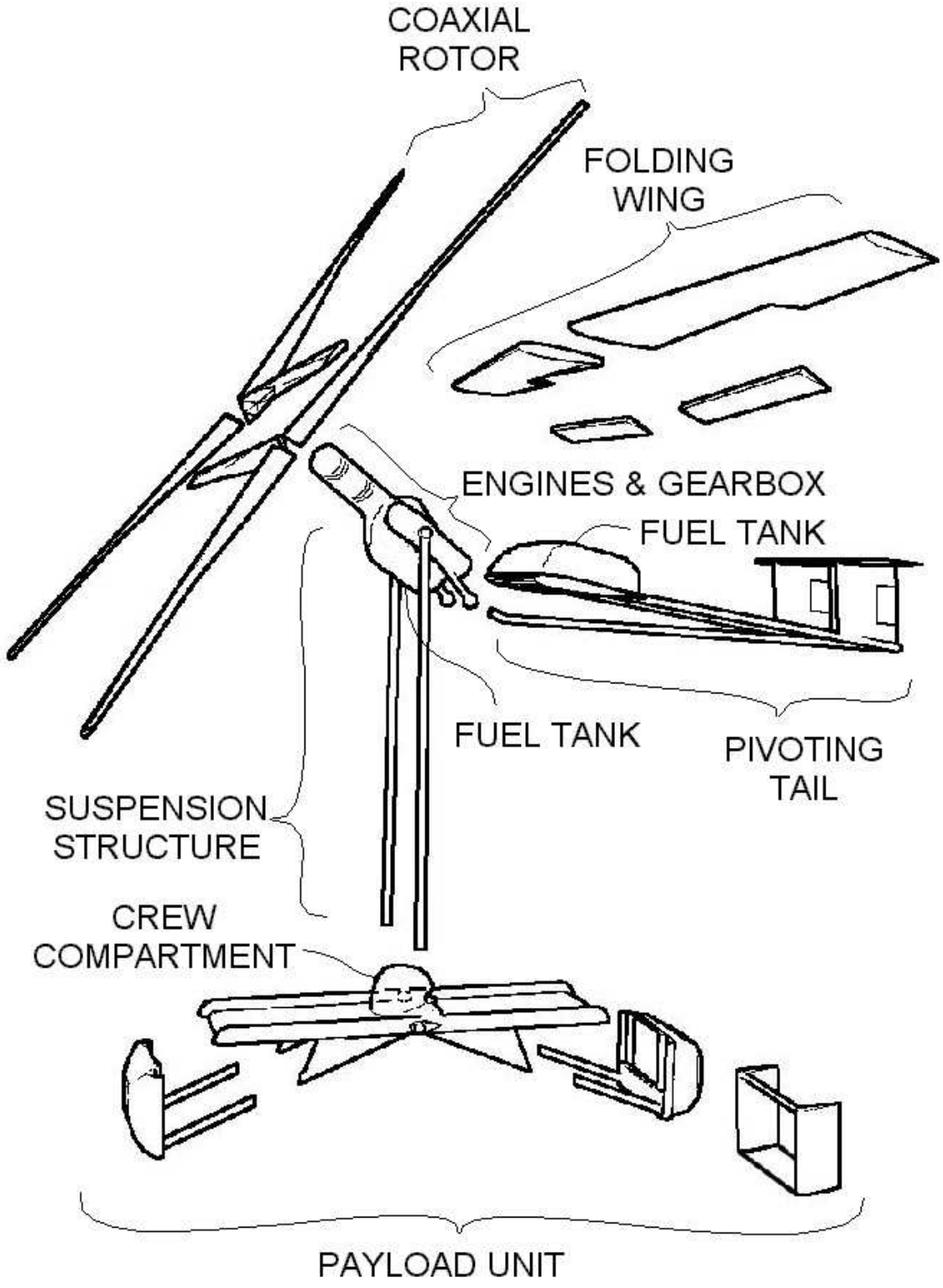

Figure 2.9: Component breakdown of the MTR architecture (BTC).

where

$$N_{\text{HUB}} = \begin{cases} 1.35 & \text{if } W_{\text{PL}} \leq 6 \text{ tons} \\ \\ 1.5 & \text{if } W_{\text{PL}} > 6 \text{ tons} \end{cases} \tag{2.64}$$

and where

$$f_{\text{Z}_{\text{MR}}} = \begin{cases} 1 & \text{if } N_{\text{B}_{\text{MR}}} \leq 4 \\ \\ 1 + 0.05(N_{\text{B}_{\text{MR}}} - 4) & \text{if } N_{\text{B}_{\text{MR}}} > 4 \end{cases} \tag{2.65}$$

The centrifugal force acting on any one main rotor blade is given by [22]

$$F_{\text{CF}_{\text{MR}}} = \left(\frac{W_{\text{B}_{\text{MR}}}}{N_{\text{B}_{\text{MR}}}}\right)\left(\frac{(\Omega R)_{\text{MR}}}{R_{\text{MR}}}\right)^2 \frac{R_{\text{MR}}}{2g} \tag{2.66}$$

In the case of the coaxial rotor system, there are two main rotor hubs and the weight of the hub must doubled (if all other factors were held constant) giving an equation for the hub weight as

$$W_{\text{HUB}_{\text{MR}}} = 2.25\ k_{\text{HUB}_{\text{MR}}} N_{\text{B}_{\text{MR}}}\ f_{\text{Z}_{\text{MR}}} \left(10^{-4} F_{\text{CF}_{\text{MR}}}\right)^{N_{\text{HUB}}} \tag{2.67}$$

where there is a penalty factor of 25% imposed on the net hub weight that accounts for structural redundancy and the typically longer shaft length that is needed with a coaxial rotor design to accommodate the dual hubs with sufficient separation distance between the rotors.

2.4.2 Transmission Weights

The weight of the main rotor transmission is defined in terms of the shaft torques required on the basis of Eq. 2.25. For the coaxial rotor system of the MTR, the weight of the main rotor gearbox, $W_{\text{GB}_{\text{MR}}}$, is defined using

For the coaxial rotor system, the rotor gearbox weight is assumed to vary according to the equation

$$W_{\mathrm{GB_{MR}}} = 1.3\, k_{\mathrm{GB_{MR}}} (Q_{\mathrm{MR}})^{0.8} \tag{2.68}$$

where the factor of 1.3 accounts for the additional planetary gearing required to produce two concentric output shafts. Additional transmission weights that would be necessary for powering a tail rotor, such as intermediate gear box, tail rotor gear box and tail rotor shaft weights are included in the helicopter calculations of Appendix A.

2.4.3 Rotor Control Weights

The rotor control mechanism comprises the swashplate and pitch links (assuming a swashplate is used), the booster servo hydraulics and the automatic flight control system. The weight of the swashplate and control linkages depends on the blade loads, which depend in turn on the blade area and forward speed. The swashplate and control linkage weight is found to correlate with the equation

$$W_{\mathrm{SP}} = k_{\mathrm{SP_1}}\, c_{\mathrm{MR}}^2 R_{\mathrm{MR}}\, \mu + k_{\mathrm{SP_2}} \tag{2.69}$$

where $k_{\mathrm{SP_1}}$ and $k_{\mathrm{SP_2}}$ are constants and μ is the main rotor advance ratio in helicopter cruise mode, which is defined as

$$\mu = \frac{V_{\mathrm{hel}} \cos \alpha_{\mathrm{TPP}}}{(\Omega R)_{\mathrm{MR}}} \tag{2.70}$$

In the case of a coaxial rotor system, the weight of the swashplate and control system is higher because of the need to control two rotors. A parametric equation

was developed in the form

$$W_{\mathrm{SP}} = 1.75 \left(k_{\mathrm{SP}_1} \, c_{\mathrm{MR}}^2 R_{\mathrm{MR}} \, \mu + k_{\mathrm{SP}_2} \right) \tag{2.71}$$

The weight of the servo or hydraulic booster control system W_{BCS} is proportional to the size and weight of the swashplate and is defined as

$$W_{\mathrm{BCS}} = k_{\mathrm{BCS}_1} \, c_{\mathrm{MR}}^2 R_{\mathrm{MR}} \, \mu + k_{\mathrm{BCS}_2} \tag{2.72}$$

Finally, the weight of the automatic flight control system W_{AFCS} is assumed to be a binary value that depends on the payload of the machine, i.e.,

$$W_{\mathrm{AFCS}} \begin{cases} 165 \text{ lb} & \text{if } W_{\mathrm{TO}} \leq 6 \text{ tons} \\ \\ 330 \text{ lb} & \text{if } W_{\mathrm{TO}} > 6 \text{ tons} \end{cases} \tag{2.73}$$

2.4.4 Airframe Weights

The MTR is essentially an unmanned lifter with suspended load, where the load includes a container handling system topped by a manned crew compartment. The rotating-wing portion of the unmanned lifter consists of engines, gearbox, rotor, fuel tank, and biped landing struts all connected together as a single unit having no conventional fuselage. The fixed-wing portion of the MTR also has no fuselage, but consists of a pivoting tailboom with tilt actuator, fuel tank and empennage, and folding wing panels pinned to a center wing box. The load bearing members of the suspension structure and the container handling system carry tensile loads only to minimize structural weight. The container itself provides structural support for enveloping and streamlining fairings. For the studies contained in this work, an

empty container weight of 5,000 lb was accounted for as payload weight, consistent with a 20 ft MILVAN container.

Because the MTR carries an external load, the weight of the cargo handling system is an integral part of the overall design and not necessarily a function of payload weight. In this regard a structural analysis was performed to calculate the weight required to support a 20 foot long MILVAN container with cargo giving a 20 ton payload. This container was used in these studies for payloads ranging from 10 to 32.5 tons. Therefore, over this range the size and weight of the payload handling unit is held constant when the mission requires the deployment of a MILVAN container, i.e.,

$$W_{\text{CHS}} = 2000 \text{ lb} \tag{2.74}$$

This value is based on a detailed structural weight analysis provided by BTC. For smaller payloads, the weight of the cargo handling system is varied proportionally to the payload weight using

$$W_{\text{CHS}} = k_{\text{CHS}} W_{\text{PL}} \tag{2.75}$$

The cargo handling system weight includes the tail capture mechanism. Recent work has led to a cargo handling system designed for carrying payload packages that would not fit into a standard MILVAN container, such as a Stryker assault vehicle. The weight of this unit is considerably higher than that used to carry MILVAN containers as it is forced to provide more structural strength and folding ramps for vehicle deployment. This longer, heavier cargo unit is pictured in Figures 1.2 and 1.3, compared to the unit designed to envelop and streamline a MILVAN container

which is shown Figure 2.5.

The weight of the trapeze struts of the suspension structure was estimated using

$$W_{\mathrm{SS}} = 2\, k_{\mathrm{SS}_1}\, l_{\mathrm{SS}} \left(\frac{P_{\mathrm{crit}} - k_{\mathrm{SS}_3}}{k_{\mathrm{SS}_2}} \right) \tag{2.76}$$

where k_{SS_1} is the mass density of the struts. The parameter P_{crit} represents a critical load for the trapeze design defined as a fraction of the vehicle weight. The suspension struts were optimized for tensile loads in a study provided by the Baldwin Technology Company. It is possible that in some maneuvering conditions that the struts would undergo compression loads, in which case the size and weight of these struts may be required to increase, which would result in increased empty weight and drag. Possible drag increases in the cargo handling system are explored in the following chapter (Section 3.4).

The MTR crew compartment is simply a canopy installed atop the container handling system and supported through the suspension structure. For this conceptual design, the weight of the structure of MTR crew compartment W_{CC} was assumed constant and was represented using

$$W_{\mathrm{CC}} = 500 \text{ lb} \tag{2.77}$$

Cockpit instrumentation, avionics, sensors and cockpit furnishings were assumed to be given by the equation

$$W_{\mathrm{INST}} = 0.075\, W_{\mathrm{PL}} \tag{2.78}$$

based on the work of Tishchenko et al. [11].

2.4.5 Wing and Tail Weights

The MTR fixed lifting surfaces (wing and tail) were sized similarly to that of a fixed-wing aircraft, rather than a helicopter, using established parametric equations. The wings of the MTR comprise a significant part of the overall airframe weight. The wings were designed to be as light as possible because they are primarily self-actuated by dynamic pressure as the MTR transitions to and from forward flight. The parametric equation used for the wing weight [25] is

$$\begin{aligned} W_{\mathrm{w}} &= 0.0051\,(W_{\mathrm{DG}}\,N_{\mathrm{ult}})^{0.557}\,S_{\mathrm{w}}^{0.649}AR^{0.5}\,(t/c)_{\mathrm{w}})^{-0.4} \\ &\quad (1+AR_{\mathrm{w}})^{0.1}\cos^{-1}\Lambda_{\mathrm{w}}\,(0.09S_{\mathrm{w}})^{0.1} \end{aligned} \tag{2.79}$$

where

$$W_{\mathrm{DG}} = W_{\mathrm{TO}} - 0.5\,W_{\mathrm{fuel}} \tag{2.80}$$

An allowance was made for the wing folding mechanism using

$$W_{\mathrm{WFM}} = k_{\mathrm{WFM}}W_{\mathrm{w}} \tag{2.81}$$

Additional weight was added to the system in terms of a fuel pod on each wing, but this is taken into account in fuel system weight calculations. In the case of the horizontal tail the weight equation used, W_{HT}, [26] is

$$W_{\mathrm{HT}} = 5.25\,S_{\mathrm{HT}} + 0.8\times10^{-6}\frac{N_{\mathrm{ult}}b_{\mathrm{HT}}^3W_{\mathrm{TO}}\,\bar{c}_{\mathrm{w}}\sqrt{S_{\mathrm{HT}}}}{(t/c)_{\mathrm{HT}}\,\cos^2\Lambda_{\mathrm{HT}}\,l_{\mathrm{sep}}S_{\mathrm{w}}^{3/2}} \tag{2.82}$$

where N_{ult} is the ultimate load factor for the design. The weight of the vertical tail, W_{VT}, is given by

$$W_{\mathrm{VT}} = 2.65\,S_{\mathrm{VT}} + 0.8\times10^{-6}\frac{N_{\mathrm{ult}}b_{\mathrm{VT}}^3(8.04+0.44(W_{\mathrm{TO}}/S_{\mathrm{w}})}{(t/c)_{\mathrm{VT}}\,\cos^2\Lambda_{\mathrm{VT}}} \tag{2.83}$$

Finally, the weight of the tail boom structure, W_{TAIL}, is estimated using

$$W_{\text{TAIL}} = 0.998\, W_{\text{DG}}^{0.35}\, N_{\text{ult}}\, l_{\text{TAIL}}^{0.5}\, D_{\text{TAIL}}^{1.534} \tag{2.84}$$

2.4.6 Power Plant & Fuel System Weights

The weight of the engine is essentially proportional to its power output. For a turboshaft engine the net uninstalled engine weight is given by the equation

$$W_{\text{ENG}} = N_{\text{ENG}}\,(k_{\text{ENG}_1}\, P_{\text{ENG}} + k_{\text{ENG}_2}) \tag{2.85}$$

To take account of the engine installation (intake, exhaust, mounts etc.) the power plant installation system weight was assumed to be proportional to the engine weight, i.e.,

$$W_{\text{PIS}} = k_{\text{PIS}} W_{\text{ENG}} \tag{2.86}$$

The weight of the engine fuel system is governed by the amount of fuel carried (i.e., by the size of the tanks) and by the lengths of the fuel lines and number of fuel pumps. The fuel system weight W_{FS} is given by the equation

$$W_{\text{FS}} = k_{\text{FS}} W_{\text{FUEL}} \tag{2.87}$$

In addition to the main engines, the weight of an auxiliary power unit (APU) for main engine starting and to power various electrical and hydraulic systems prior to engine start must be taken into account. The weight of the APU is essentially proportional to the power of one of the main engines and can be written as

$$W_{\text{APU}} = k_{\text{APU}_1}\, P_{\text{ENG}} + k_{\text{APU}_2} \tag{2.88}$$

2.4.7 Tilt Boom & Actuator Weights

The tilt boom is the third structural member of the pivoting tail unit, which supports compression loads during takeoff and landing. The weight of the tilt boom on the MTR is related to the vehicle size and its takeoff weight. The weight was assumed to be proportional to takeoff weight and in the conceptual design studies it was modeled using the equation

$$W_{\mathrm{TB}} = k_{\mathrm{TB}} W_{\mathrm{TO}} \tag{2.89}$$

Similarly, the weight of the actuator used to tilt the coaxial rotor system was modeled using

$$W_{\mathrm{TM}} = k_{\mathrm{TM}} W_{\mathrm{TO}} \tag{2.90}$$

where the coefficient k_{TM} has been determined based on weight estimates that were conducted for the tilt actuators used on conventional tiltrotor aircraft, such as the V-22 Osprey [19].

2.4.8 Electrical System Weight

The weight of the electrical system is driven, on average, by the size of the machine and, in particular, the need for any anti-icing system. The parametric equation used for the electrical system weight was

$$W_{\mathrm{ES}} = k_{\mathrm{ES}} \left(1 + 0.08\, N_{B_{\mathrm{MR}}} c_{\mathrm{MR}} R_{\mathrm{MR}}\right) \tag{2.91}$$

where the second term accounts for the extra electrical power required for anti-icing, if included.

2.4.9 Landing Gear Weight

For the MTR with a self-supporting payload, landing gear weight was assumed to be proportional to the maximum takeoff weight less payload, which is supported by the cargo handling system, giving the equation

$$W_{\mathrm{LG}} = k_{\mathrm{LG}} \left(W_{\mathrm{TO}} - W_{\mathrm{PL}} \right) \tag{2.92}$$

This complete set of performance, fuel burn, sizing and weight equations are integrated into a series of numerical codes compiled in MATLAB (see Appendix C for examples), which maintain the overall structure depicted in Figure 2.1. This comprehensive sizing analysis was validated and applied to perform numerous trade, optimization and performance studies, as detailed in the following chapter.

Chapter 3

Results

The results contained in this chapter cover a broad spectrum of studies performed to both assess value of the MTR concept relative to legacy heavy-lift rotorcraft, and to refine the elements of this conceptual design study. These results include an initial validation of the design methodology presented in the previous chapter, mission trade studies, and the optimization of two key point designs – a heavy-lift, long range MTR and an MTR Scaled Demonstrator (MTR-SD). Also included is a comprehensive performance summary of the two optimized point designs.

3.1 Validation of Methodology

It is important to carefully validate any rotorcraft sizing analysis against weight and performance data of legacy designs. A complicating factor in the overall design approach is that the MTR is a coaxial counter-rotating rotor configuration for which limited historical weight and performance data exists, especially for larger helicopters. The largest coaxial helicopters previously developed (by Kamov in Russia) have payload capabilities of less than 5 tons. This lack of historical data requires careful validation of the analysis for larger single rotor helicopters, and also for coaxial helicopters where data is available. Only then can the analysis be used

with confidence in the conceptual design and sizing of the MTR architecture.

3.1.1 Single Rotor Helicopter

Sizing estimates for the conventional single rotor helicopter are shown in Figures 3.1 through 3.4 in terms of rotor size (rotor diameter), empty and maximum takeoff weights, and installed power requirements versus the net useful payload to be carried. Results are shown for unrefueled ranges of 110 to 330 nm (200 to 600 km), which would be typical for a conventional helicopter operating at or near its maximum payload. Data points for several helicopters are shown for reference, and to help provide an appropriate validation of the design methodology.

Figure 3.1 shows predictions of the main rotor diameter versus payload (in tons). Notice that there is a break in the correlations near the 5 ton payload mark. The reasons for this were apparent from many of the subsystem weight correlation studies, where the correlation coefficients used to develop the parametric equations were found to be different for larger versus smaller helicopters. Another break in the correlation curves is shown near the 10 ton payload mark. This is because the design analysis predicts an increase in the number of rotor blades in an attempt to maintain a high blade aspect ratio (for aerodynamic efficiency) for a given rotor solidity, σ_{MR}, and blade loading coefficient, C_{T}/σ.

Notice also from Figure 3.1 that the size of the rotor increases logarithmically with the payload required to be carried. This behavior is consistent with the square-cube law [22], which predicts that the helicopter weight will grow much faster than

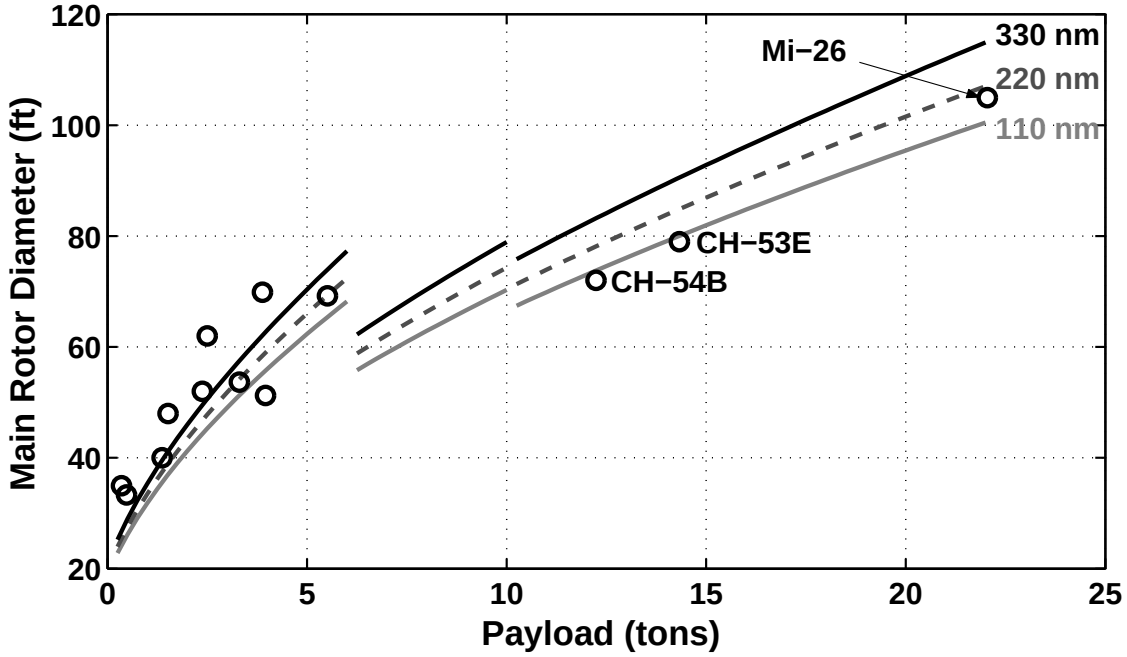

Figure 3.1: Predicted main rotor diameter versus payload for a single rotor helicopter follows the trends expected based on the square-cube law.

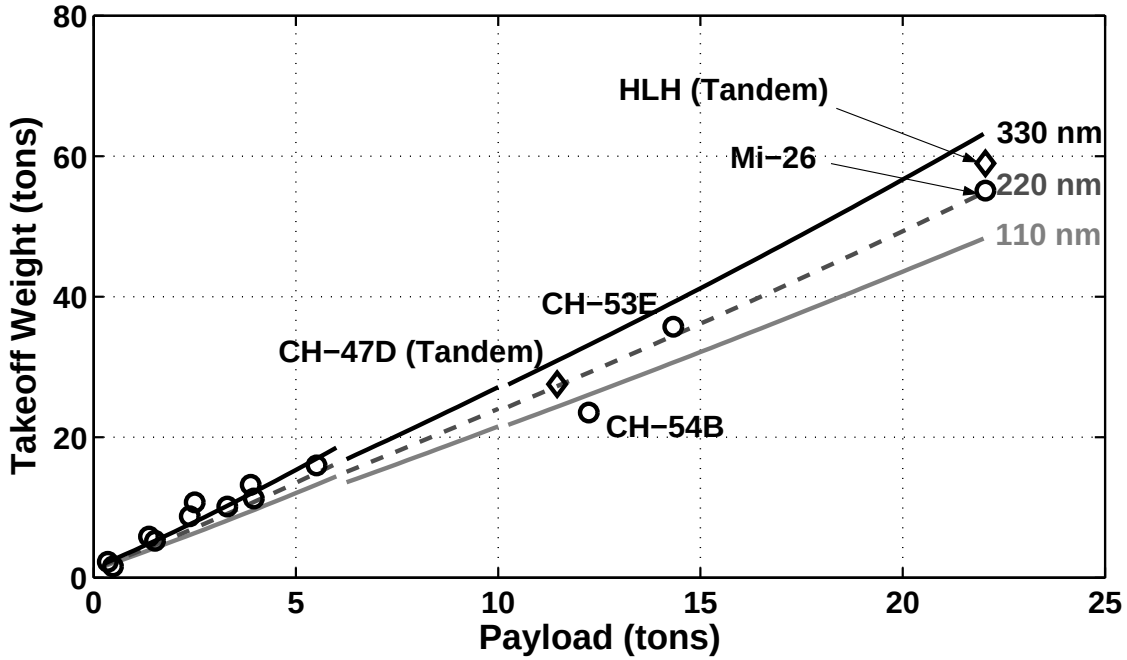

Figure 3.2: Predicted gross takeoff weight versus payload for a single rotor helicopter.

the rotor size, the rotor size being determined based on the equations given previously. This point is made further in Figure 3.2, which shows that takeoff weight is proportional to payload, so that the rotor radius is proportional to either $W_{\mathrm{PL}}^{1/3}$ or $W_{\mathrm{TO}}^{1/3}$. This means that for very large payloads (exceeding 25 tons) the size of the rotor will become extremely large, and will become harder to build successfully. This immediately points to the possibilities of a coaxial rotor configuration with its overall smaller rotor diameter in better meeting heavy-lift requirements.

The predicted empty weight versus payload for the single rotor helicopter is shown in Figure 3.3, and suggests a nearly linear relationship. Of particular interest are the results obtained for payloads of 10 tons and greater. Shown on the plots are data points for several "heavy-lift" helicopters, including the Sikorsky CH-53, CH-54 and Mil Mi-26, as well as the Boeing CH-47 and HLH, even though the latter are tandem rotor machines.

Notice that the empty weight of the helicopter designs becomes very high for the larger payloads, with empty weights of between 20 and 25 tons for a 20 ton payload, which depends also on the range requirement. A further discussion of range issues on empty weight fraction for various rotorcraft concepts is given later.

The predicted installed power requirements for the single rotor helicopter are shown in Figure 3.4 based on the performance equations laid down in the previous chapter. The agreement is considered acceptable. The predictions confirm that installed power requirements will become very large (approaching 20,000 shp) for the bigger machines carrying large payloads. Again, data points for the Boeing CH-47 and HLH are shown here for reference.

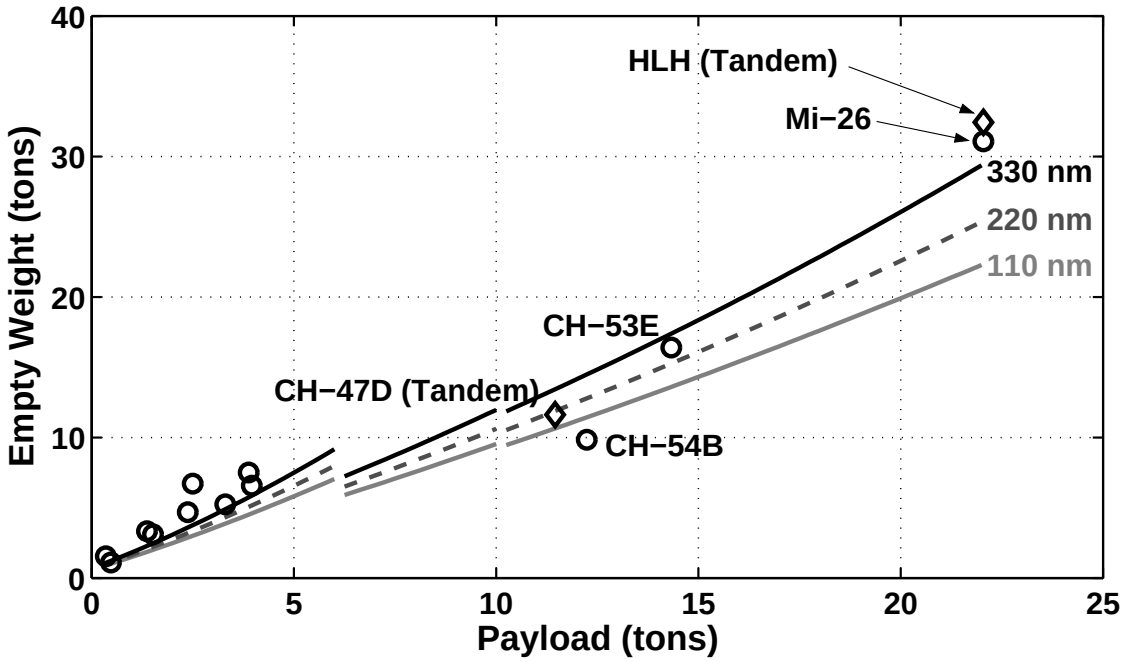

Figure 3.3: Predicted empty weight for the single rotor helicopter is very nearly proportional to payload.

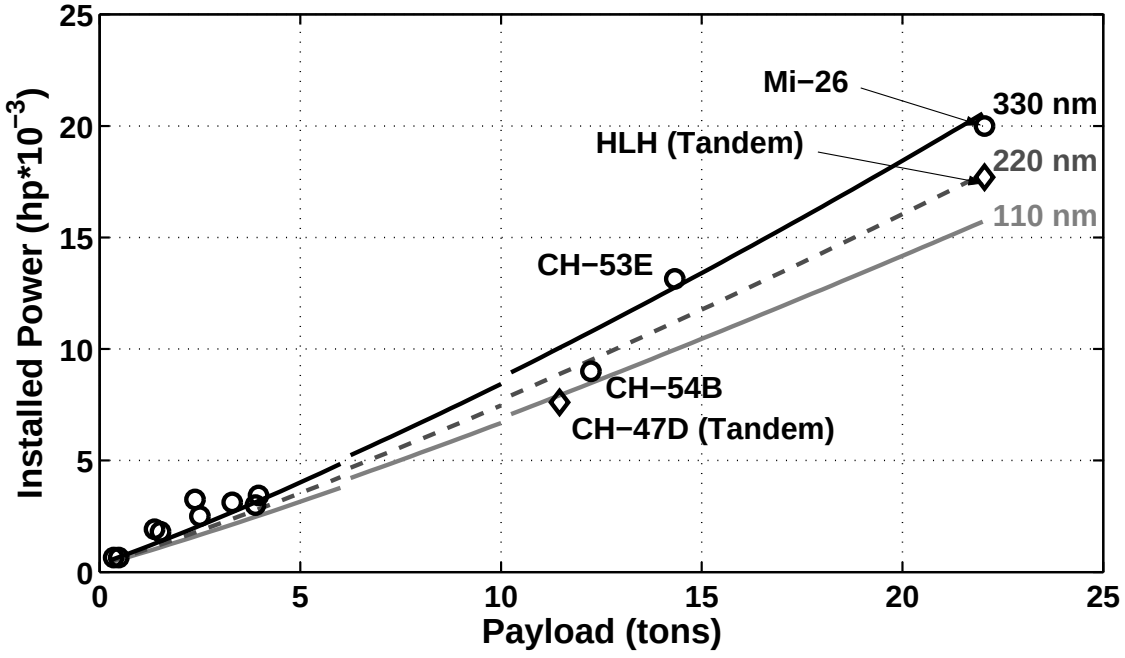

Figure 3.4: Predicted power requirements versus payload for single rotor helicopters.

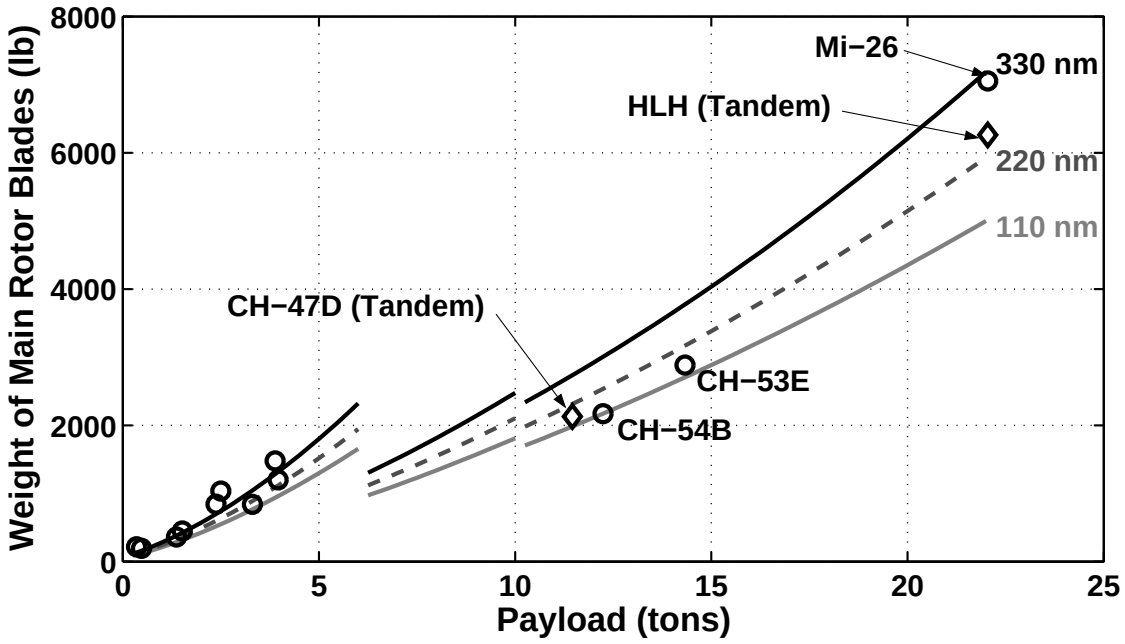

Figure 3.5: Predicted blade weights versus payload for the single rotor helicopters.

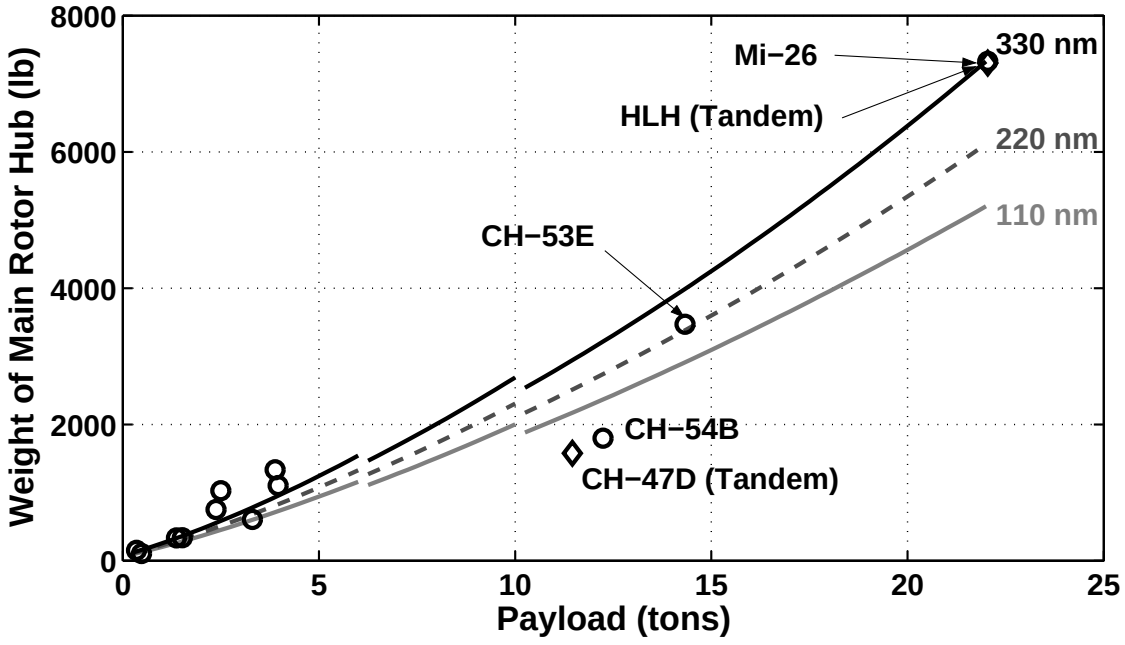

Figure 3.6: Predicted hub weights versus payload for the single rotor helicopters.

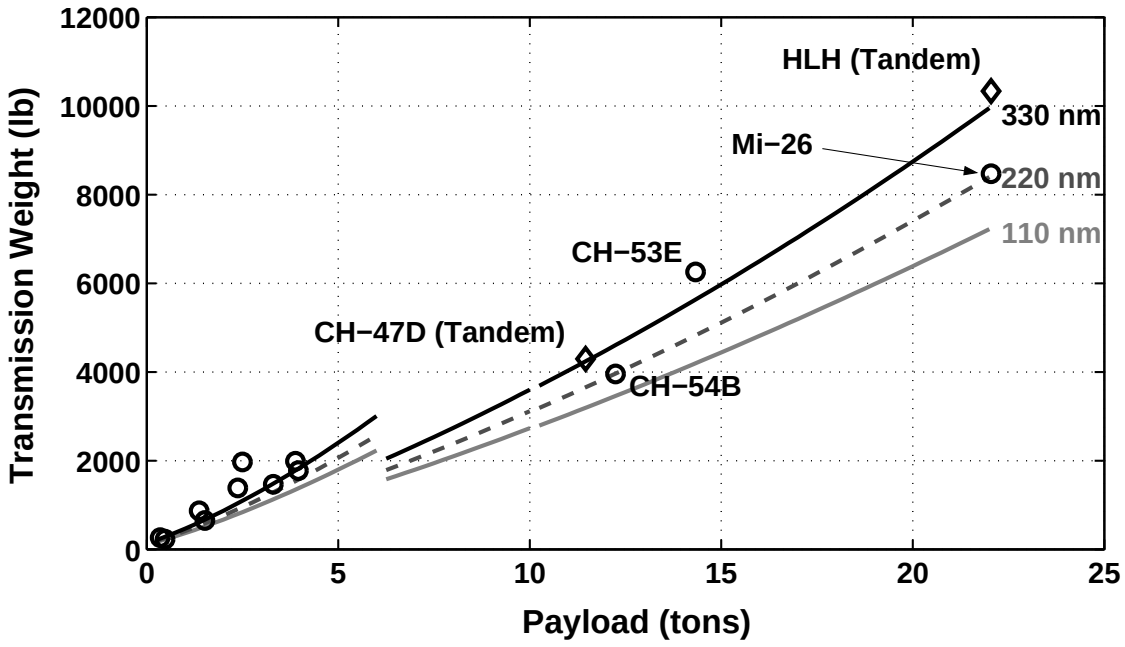

Figure 3.7: Predicted transmission weights versus payload for the single rotor helicopters.

Figures 3.5 through 3.8 show some predicted component weights for the conventional single rotor helicopter. Figure 3.5 shows the predicted total blade weight versus payload. Blade weight is driven by blade area, which increases with rotor radius (Figure 3.1). Blade weight is also determined by the need to increase chord and/or the number of blades to maintain reasonably low values of C_T/σ to retain sufficient stall margins to meet forward flight and maneuver requirements. Overall, the predictions were found to be in good agreement with historical data. Notice that the 8-bladed Mi-26 comes in slightly heavier than the 8-blades of the HLH (a tandem with two four bladed rotors [27]). This is partly because of the different types of blade construction.

Figure 3.6 shows results for rotor hub weight. Again, the agreement of the predictions with historical data is considered good. Hub weight is driven by centrifugal

forces on the blades, so inevitably hub weight grows quite rapidly with blade weight and with the overall size of the helicopter. In this case it is interesting to note that the results for the Mi-26 and HLH (sum of both rotor hub weights) are in good agreement, even though the machines are of considerably different configurations.

Figure 3.7 shows predictions of the overall transmission weight, including the main rotor and tail rotor transmissions. Transmission weight is driven by overall torque requirements. The Mi-26 and HLH [28] have the biggest transmissions ever designed for helicopters [29]. Of some interest is that the transmission weight for the HLH comes in about 20% higher than for the Mi-26. This is because the Mi-26 is a split torque design compared to the spiral bevel design on the HLH, and also reflects the need for the interconnect drive shafts with a tandem design. This is despite the fact that the Mi-26 has a very large tail rotor and a long interconnect drive with a secondary gearbox.

Figure 3.8 shows the engine weight versus payload. Overall, good correlations are shown, but the analysis tends to slightly over-predict engine weights for the CH-54 and CH-53, and to under-predict the engine weight for the large Mi-26 helicopter. The latter can be explained by the fact that, historically at least, engines designed in the West have shown better power-to-weight ratios [31]. It would be expected that these results for engine weights are on the pessimistic side overall, as they were calculated using a relatively modest power-to-weight ratio, which is controlled through the engine weight factor, k_{ENG_1} (see Section 2.4).

Figure 3.9 shows the predicted fuselage weight versus payload of the single rotor helicopter. The results were found to be in good agreement with historical

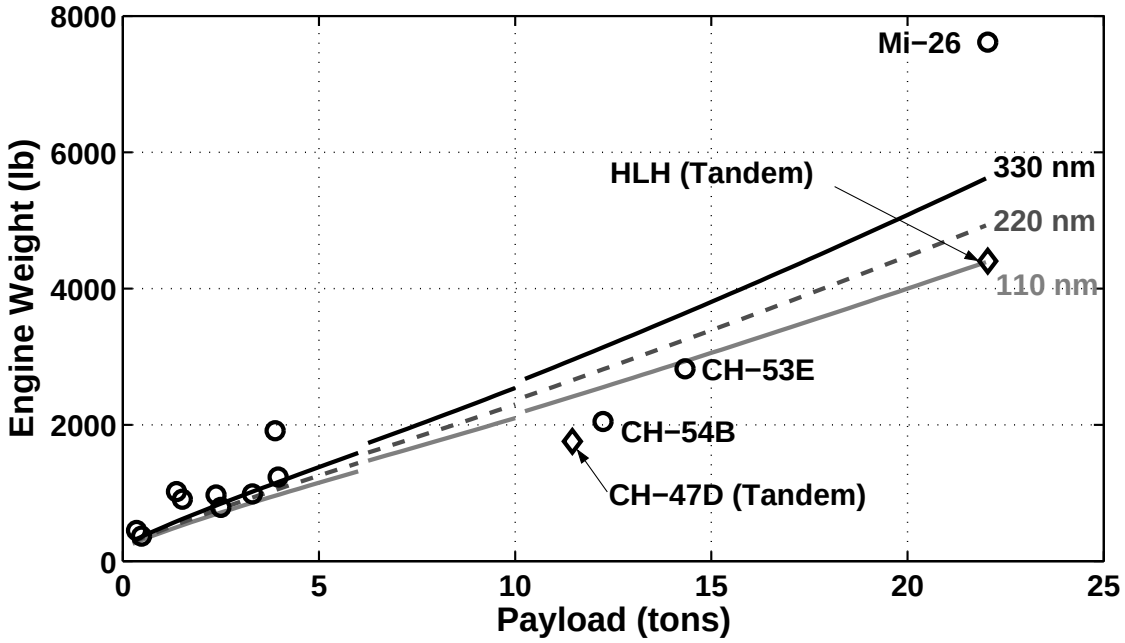

Figure 3.8: Predicted engine weights versus payload for the single rotor helicopters.

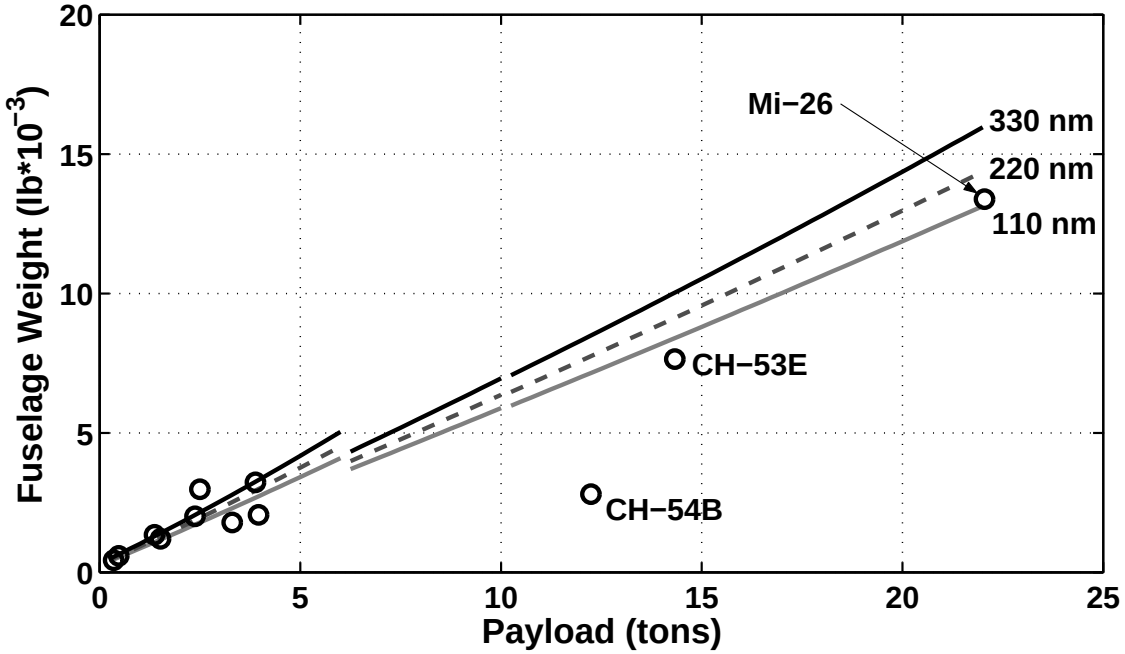

Figure 3.9: Predicted fuselage weight versus payload for single rotor helicopters.

data, where available. Notice that the CH-54 is a crane design and does not have a conventional fuselage, so this data point sits well below the correlation line.

The overall sizing and component weight correlations obtained for the single rotor helicopter designs is very encouraging, and lends to relatively good confidence levels in the design analysis developed here. While it is apparent that in some cases the correlations could be improved, the results obtained were considered sufficiently good to proceed to the analysis of a coaxial rotor helicopter.

3.1.2 Coaxial Dual Rotor Helicopter

The design analysis was extended to specifically encompass dual rotor coaxials. This involved several modifications and changes to the parametric equations, including aerodynamic changes to take into account losses that are a consequence of rotor-on-rotor interference, as well as appropriate weight estimates for the coaxial rotor hub and the different type of airframe (no tail boom but larger empennage).

A dual rotor coaxial hub is complicated by the approximate doubling of the number of total blades (but this depends on several factors), the need for a longer (and heavier) main rotor shaft, and for a secondary swashplate with control linkages and bigger and more powerful actuators. There are also modifications to the parametric equations required to represent the transmission weights. Of course the tail rotor, its transmission and associated gearboxes can be dispensed with on a dual rotor coaxial design. This is a significant weight savings.

There are no existing parametric equations based on historical data that have

been derived and published for the design of a dual rotor coaxial system, and this is probably the first time such an analysis has been undertaken outside of the helicopter industry. Historical data were obtained for Kamov dual rotor coaxial helicopters (although published data are still relatively limited in scope), and were used to help verify the modified design analysis.

The results for the general sizing of the coaxial machines are shown in Figures 3.10 through 3.13. Good correlations were obtained against the results for the Kamov machines, where historical data were available. There have been no large dual rotor coaxial helicopters designed with payloads more than 5 tons, and so there are no historical data available in this range to compare with. In this case, the design analysis proceeded on the basis of adjusted trends for large single rotor systems with further adjustments of the estimated weights and aerodynamic losses extrapolated based on results for the smaller, dual rotor coaxial machines.

Figure 3.10 shows the rotor diameter versus payload for the coaxial designs. These results basically follow the square-cube law in a manner similar to that found for the single rotor machines (Figure 3.1). However, in this case the rotor is about 25% smaller than an equivalent single rotor machine when carrying the same payload over the same range. Nevertheless, for large payloads of 20 tons or more the rotor diameter exceeds 80 ft, which is not a small rotor by any standard.

For the lighter payloads, the predictions of rotor size were found to be in good agreement with historical data for the Kamov machines. For the heavier payloads no historical data exist for coaxials, but data points for the tandem rotor CH-47 and HLH machines are shown as a reference. There is good agreement. Notice

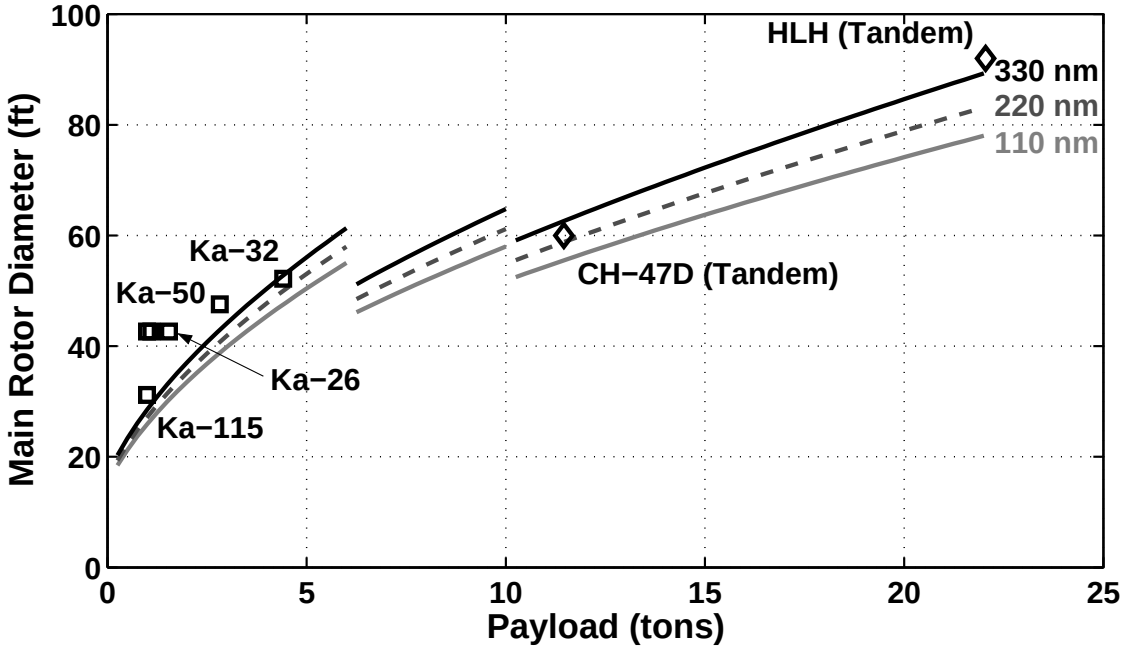

Figure 3.10: Predicted rotor diameter versus payload for a coaxial dual rotor helicopter.

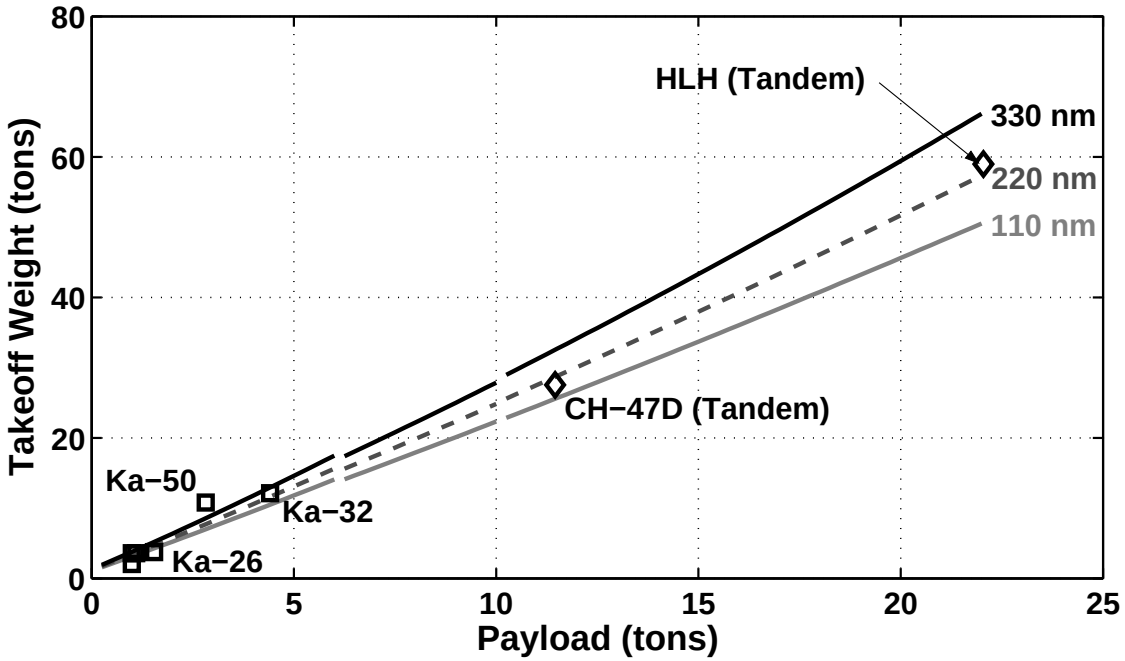

Figure 3.11: Predicted gross takeoff weight versus payload for a coaxial dual rotor helicopter.

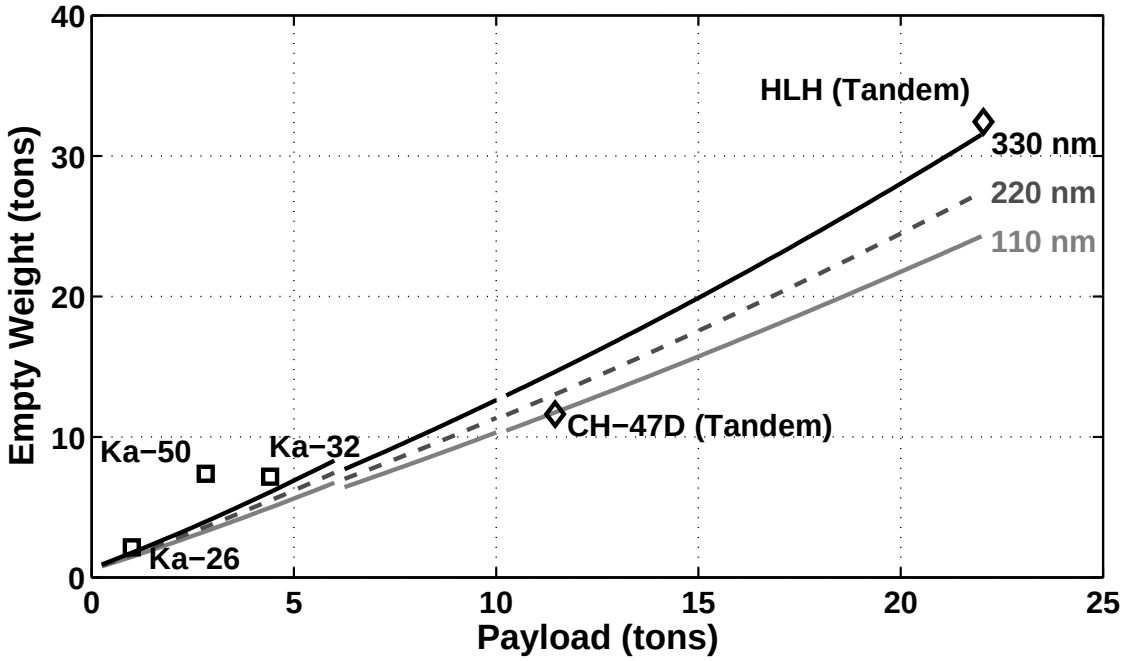

Figure 3.12: Predicted empty weight for the coaxial dual rotor helicopter is very nearly proportional to payload.

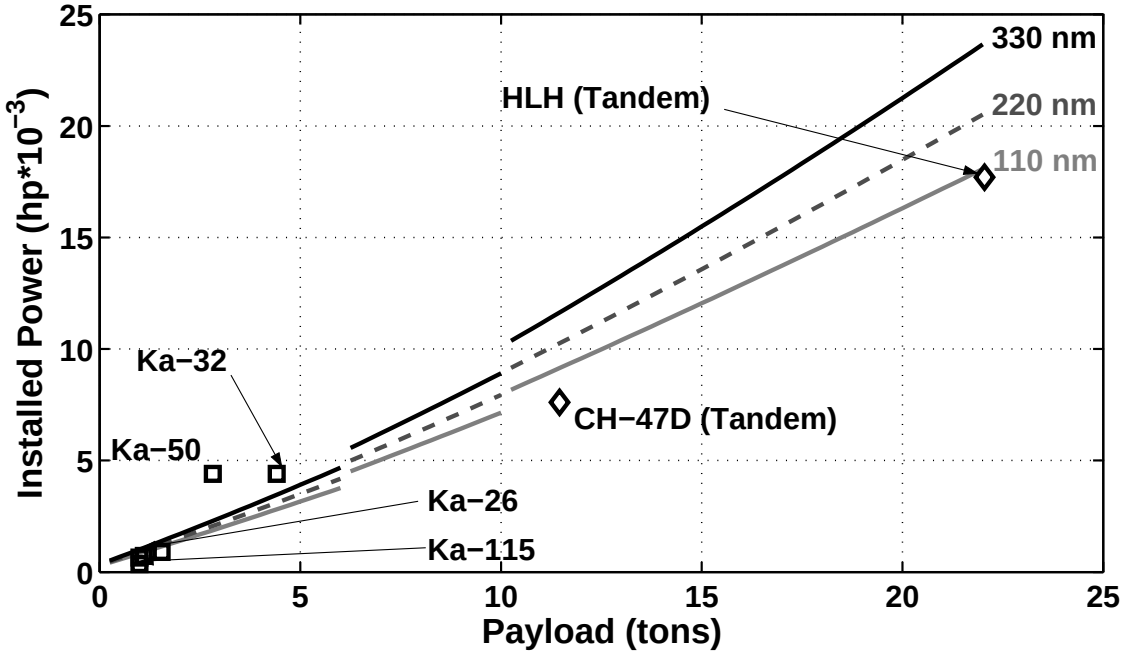

Figure 3.13: Predicted power requirements versus payload for coaxial dual rotor helicopters.

again the breaks in the correlation curves correspond to predicted discrete changes in the number of blades per rotor, which come about by minimizing weight and maximizing aerodynamic efficiency as the machine grows in size.

Figure 3.11 shows the predicted relationship between gross takeoff weight and payload for the coaxial machines. There are very little differences here between those found for the single rotor machines (Figure 3.2). The corresponding empty weight results are shown in Figure 3.12, where it is apparent that these too are comparable to single rotor machines. Therefore, the results suggest that even with the advantages of a smaller rotor a conventional coaxial helicopter concept offers very little weight saving advantage over a single rotor machine when carrying the same payload.

The net installed power requirements of the coaxial machines are shown in Figure 3.13. These were noted to be marginally higher than for an equivalent single rotor machine. This is mainly because of the loss of aerodynamic efficiency resulting from rotor-on-rotor interference, despite the absence of a tail rotor. Again, the overall results suggest few advantages in the coaxial design over the single rotor machine, other than the smaller rotor.

There are few component weight data that have been published for the Kamov machines, and without historical data points covering a range of conditions and for several different machines it was felt inappropriate to show ad hoc points less inappropriate correlation coefficients be obtained and misleading conclusions be drawn. Instead, where empirical data are unknown, the coefficients in the parametric equations used for the single rotor machines have been used. However, for reference the

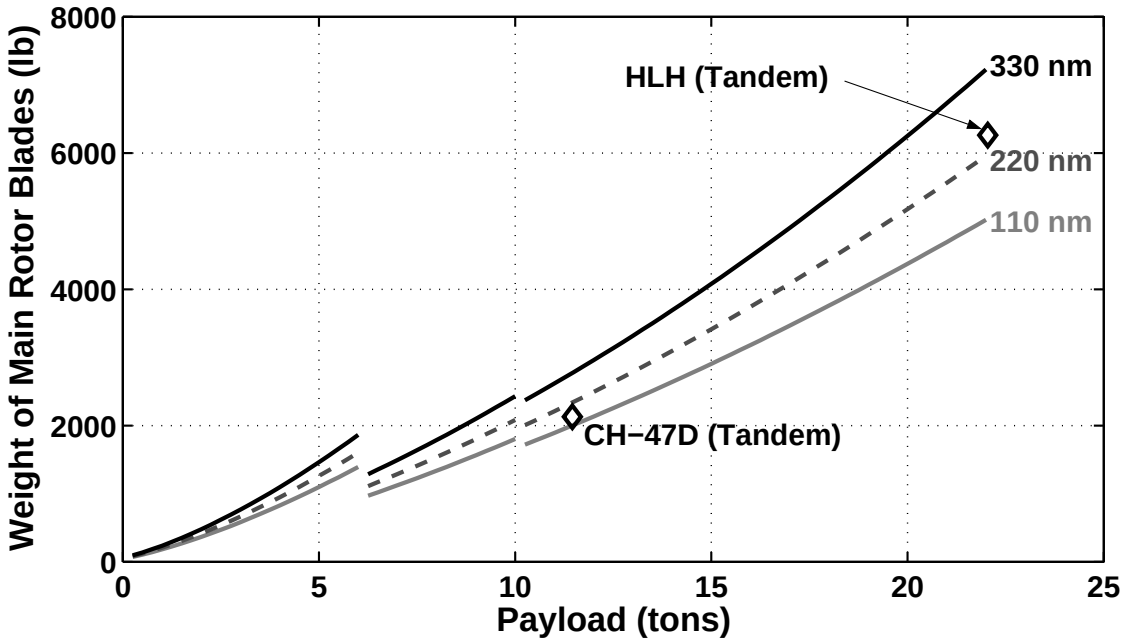

Figure 3.14: Predicted blade weights versus payload for the coaxial dual rotor helicopters.

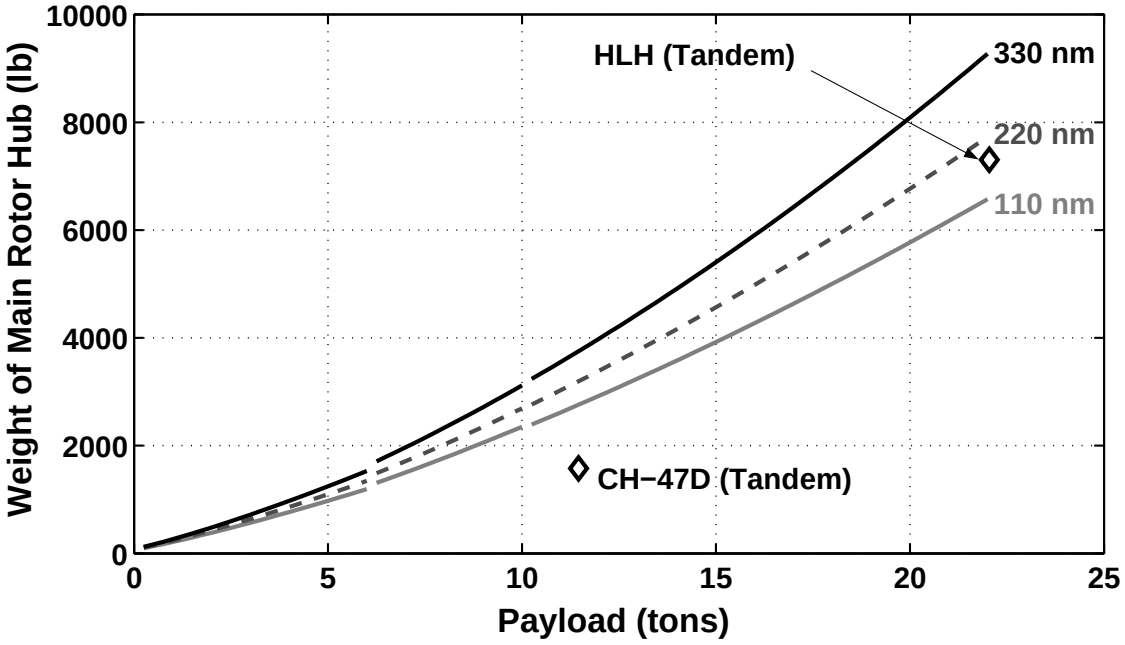

Figure 3.15: Predicted hub weights versus payload for the coaxial dual rotor helicopters.

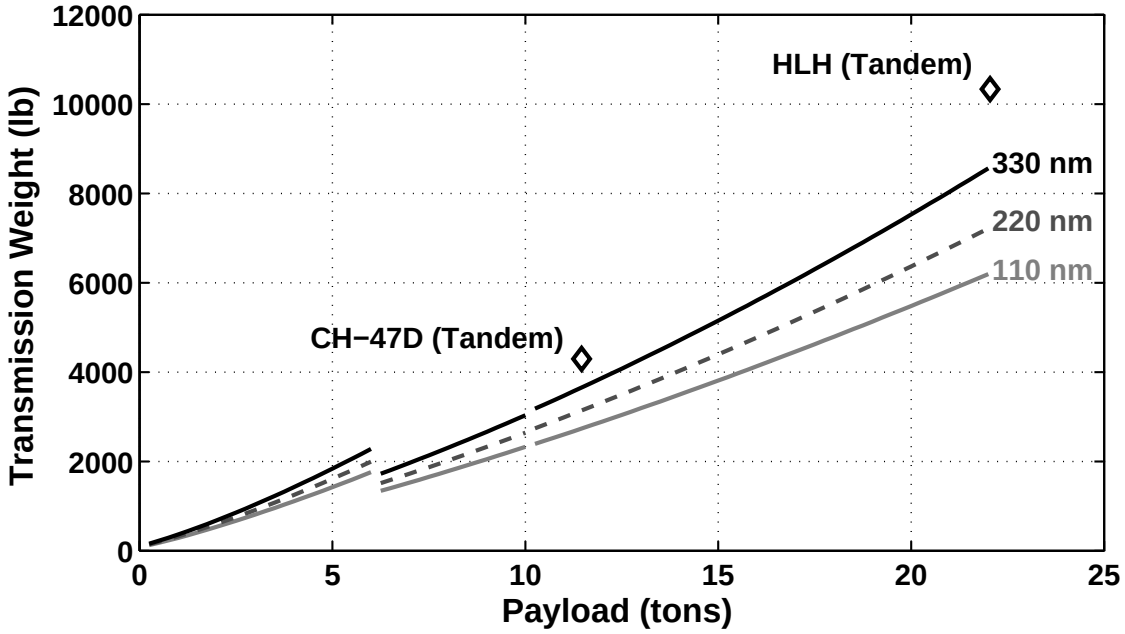

Figure 3.16: Predicted transmission weights versus payload for the coaxial dual rotor helicopters.

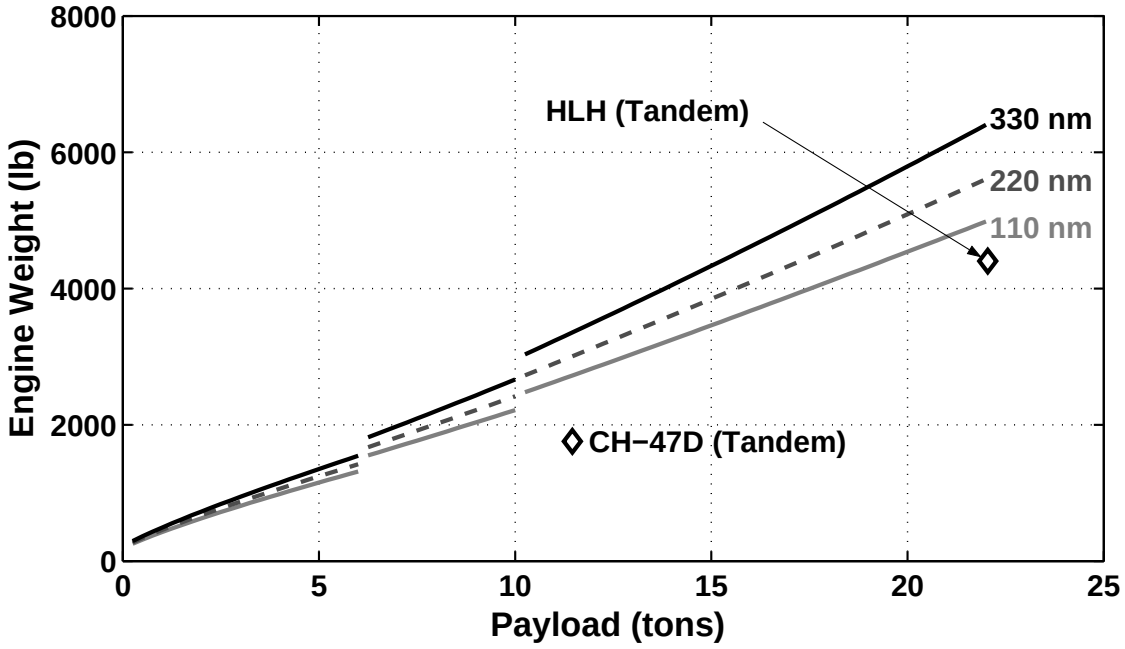

Figure 3.17: Predicted engine weights versus payload for the coaxial dual rotor helicopters.

results for the CH-47 and HLH machines have been included in the various plots, but recognizing again, of course, that these are tandem rotor machines and not coaxials.

The predicted weight of the rotor blades are shown in Figure 3.14. Despite the larger number of blades typical of a coaxial rotor system, the net blade weight was found to be comparable to the single rotor system (Figure 3.5). This is a consequence of the lower blade radius, which offsets the increase in weight associated with the larger number of blades. However, the hub weights shown in Figure 3.15 are notably larger than for a single rotor machine. This is because of two factors. First, the hub weight is driven by the structural strength requirements to counteract the net centrifugal effects on the blades, this being higher for a coaxial rotor system than an equivalent single rotor system. Second, there is a weight penalty associated with the extra shaft length on a coaxial rotor system. This higher hub weight, however, is offset by the lower transmission weight (Figure 3.16). Engine weight is predicted to be higher for the coaxial rotor helicopter (Figure 3.17) because of the increase in power requirements associated with the interference effects between the upper and lower rotors. These results can be compared with the results of Figures 3.7 and 3.8 for the single rotor helicopters. Based on the previously shown results obtained for the single rotor helicopter, the performance predictions for the coaxial machines have been assigned relatively good confidence levels.

3.2 Comparison Studies

Once the MTR design analysis was validated against legacy rotorcraft data, the first study performed was to compare the potential of the MTR concept with that of the conventional helicopter, particularly for long-range, heavy-lift missions. In one study, the conventional, single-rotor helicopter was extrapolated to extremely long ranges to examine the effect on the aircraft size to meet mission requirements similar to those that the MTR is targeted to fill. Another study makes direct comparisons of the MTR aircraft size, requirements and capability versus those predicted for conventional and coaxial helicopter designs.

3.2.1 Long-Range Heavy-Lift Helicopter

A requirement that motivated, in part, the design of the MTR was to meet a military goal that a vertical-lift aircraft be able to carry at least a 20 ton useful payload efficiently and economically over an unrefueled distance of 1,000 nautical miles. This is an unprecedented range for a conventional helicopter when carrying this payload. To examine the possible hypothetical designs that might result from attempting to meet such a requirement, a design analysis was undertaken to meet a 1,000 nm unrefueled range specification with a range of payloads from as little as one ton to over 20 tons.

The results in Figure 3.18 show the predicted size (rotor diameter) of the single rotor helicopter versus payload to meet both 220 nm and 1,000 nm range goals. Notice that the machines become extremely large in size for larger payloads,

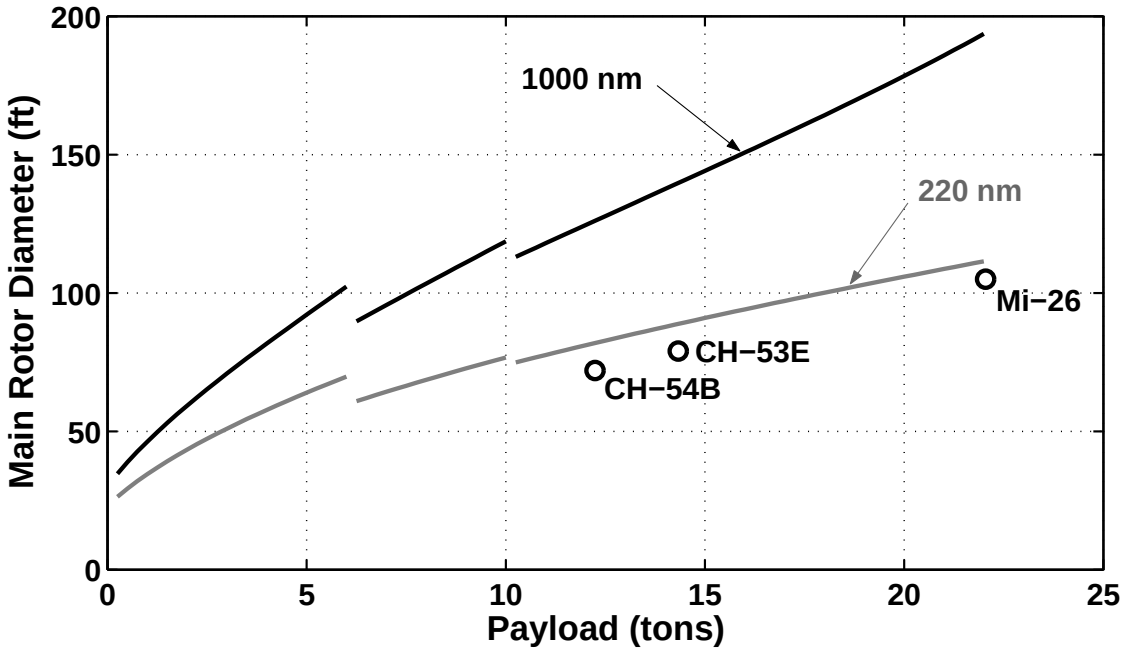

Figure 3.18: Predicted rotor size versus payload for a single rotor helicopter with ranges of 220 nm and 1,000 nm.

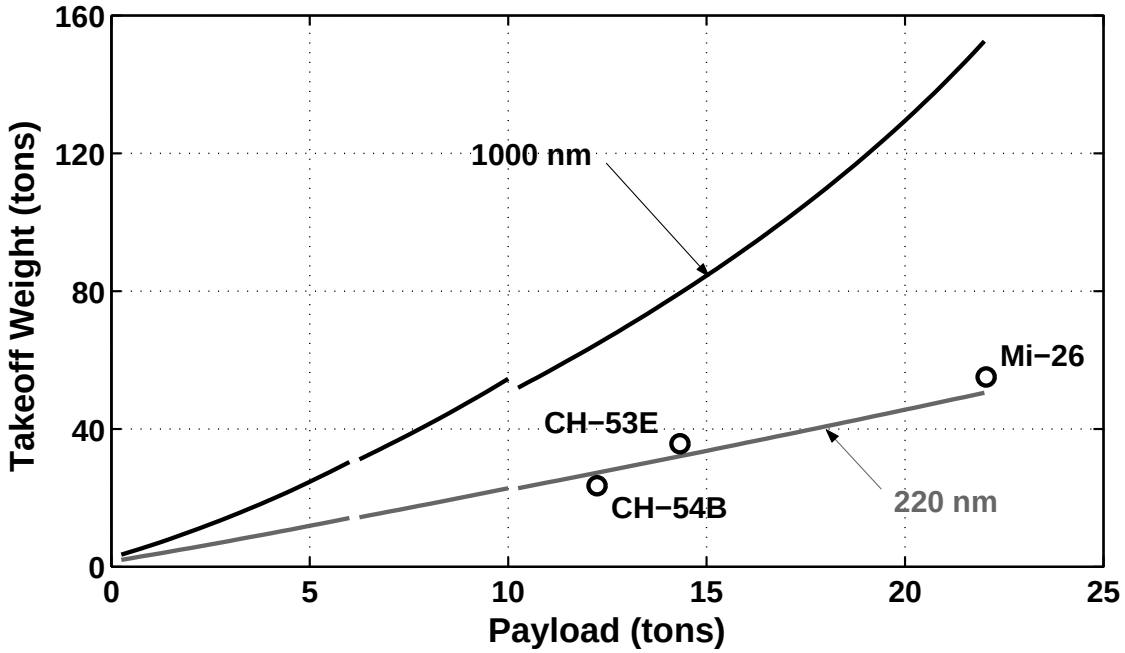

Figure 3.19: Predicted takeoff weight versus payload for a single rotor helicopter with ranges of 220 nm and 1,000 nm.

and especially so when longer ranges are required. To meet the 20 ton useful payload over 1,000 nm goal, a rotor diameter of over 170 ft would be required. This is too large to be practical, especially when considering that the world's largest helicopter currently in service, the Mi-26, has a rotor diameter of 105 ft. The results for a coaxial machine (shown in the next section) suggest that a 125 ft diameter rotor would be necessary, but this too is extremely large and probably infeasible because of the mechanical complexity of coaxial rotor systems.

The corresponding takeoff weights for the designs are shown in Figure 3.19. For range requirements typical to modern helicopters (220 nm) the predicted takeoff weights agree closely with legacy designs. However, when the range requirements are extended to 1,000 nm, the aircraft weight increases very rapidly. For instance, the predicted takeoff weight for a conventional helicopter required to carry 20 tons 1,000 nm exceeds 125 tons, which is more than twice that of the world's largest operational helicopter – the Mi-26.

The primary driver for these dramatic size increases is the increase in required fuel weight to perform this long range mission as shown in Figure 3.20. The required fuel weight for a helicopter to carry a 20 ton payload 1,000 nm unrefueled range is approximately 50 tons, which is an order of magnitude greater than that predicted for a more typical heavy-lift mission. This result reflects the relative fuel inefficiency of the conventional helicopter when compared to tiltrotor or fixed-wing aircraft. Some of the rapid increase in fuel weight is also related to the recursive nature of the sizing analysis. As the fuel requirements increase, the additional fuel increases the overall gross weight, which in turn increases the required size of the rotor, engine

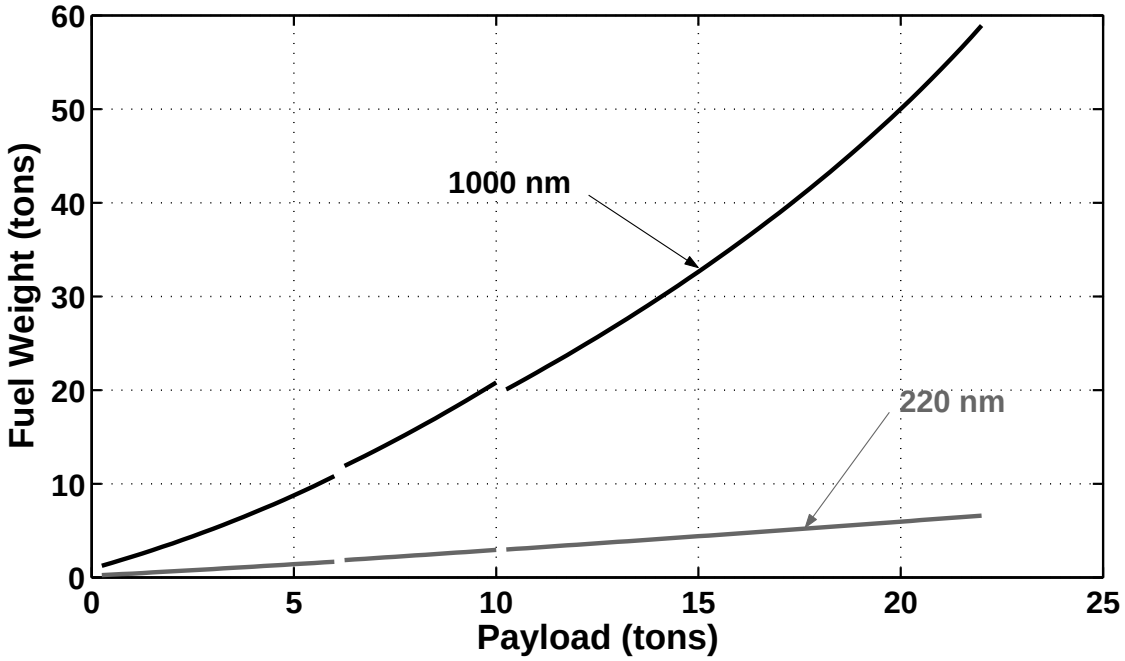

Figure 3.20: Predicted fuel weight versus payload for a single rotor helicopter with ranges of 220 nm and 1,000 nm

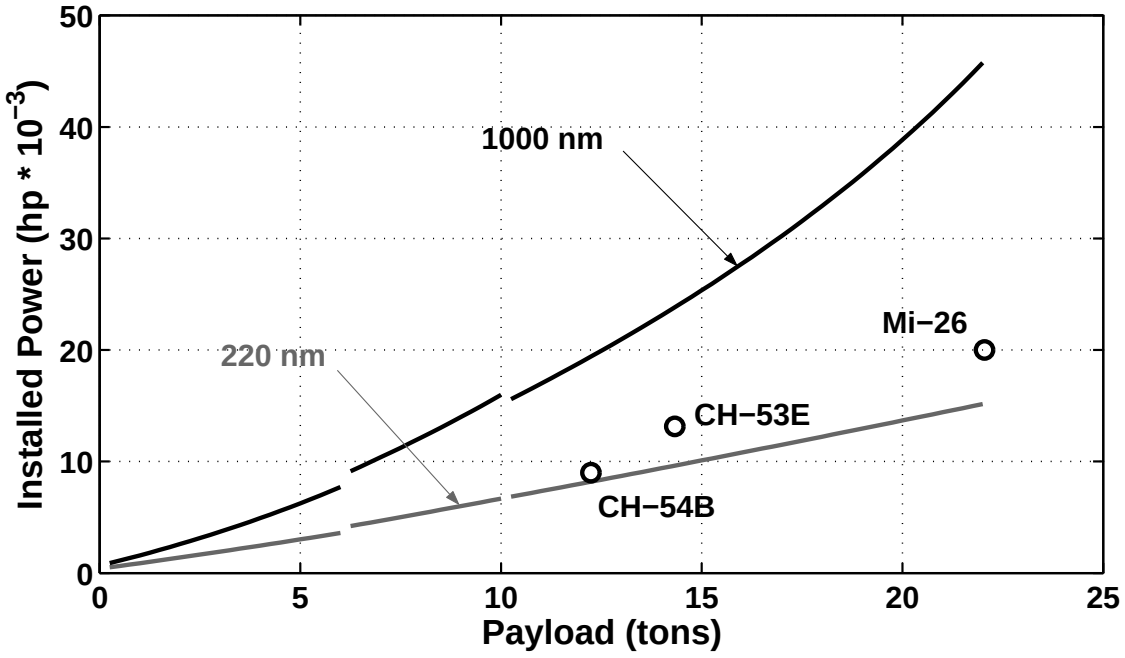

Figure 3.21: Predicted power requirements versus payload for a single rotor helicopter with ranges of 220 nm and 1,000 nm.

power requirements leading to further increases to the required fuel weight. This process continues until convergence is achieved.

The rapid increase in power requirements is shown in Figure 3.21. It is predicted that a conventional helicopter designed to achieve the heavy-lift, long-range mission (20 tons, 1,000 nm) would require nearly 40,000 shp out of the engine package. This is a tremendous amount of power and the resulting torque would likely lead to great difficulty in the design of the transmission. This in combination with the unprecedented size, weight and fuel requirements makes it seem unrealistic that a conventional helicopter could be built to meet these large payload and long-range requirements.

3.2.2 MTR Comparison to Legacy Rotorcraft

The MTR has primarily been targeted toward heavy-lift, long-range applications. If technically realizable, the ability to morph between an effective lifting platform to an efficient fixed-wing cruising vehicle make the MTR concept uniquely capable of missions that are not necessarily feasible with a conventional helicopter design. To further investigate this problem, a study was performed to compare the predicted sizing and performance characteristics of the MTR to those predicted for a conventional single-rotor and coaxial dual-rotor helicopters performing the same long-range, heavy-lift missions.

For this study, a fixed unrefueled range of 1,000 nm was used with a wide range of payload weights. A non-optimized, long range cruise mission profile (see

Figure 2.2) was used in all cases with takeoff, landing and cruise at mean sea level (MSL) conditions. It should be noted that this is a non-optimized mission profile in terms of cruise performance for the MTR design, because it is possible to cruise at high altitudes to greatly reduce drag and required fuel. Yet, this case was used to make a fair comparison between the MTR concept and legacy helicopter designs.

There was no hover time assumed beyond what was required for takeoff and landing. For simplicity, the lift-to-drag ratio of the MTR was assumed to be fixed and given a value of 10, which was previously shown to be a conservative value (see Figure 2.6). The lift-to-drag ratio of the conventional helicopter was assumed to be 4.6, which is a representative value for legacy helicopters. Similarly, the coaxial helicopter was assumed to have a lift-to-drag ratio of 4.2, with the lower value accounting for higher hub and shaft drag. The cruise speed assumed for the MTR was 240 knots, with cruise speeds for the helicopter cases being approximately half of that value, as is typical with large, transport helicopters. As a first approximation, propulsive efficiency of a fixed geometry proprotor in airplane mode was estimated to be 0.6, which is considered to be a conservative value.

The rotor disk loading was held constant across design concepts and constrained to values typical of legacy helicopters to maintain adequate hover efficiency and relatively low downwash velocities for cargo loading and unloading, and also for operations in austere environments. The values of disk loading used for all three configurations for the range of payloads in question are shown in Figure 3.22. While the relatively low disk loading may somewhat compromise the propulsive efficiency of the MTR in airplane mode, the need for good hovering efficiency and low down-

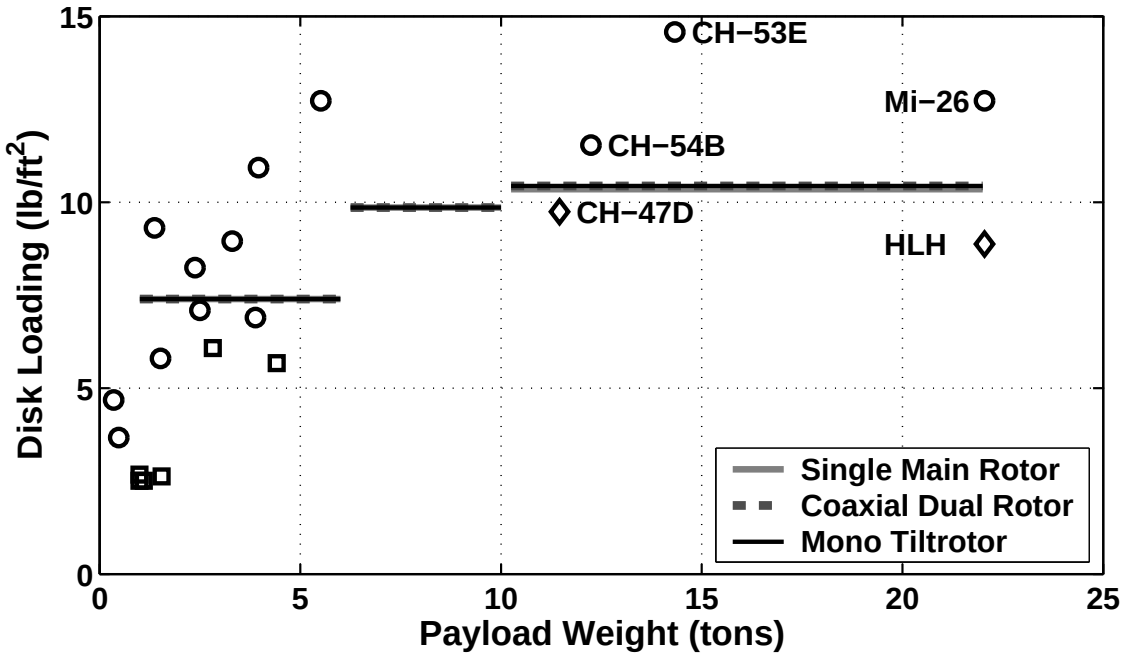

Figure 3.22: Predicted disk loading of the MTR architecture versus historical data for conventional (single) and coaxial rotor helicopters.

wash velocities in hover was considered more important because a coaxial operated at the same equivalent disk loading as a single rotor machine will have a higher wake slipstream velocity [32]. This is an important operational issue that can subtract from the value of a coaxial rotor configuration, but is offset somewhat on the MTR because of the higher position of the rotor relative to the ground.

Aircraft Sizing Comparison

Sizing results comparing predictions for the MTR concept to those of conventional and coaxial helicopters are shown in Figures 3.23 through 3.30 using the previously stated assumptions. Overall, the results suggest that if the MTR concept were to be technically realized then it could be up to 50% smaller in terms of rotor size (see Figure 3.23) with a 50% lighter gross takeoff weight (see Figure 3.25) com-

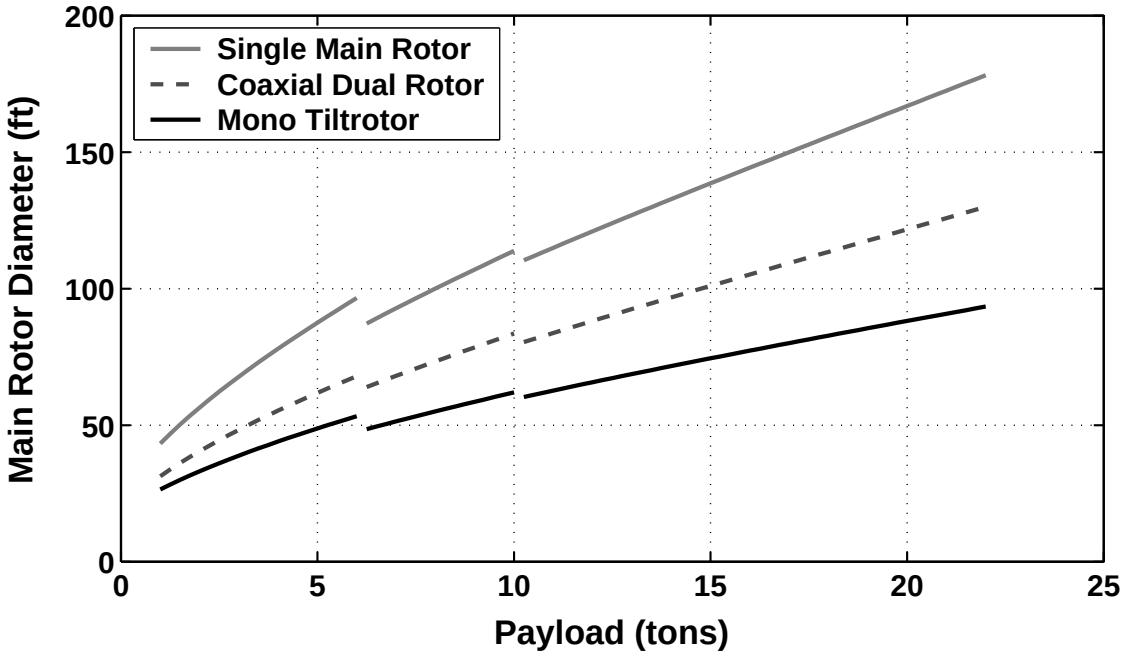

Figure 3.23: Predicted rotor size (diameter) for the MTR architecture to meet a 1,000 nm range requirement versus hypothetical conventional (single) and coaxial rotor helicopters.

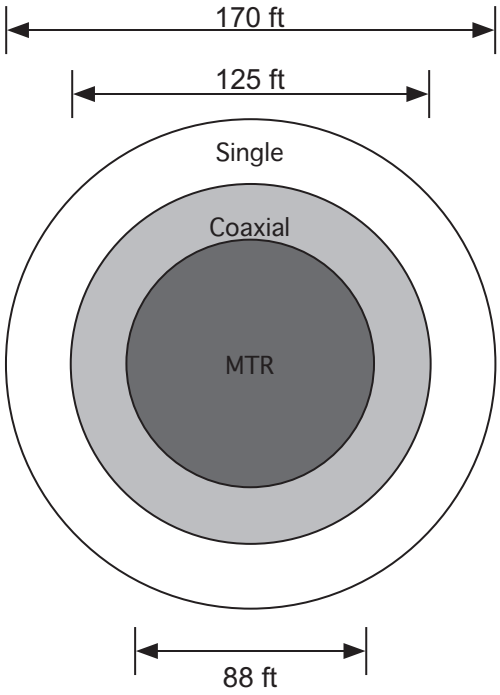

Figure 3.24: Comparison of rotor diameters for the hypothetical conventional (single) and coaxial rotor helicopters versus the MTR to meet the 1,000 nm range and 20 ton payload requirement.

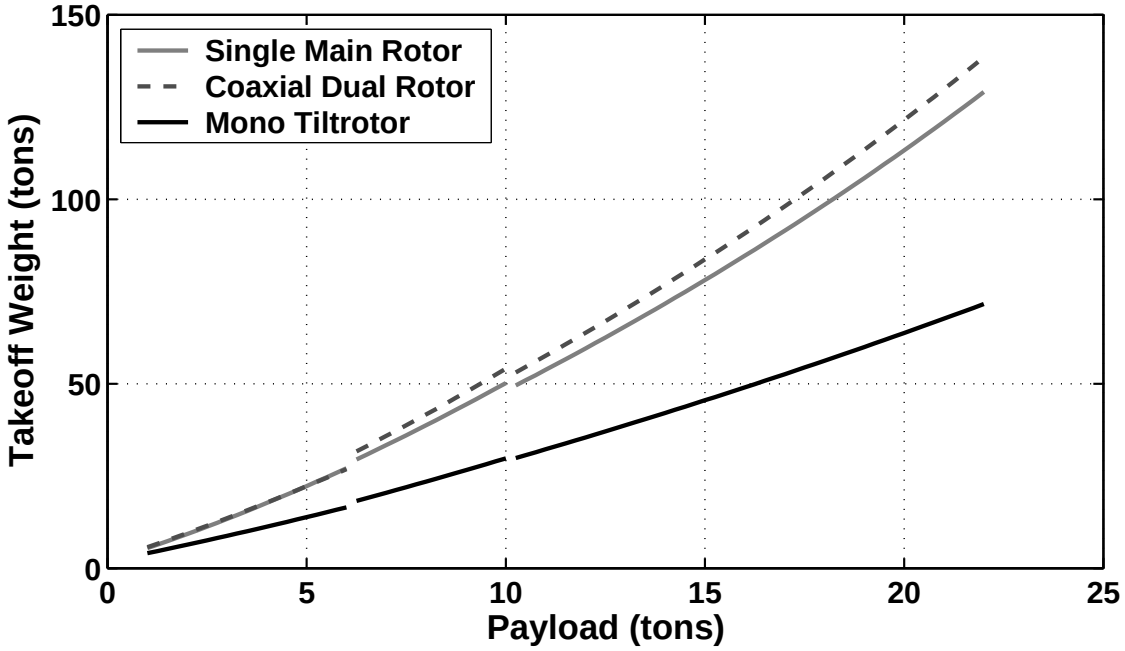

Figure 3.25: Predicted gross takeoff weight for the MTR architecture to meet a 1,000 nm range requirement versus payload compared with hypothetical conventional (single) and coaxial rotor helicopters.

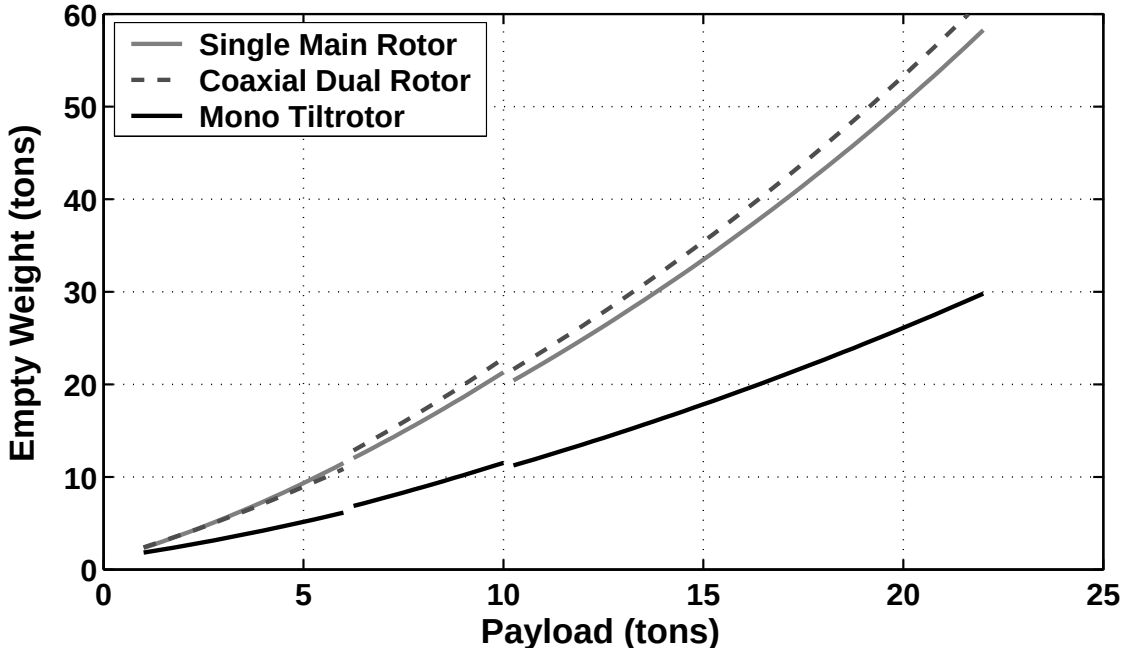

Figure 3.26: Predicted empty weight for the MTR architecture to meet a 1,000 nm range requirement versus payload compared with hypothetical conventional (single) and coaxial rotor helicopters.

pared to a conventional helicopter when carrying the same useful payload over the same distance. According to this initial comparison study, the heavy-lift, long-range (20 ton, 1,000 nm) mission requirement could be met with a MTR vehicle that has about an 88 ft diameter rotor with a gross takeoff weight of 65 tons.

Of significance in this design study is that a coaxial rotor system could (in theory) be designed that is smaller and lighter than an equivalent single rotor system. However, to achieve the long-range, heavy-lift mission of 1,000 nm and 20 tons, the required rotor diameter for a coaxial helicopter is still very large ($\approx$ 125 ft). The practical difficulties in building a coaxial rotor of this size are unknown, but must be expected to be considerable. While the MTR uses a coaxial rotor, it is about 25% smaller than this and the feasibility of successful construction of an 88 ft diameter rotor is more likely, but certainly not without its issues. The relative size of the rotors for the single, coaxial and MTR to perform the long-range, heavy-lift mission are compared in Figure 3.24, where it is apparent that the difference in rotor diameter and disk area is dramatic. Besides feasibility issues that would be present in producing and flying with these huge rotor systems, the very large vertical footprints associated with these designs would prevent any sort of sea-basing mission capability, which with the MTR design is still a definite possibility.

The MTR's empty weight as shown in Figure 3.26 was found to be 65% less than a conventional helicopter for the same payload and range requirements. The MTR has such a lower empty weight than a conventional helicopter, in part because of its minimal "crane" type of airframe design, even when including the deployable wings and cargo suspension unit. Because the MTR is so much lighter than

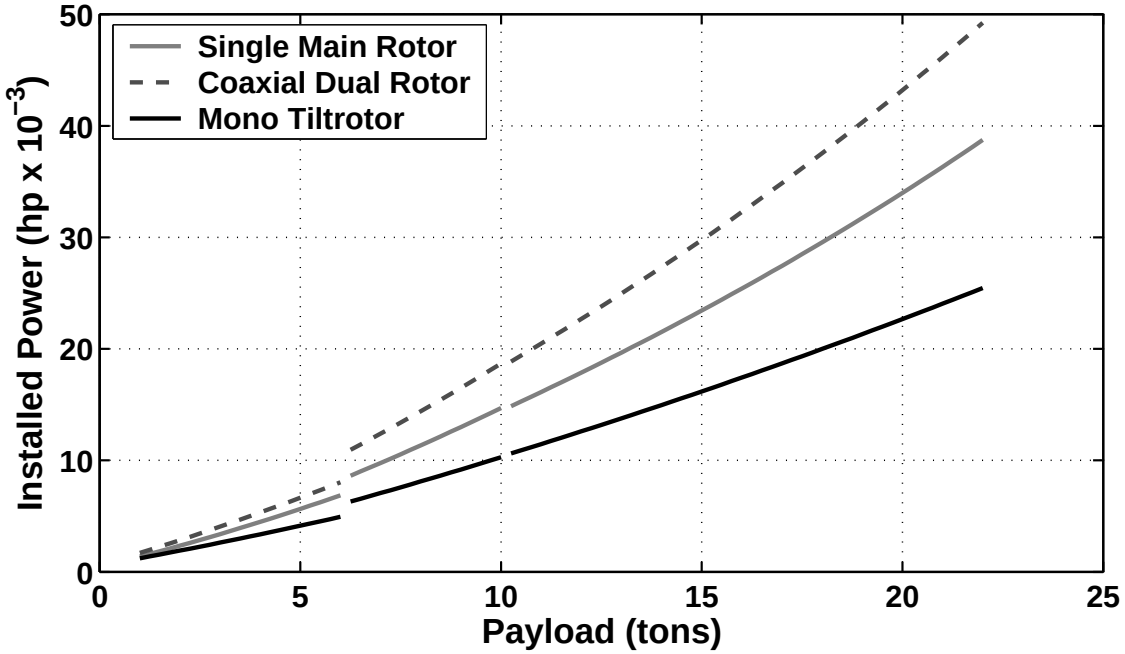

Figure 3.27: Predicted power requirements for the MTR architecture to meet a 1,000 nm range requirement versus payload compared with hypothetical conventional (single) and coaxial rotor helicopters.

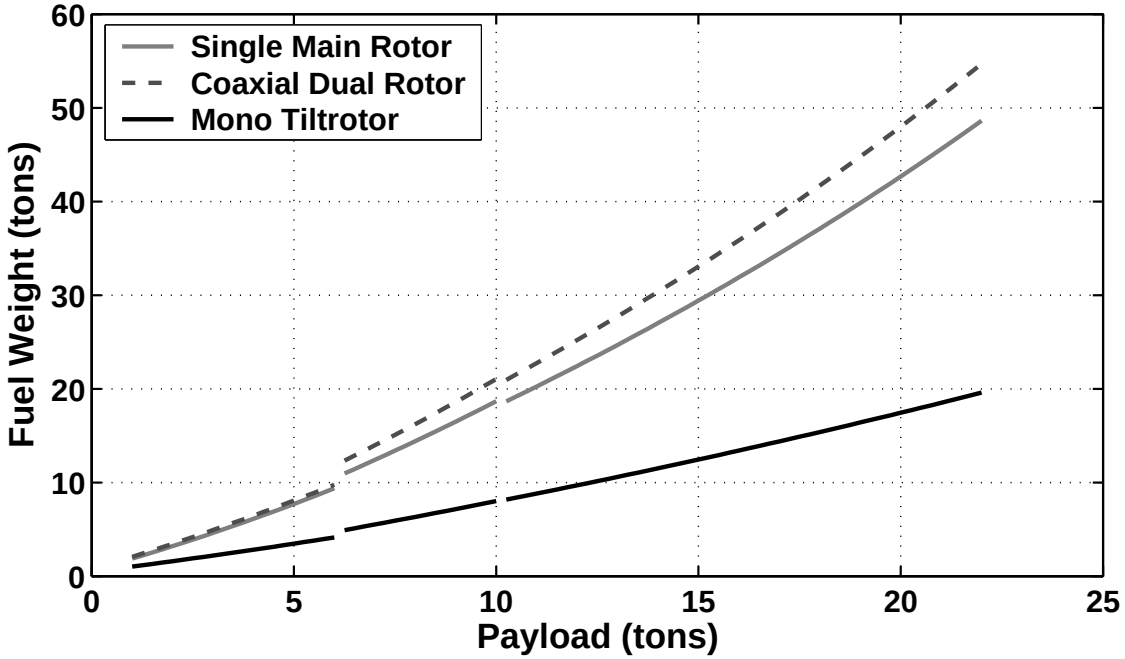

Figure 3.28: Predicted fuel weight for the MTR architecture to meet a 1,000 nm range requirement versus payload compared with hypothetical conventional (single) and coaxial rotor helicopters.

a conventional helicopter to perform the same mission, significantly less installed engine power is required for flight, as shown in Figure 3.27. While the MTR's power requirements are still relatively large ($\approx$ 20,000 shp), they are more realistically achievable than the 35,000+ shp net installed power that would be required to meet the same goals using a conventional helicopter configuration.

The reduced power requirements serve to contain net empty vehicle weight, and also have an impact on reducing the MTR's required fuel weight. The compared predictions for fuel weight are given in Figure 3.28. The results show that for most missions, the MTR requires less than half of the fuel that would be required of a conventional helicopter. This is both a result of the smaller and lighter vehicle as well as the MTR's ability to morph into a more fuel-efficient fixed-wing cruising configuration, with a significantly higher lift-to-drag ratio than is achievable with a conventional helicopter.

To quantify the discrepancy in cruise efficiency, a range specific transport efficiency, E_{RST}, can be defined using

$$E_{\mathrm{RST}} = \frac{W_{\mathrm{PL}}}{W_{\mathrm{fuel}}} \tag{3.1}$$

This quantity (shown in Figure 3.29) measures the payload weight moved per unit weight of fuel over a specific range. According to these results, the MTR would transport 1.2 pounds of payload per pound of fuel, whereas a helicopter would transport only about 0.5 pounds per pound of fuel. This result suggests that the MTR architecture, if technically realized, would be over twice as efficient at transporting payload as a conventional helicopter.

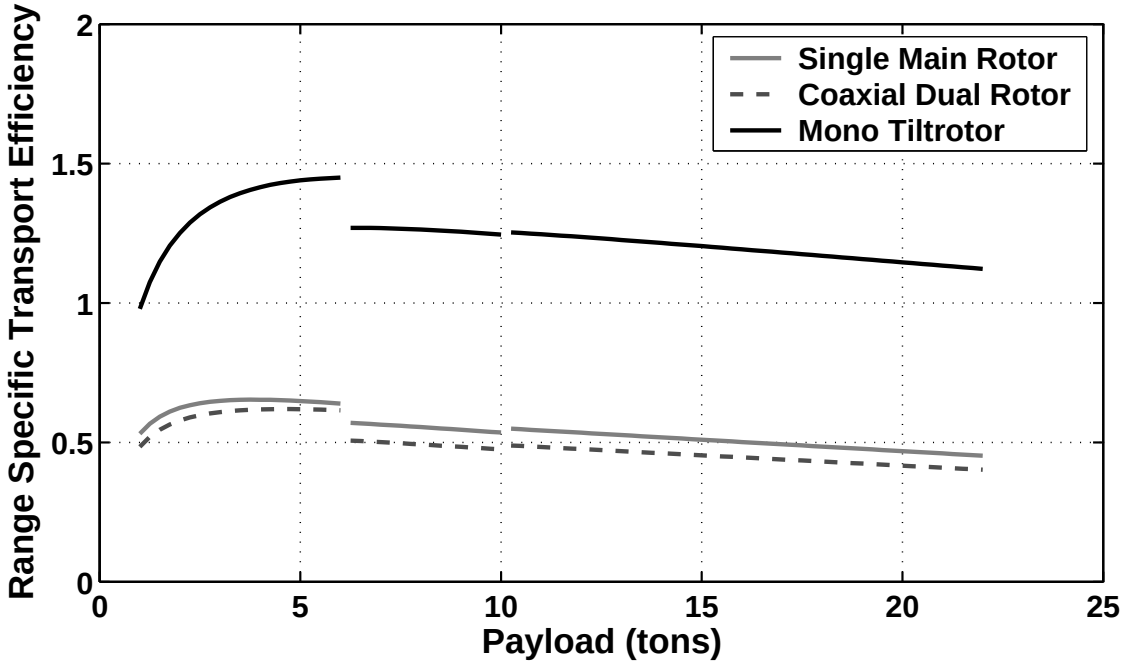

Figure 3.29: Predicted specific transport efficiency of the MTR versus payload compared with hypothetical conventional (single) and coaxial rotor helicopters.

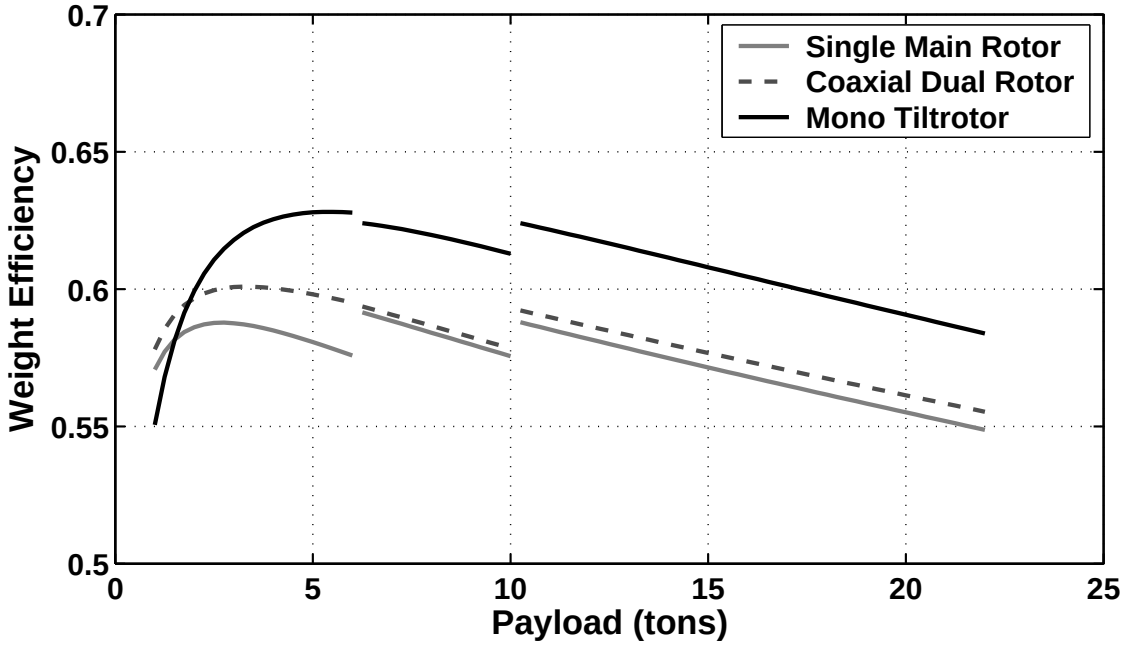

Figure 3.30: Predicted weight efficiency for the MTR architecture to meet a 1,000 nm range requirement versus payload compared with hypothetical conventional (single) and coaxial rotor helicopters.

Structural weight efficiency (Eq. 2.14) measures the proportion of takeoff gross weight dedicated to fuel and payload. Distance traveled does not factor into this equation, only the efficiency of the aircraft in lifting a payload vertically.

Because the MTR aircraft architecture is proposed mostly as an assemblage of off-the-shelf component technologies, it should at best have a weight efficiency comparable to helicopters. Indeed, Figure 3.30 shows the MTR to have improved weight efficiency – bearing more resemblance to a crane type helicopter than a conventional helicopter in this respect, which is fair considering that the MTR is similarly dedicated to carrying external loads.

Payload–Range Comparison

Results for payload versus range performance of the MTR are shown in Figure 3.31 compared with the performance of legacy heavy-lift rotorcraft. The same assumptions were used for MTR performance as detailed previously. It was also assumed that useful payload could be traded off for fuel and vice-versa, until the designed tank capacity was reached. To exceed the tank capacity, it is necessary to account for auxiliary fuel tanks to house the additional fuel. For this analysis, an auxiliary fuel tank was added to the aircraft, when needed, with weight equal to 10% of its maximum auxiliary fuel capacity for self-deployment (20 tons). This is shown in Figure 3.31 as a step drop in payload capability of the MTR with the addition of the tank.

Figure 3.31 shows that the MTR offers a payload-range capability that cannot

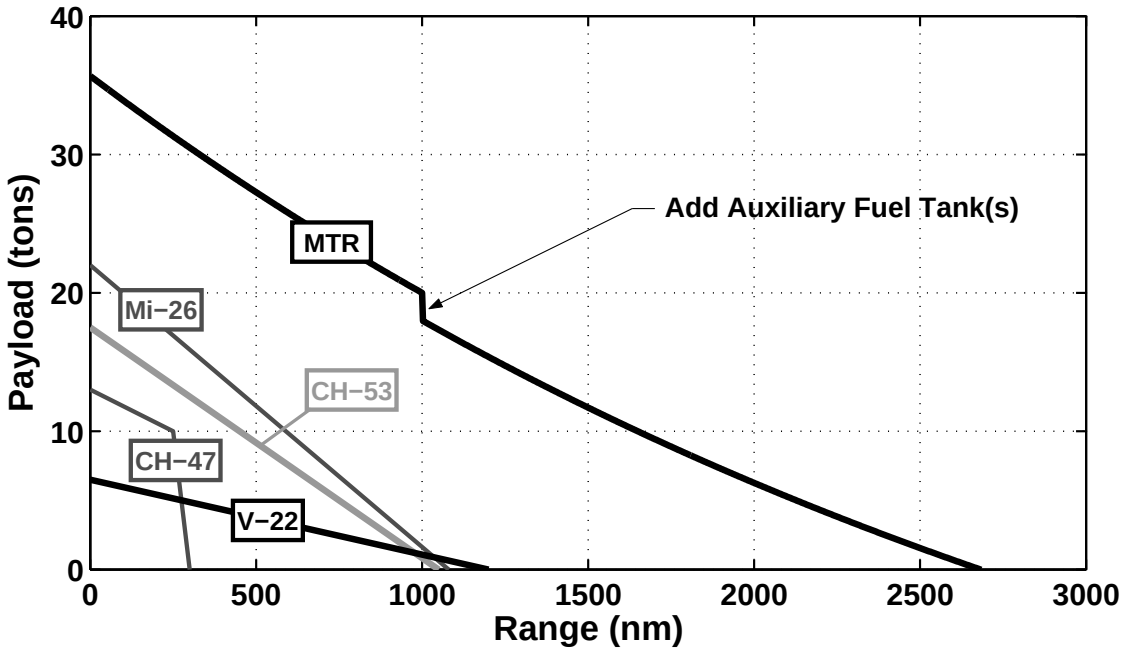

Figure 3.31: Predicted payload/range graph for the MTR concept when compared with a legacy helicopter design.

be approached by current rotorcraft. According to these results, not only would the MTR have the capability to carry 20 tons of payload over an unrefueled range of 1,000 nm, it would also be able to carry 27 tons over 500 nm or 10 tons over 1,700 nm. The self-deploy or maximum ferry range of the MTR is shown to be over 2,500 nm with the use of the auxiliary fuel tank. Meanwhile, the maximum ferry ranges of the legacy helicopters shown are in the neighborhood of only 1,000 nm. Overall, the MTR is shown to have the potential for unprecedented payload-range performance capability for a rotorcraft, if technically realized. It should be noted that these results were obtained with a non-optimized mission profile. Optimization through mission and design trade studies gives the potential to greatly enhance aircraft performance, which is the focus of the following section.

3.3 Design and Optimization Trade Studies

In previous sections, a comprehensive sizing methodology has been developed, validated and implemented to compare the relative merits of the MTR concept to legacy helicopters designs. This section takes an in-depth look at sizing the MTR concept by completing a series of trade studies. These studies were designed to study the influence of mission and design parameters on the overall vehicle, as well as to determine optimum designs for key MTR configurations including a heavy-lift, long-range MTR and an MTR Scaled Demonstrator (MTR-SD). The first of these studies details the influence on changes to the mission requirements on the overall design of the MTR.

3.3.1 Mission Design Trade Studies

Several trade studies were performed to determine the sensitivity of the overall MTR design to changes in key mission parameters, such as hover time and operational density altitudes. The studies detailed here include the variation in destination hover time and takeoff density altitude. The default mission used for these studies requires a 500 nm radius of action (ROA), in which the MTR deploys and returns with a range of payload weights. The MTR cruises at 10,000 ft at 240 kts, and hovers for 20 minutes at the destination. The takeoff, landing and destination sites were all considered to be at MSL in the default case. Elements of this default mission were then varied to study the effects on the overall design. A constant rotor disk loading of approximately 10.5 lb/ft^2 was assumed for all design points.

Destination Hover Time

The first study examined the effects of changes in the destination hover time on the overall design. While the MTR design features rapid container deployment and acquisition capability, certain missions may require longer hover times than necessary for a simple payload deployment. Figure 3.32 shows the effect of increasing the destination hover time on the takeoff weight of the MTR for various mission payloads. Increases in destination hover time tend to increase the takeoff weight of the MTR substantially for large payloads. For a 20 ton payload, the takeoff weight was increased from 60 to 65 tons when increasing the destination hover time from 20 minutes to 40 minutes. An additional 20 minutes of hover time increases the takeoff weight to over 70 tons. Figures 3.33 and 3.34 show the variation in MTR rotor size and wing span, respectively, with payload and destination hover time. It is shown that increases in destination hover time also lead to marked growth in the size of the rotor system. Figure 3.33 shows that for a 20 ton payload, increasing the destination hover time to 60 minutes results in a 7 ft increase in the MTR's required rotor diameter, as well as a 7 ft increase in its wing span.

These increases in overall size are a result of the high power and high fuel requirements in the hover condition. The effects on the fuel requirements of the MTR with variation in payload and hover time are shown in Figure 3.35. Fuel weight is shown to increase dramatically with hover time. For an MTR designed to carry a 20 ton payload, fuel weight was predicted to increase by nearly 40% to increase the destination hover requirements from 20 to 60 minutes. This increase is far greater

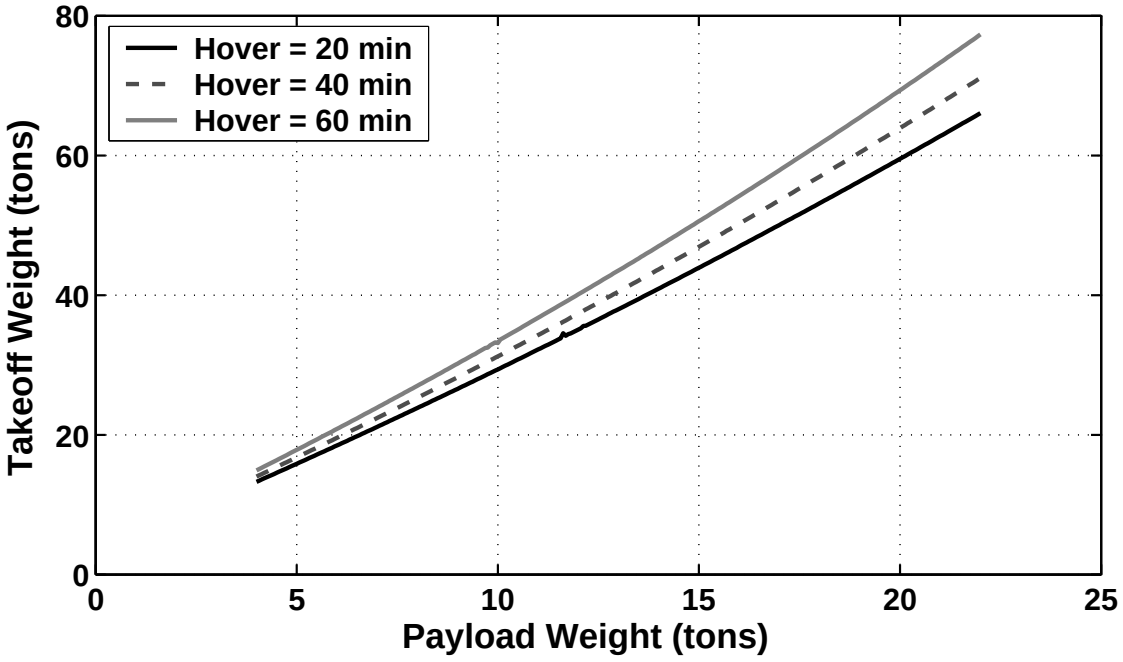

Figure 3.32: MTR takeoff weight versus payload and destination hover time.

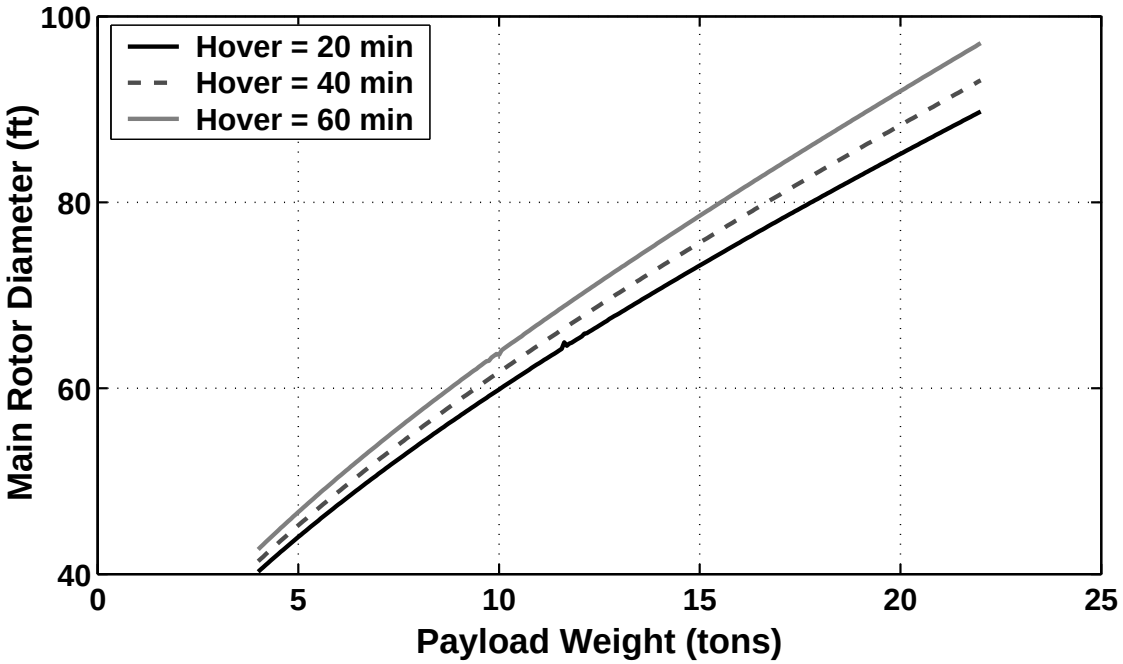

Figure 3.33: MTR rotor diameter versus payload and destination hover time.

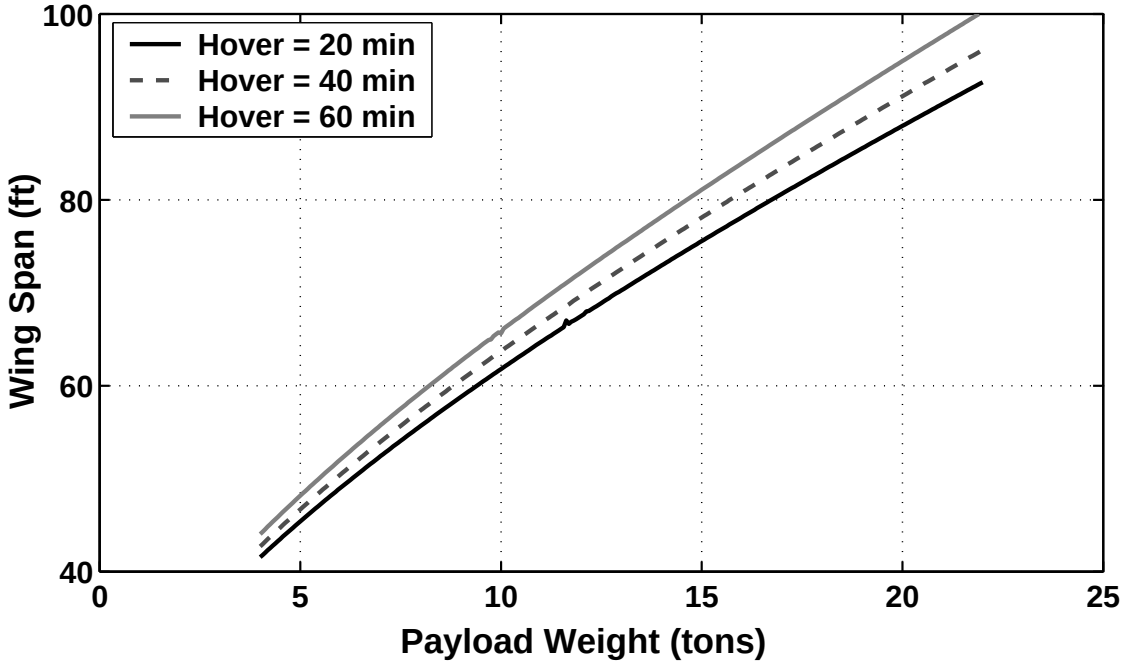

Figure 3.34: MTR wing span versus payload and destination hover time.

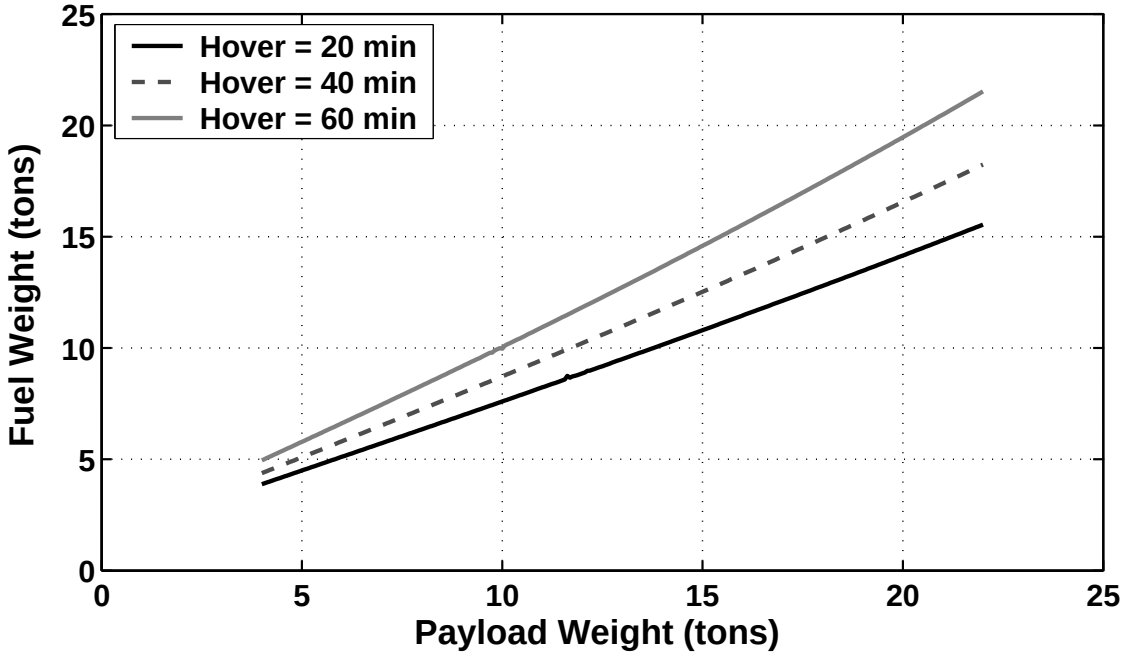

Figure 3.35: MTR required fuel weight versus payload and destination hover time.

proportionally than the overall size increase of the vehicle, thereby making this the clear driver for the overall vehicle size increases. Therefore, missions with high hover time demands will either require a significantly larger aircraft to achieve them, or a reduction in the payload and/or range capabilities for that mission. For instance, if the destination hover requirements were increased from 20 to 60 minutes for an MTR aircraft designed to carry 20 tons over a 500 nm ROA, the payload capacity would have to be decreased to 17.5 tons for that range according to Figures 3.32 through 3.34.

Takeoff Density Altitude

The next study examined the influence of the takeoff density altitude on the overall vehicle size. There are many situations in which an aircraft may be required to take off from density altitudes that are above MSL. If the aircraft is taking off from a higher altitude or on a hot day, the aircraft will have less power available, therefore making takeoff and hovering flight much more difficult. The effects of changes in the takeoff density altitude on the MTR gross takeoff weight, rotor size and wing span are shown in Figures 3.36 through 3.38, respectively. It is shown that the size of the MTR required to perform the same mission while taking off at H_{TO} = 6,000 ft density altitude is much larger relative to an aircraft designed to takeoff at MSL. For a 20 ton payload, this would require an increase in maximum vehicle gross weight of over 20 tons, and increases in rotor diameter in wing span of over 20 ft.

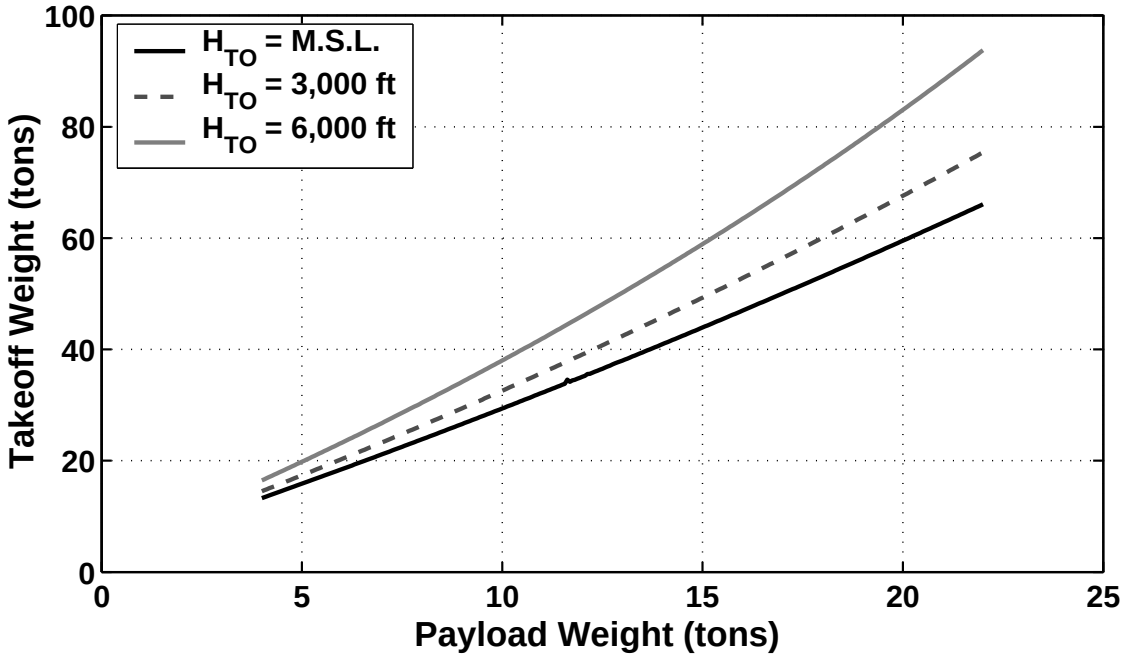

Figure 3.36: MTR gross takeoff weight versus payload and takeoff density altitude.

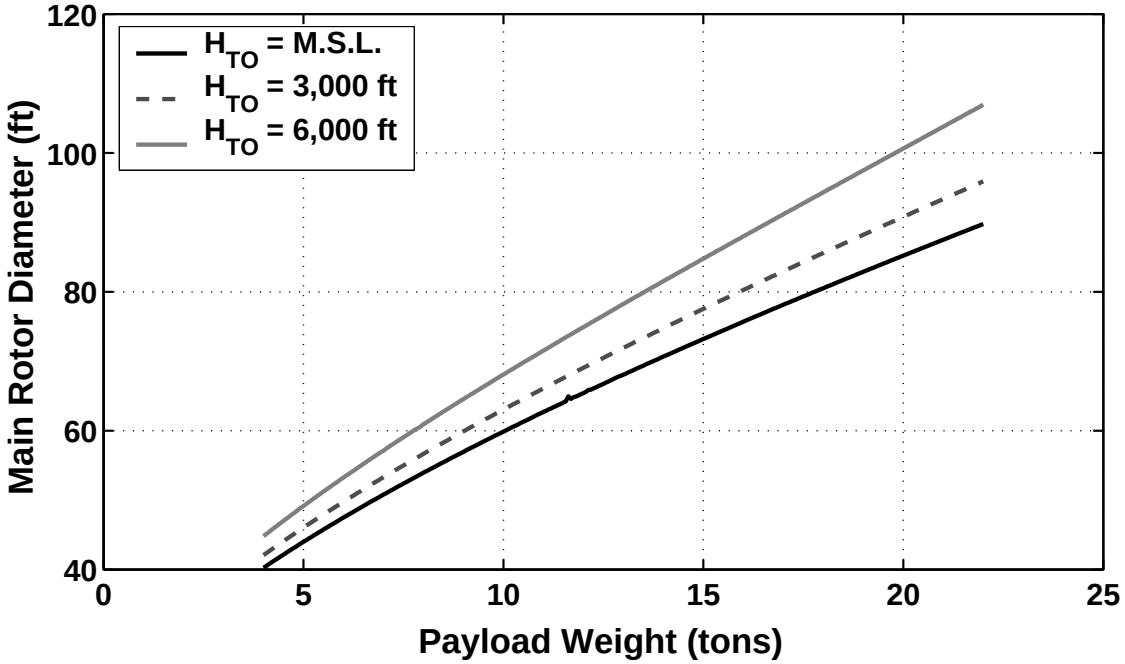

Figure 3.37: MTR rotor diameter versus payload and takeoff density altitude.

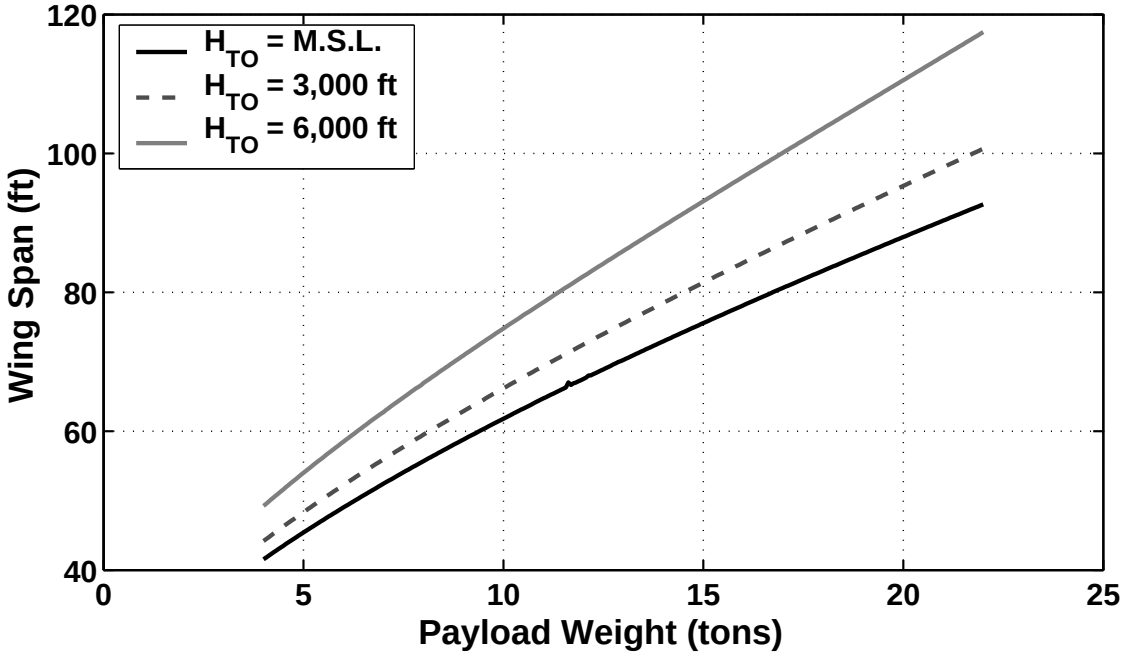

Figure 3.38: MTR wing span versus payload and takeoff density altitude.

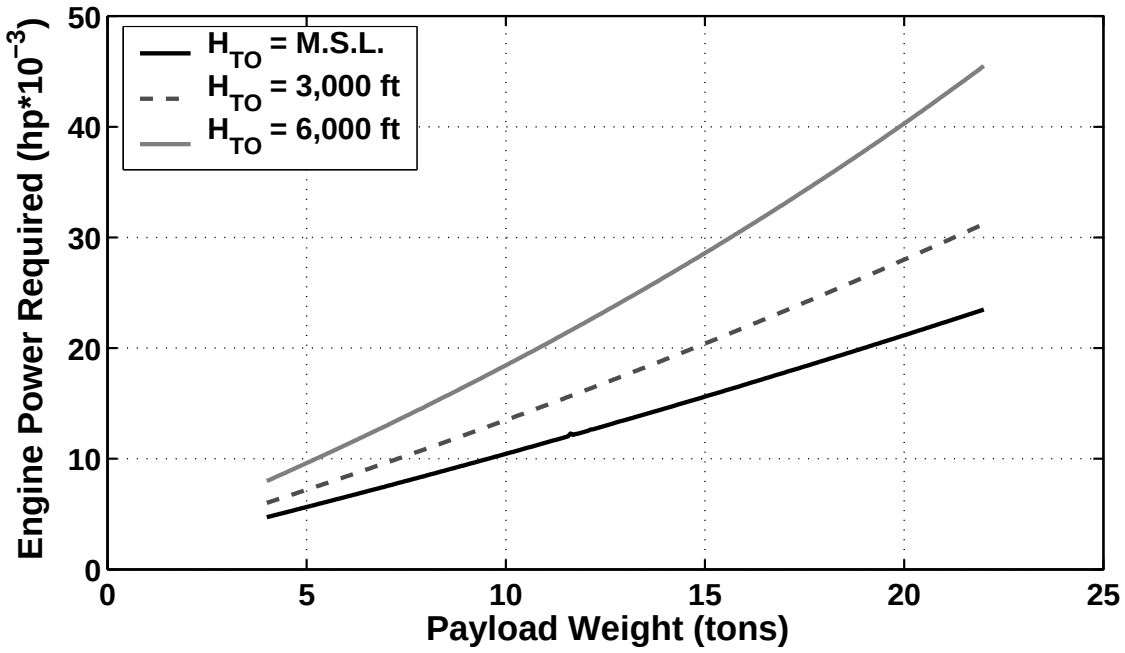

Figure 3.39: MTR engine power required versus payload and takeoff density altitude.

The primary driver for this dramatic size difference is the increase in the engine power requirements to take off under these conditions, as shown in Figure 3.39. The growth in engine power requirements leads to increased engine weight, vehicle empty weight and ultimately to increases in the overall vehicle size through design iteration. The engine power requirements were noted to increase by nearly 50% for the case the MTR designed for takeoff with a payload of 20 tons at a density altitude of 6,000 ft. Clearly in such equivalent "hot and high" conditions, which are key to the success of many military missions, less payload can be carried or less range can be achieved if the design is to remain fixed. This is shown in Figure 3.36 through 3.38, where an MTR designed to carry a 20 ton payload taking off at MSL is approximately the same size as an MTR designed to carry a 15 ton payload taking off at a density altitude of 6,000 ft.

3.3.2 Design Optimization for Heavy-Lift MTR

To tailor the MTR design for heavy-lift, long-range missions, it is necessary to optimize key design parameters such that the mission can be performed in the most efficient manner, in terms of the required vehicle size, mission time and operational costs. One key optimization that must take place is that of the mission profile, particularly the cruise leg in airplane mode in which the MTR would cover the most distance and spend the majority of its operational life. By selecting the optimum combination of cruise speed and cruise altitude to perform the heavy-lift, long-range mission, it is possible to greatly reduce the fuel requirements and overall size of the vehicle. Additionally, it is important to select an engine package that will give the best potential performance for the aircraft and tailor that design to take full advantage of the capabilities offered by the power plant. This can be accomplished by adjusting the rotor disk loading and solidity.

Cruise Optimization

Previously reported MTR sizing and performance studies have used non-optimized mission profiles often cruising at MSL conditions at a design cruise speed of 240 knots. It is known that cruising at higher altitudes can lead to great benefits such as drag reduction related to decreased air density. This drag reduction can lead to increases in vehicle lift-to-drag ratio and lower power requirements and required fuel burn. If the required fuel weight is decreased, it can lead to a significantly smaller vehicle, as well as greatly reduced operating costs. However, there are also

penalties associated with high altitude cruise such as the loss of lifting capacity of the wings, which leads to increases in the required wing area to maintain stall margins and therefore, empty weight of the vehicle for the same cruise lift coefficient. Additionally, cruising at higher altitudes decreases the available power, which can reduce performance capability. Cruising at higher speeds can reduce required wing area and empty weight for the same cruise lift coefficient. Higher cruise speeds also reduce mission time, which is always desirable from a tactical standpoint. However design cruise speed is limited by available power.

An optimal combination of cruise speed and cruise density altitude is one which would achieve a minimum vehicle size and maximum fuel efficiency while working within the limits of the power plant. To maximize the fuel efficiency of the design, it is important for the aircraft to fly at the cruise speed for maximum range (maximum L/D) and at or near the maximum continuous power rating of the engine for best specific fuel consumption. Ultimately, this combination of factors will lead to the lowest fuel burned per mile, which is important for any long-range aircraft. A wide range of combinations of design cruise altitude and cruise speed were examined to optimize the long-range, heavy-lift (20 ton, 500 nm ROA) MTR. Figures 3.40 through 3.43 show a sampling of possible combinations of cruise speed and altitude and their effects on the overall design of the MTR. For this study, 20 minutes of hover time was assumed at the destination site, with takeoff, landing and destination at MSL conditions.

Figure 3.40 shows results for the relative power in cruise for various combinations of cruise speed and altitude. A relative power of one is the maximum power

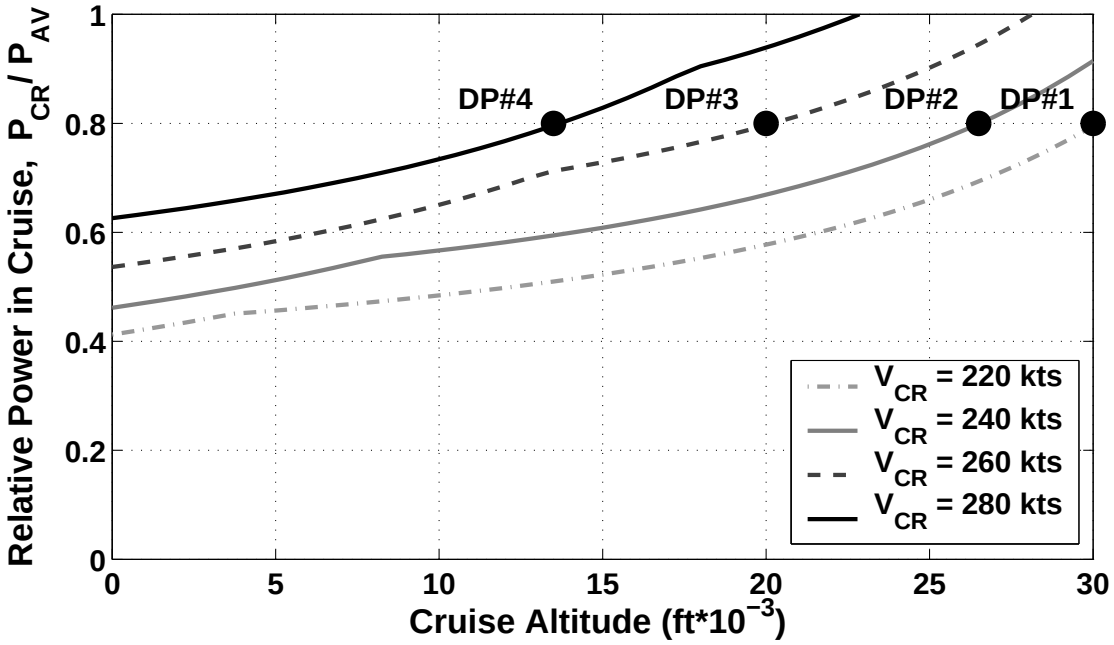

Figure 3.40: Relative power in cruise versus cruise density altitude and cruise speed.

available from the engine package and a relative power of approximately 0.8 was estimated to be the maximum continuous power available. It is shown that there are several sample design points that cruise at the estimated maximum continuous power rating. These sample design points are:

$$\text{DP\#1: } V_{\text{cr}} = 220 \text{ kts}, H_\rho = 30,000 \text{ ft}$$

$$\text{DP\#2: } V_{\text{cr}} = 240 \text{ kts}, H_\rho = 27,000 \text{ ft}$$

$$\text{DP\#3: } V_{\text{cr}} = 260 \text{ kts}, H_\rho = 20,000 \text{ ft}$$

$$\text{DP\#4: } V_{\text{cr}} = 280 \text{ kts}, H_\rho = 13,000 \text{ ft}$$

There are clearly many intermediate choices possible, but these design points serve as a basis to study the behavior of the MTR's design characteristics with changes in defined cruise speed and altitude, while attempting to maintain overall maximum flight efficiency. Out of all four sample design points, the minimum takeoff weight and rotor size are achieved at design point 3 (Figures 3.41 and 3.42). The

design points with higher cruise altitudes and lower cruise speeds have improved fuel efficiency, but this is overcome by reductions in weight efficiency from rapidly increasing wing spans (Figure 3.43). The design points with lower cruise altitudes and higher cruise speeds have improved weight efficiency stemming from reductions in the required wing area, but this is overcome by degraded aerodynamic efficiency (decreased L/D) and higher fuel requirements.

Design point 4 might be a reasonable choice because it possesses a significantly smaller wing span (by nearly 10 ft) than design point 3. However, this is offset by increases in takeoff weight (2 tons), rotor diameter (2 ft), and fuel weight (4 tons). Therefore, the vehicle size (in terms of gross weight and rotor size) are significantly larger, and the vehicle is much less efficient in terms of fuel requirements. While the larger wing span for design point 3 could be undesirable, it falls well within the kinematic limits set on the wing design. Additionally, the rotor size would likely be the primary driver in any shipboard compatibility issues because of the unique wing folding design characteristics.

Both design points 3 and 4 were examined further using the derived power required curves, along with many intermediate design points to determine whether these selected combinations were optimized for the resulting aircraft design. It was found that the large discrepancy in fuel requirements in the designs was, in part, a result of cruising at a velocity higher at design point 4 than its best range speed (maximum L/D). The result is a far less efficient design because a simple reduction in cruise speed would result in a higher wing lift coefficient and induced drag, possibly resulting in an increase in fuel requirements.

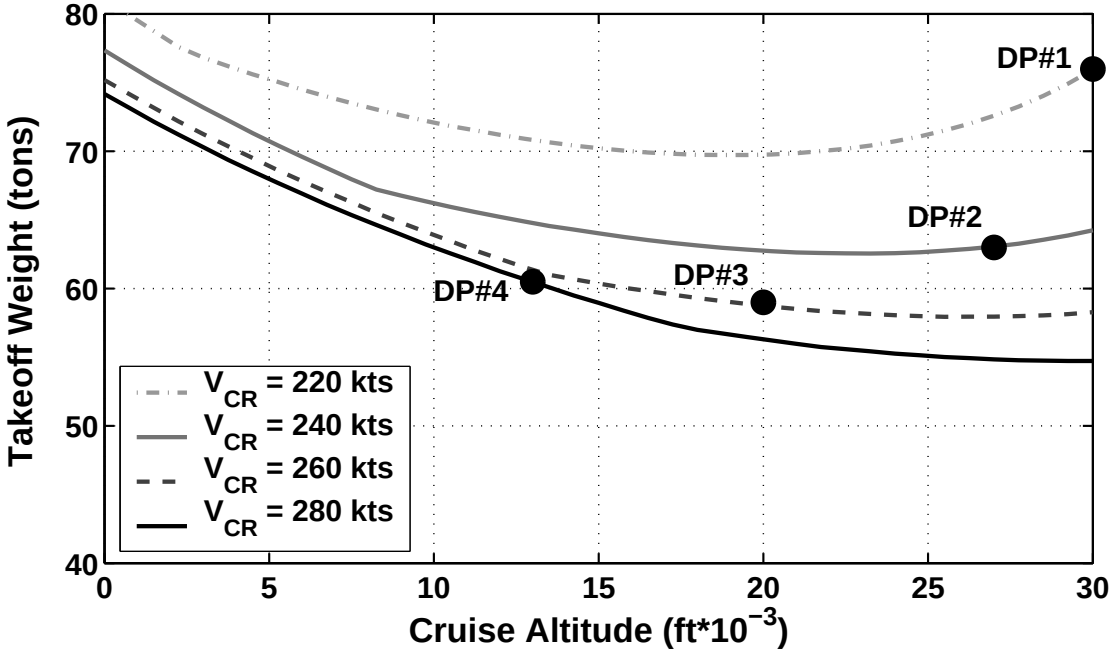

Figure 3.41: MTR takeoff weight versus cruise density altitude and cruise speed.

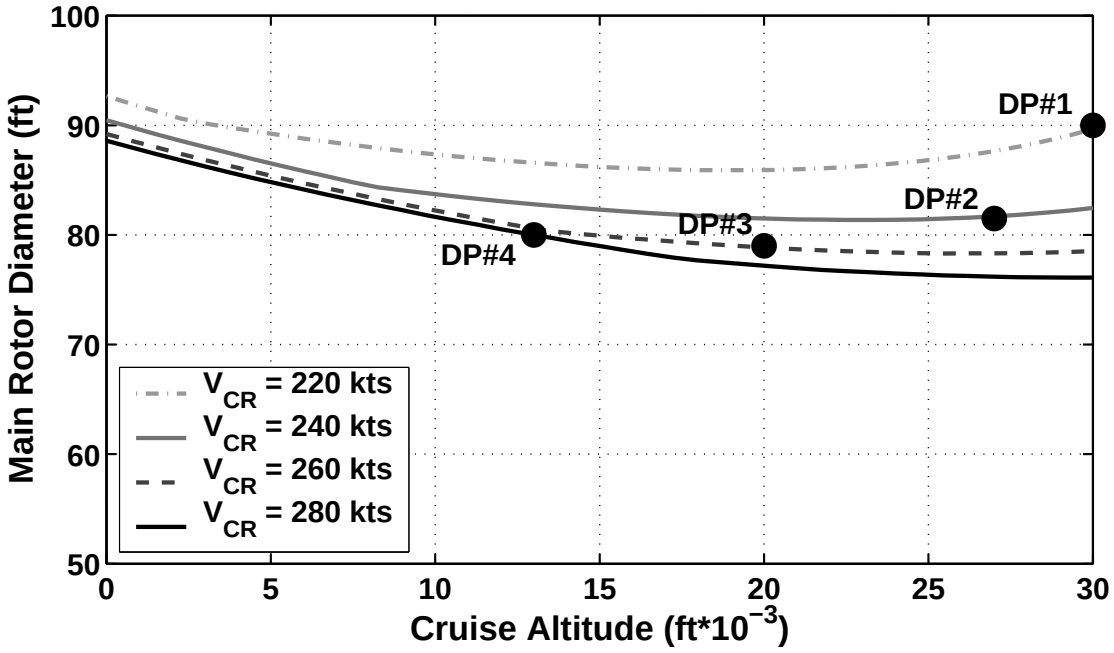

Figure 3.42: Rotor size versus cruise density altitude and cruise speed.

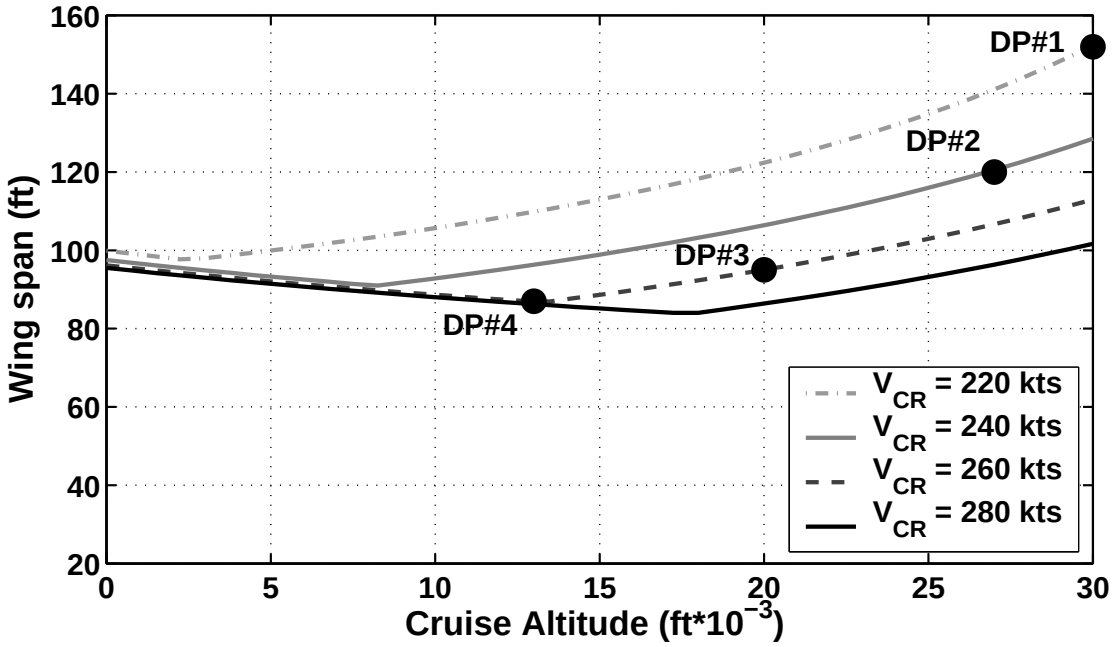

Figure 3.43: MTR wing span versus payload and takeoff density altitude – break in span predictions marks the change in the wing sizing driver from conversion to cruise stall margins.

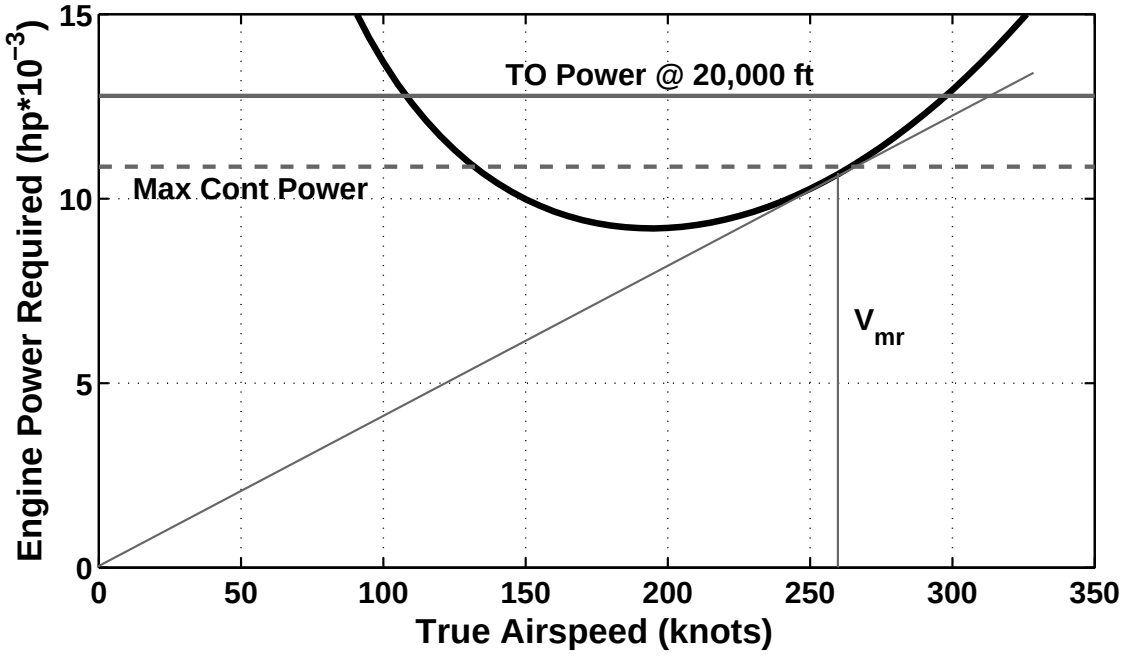

Figure 3.44: Power required curve of design point 3 at 20,000 ft density altitude.

Meanwhile, it was found that design point 3 did result in an optimized combination of design cruise speed and cruise altitude for the resulting design. It is shown in Figure 3.44 that design point 3 is the cruise speed for maximum range (maximum L/D) and the maximum continuous power rating (minimum SFC) at the design cruise altitude altitude. Therefore, the combination of design cruise speed and cruise altitude given by design point 3 was selected for the heavy-lift, long-range MTR point design.

Engine Selection

In previous studies, the MTR engine sizing was based on the idea of a "rubber engine." This means that a hypothetical engine was created for each design output based on the predicted power requirements and values of power-to-weight ratio comparable to legacy turboshaft engines. For the heavy-lift, long range (20 ton, 500 nm ROA) MTR design, the decision was made to focus the design around the existing Allison AE 1107C engine, which is used on the V-22 Osprey. This engine is already designed for tiltrotor operation and has a superior power-to-weight ratio ($P/W = 6.3$ shp/lb) and specific fuel consumption over legacy rotorcraft turboshaft engines. The engine power requirements of the heavy-lift, long-range MTR exceed 20,000 shp, requiring the use of four engines, for a total of 24,600 shp takeoff power available at MSL conditions.

With the design analysis updated for the selections of design cruise speed, cruise altitude, and engine weight, it was found initially that the power available

exceeded the power required to takeoff by a significant margin. It is important for the aircraft to be designed in such a way that that it utilizes all of the power that is given by the engines selected. Otherwise, the lower power settings will result in significant increases in specific fuel consumption.

The surplus available power in this design allowed the opportunity to increase the disk loading of the MTR aircraft, thereby decreasing the size of the coaxial rotor without a significant weight penalty. To take full advantage of the powerplant, the disk loading and rotor solidity of the aircraft were increased iteratively until the power required to takeoff approached the power available at MSL conditions. This was done parallel to the cruise optimization study, and had the effect of significantly reducing the size of the main rotor. The disk loading was increased from 10.4 lb/ft^2 to 12 lb/ft^2, which is still comparable to legacy heavy-lift helicopters. The main rotor solidity was also increased from 0.11 to 0.13, to maintain appropriate blade loading coefficients, which reduced the predicted main rotor diameter considerably. The predicted result of the vehicle optimization was a very compact, efficient vehicle design relative to the mission requirements and potential performance capabilities.

MTR Heavy-Lift Preliminary Sizing Results

The following is a summary of a preliminary result for the MTR point design optimized to efficiently perform a long-range, heavy-lift mission. Table 3.1 summarizes the key design and mission inputs for this particular design. The MTR was designed in this case to carry a 20 ton payload over a 500 nm ROA mission with 20

minutes of hover time at the destination.

The resulting preliminary MTR design is summarized in Table 3.2. It is shown that the maximum takeoff weight has been reduced to under 59 tons, and the main rotor has a diameter of less than 79 ft. This is a significant size reduction from that previously proposed, where takeoff weights approaching 65 tons and rotor diameters of nearly 90 ft were predicted (see Section 3.2). The significant reduction in overall size can be attributed to several factors, including the reduction in fuel burn because of an optimized mission profile, and the design of the aircraft around the AE 1107C engine, which, as previously mentioned, has an excellent power-to-weight ratio. The MTR's wing span is slightly larger than predicted in previous studies because of the more stringent wing area requirements based on stall margins at high altitudes. The empty weight fraction of 0.44 is comparable to that of a conventional crane helicopter. The higher disk loading and main rotor solidity is beneficial in the performance of the rotor system in terms of propulsive efficiency, while the smaller rotor size improves the shipboard compatibility of the design. This increase in disk loading will result in higher downwash velocities, but they should still remain comparable to those of a large, heavy-lift helicopter.

Table 3.3 lists the component weights predicted by the analysis for this heavy-lift, long-range MTR point design. It is shown that the rotor system, gearbox, and powerplant and fixed lifting surfaces (wing and tail) are the heaviest aircraft components, with the cargo handling system, landing gear, rotor tilt mechanism and cockpit furnishings also making significant contributions to the total gross weight. The blade and hub weights were found to be comparable to those of the Boeing HLH

Design Payload (tons)	20
Radius of action (nm)	500
Dest. Hover Time (min)	20
Design Cruise Speed (kts)	260
Design Cruise Altitude (ft)	20,000

Table 3.1: Mission profile for heavy-lift, long-range MTR point design.

Max Takeoff Weight (lb)	116,600
Empty Weight (lb)	51,500
Empty Weight Fraction	0.442
Main Rotor Diameter (ft)	78.6
Rotor Disk Loading (lb/ft^2)	12.0
Number of M/R Blades (per rotor)	6
Main Rotor Solidity	0.130
TO Power @ MSL (shp)	24,600
Number of Engines	4
Fuel Weight (lb)	24,682
Fuel Fraction	0.212
Wingspan (ft)	94.7
Wing Aspect Ratio	7.5

Table 3.2: General sizing for heavy-lift, long-range MTR point design.

MTR Component	Weight (lb)
Main Rotor Blades (6x2)	5,615
Main Rotor Hubs (2)	7,360
Main Rotor Gear Box	8,697
Swashplate	597
Control Hydraulics	187
Automatic Flight Control System	330
Engine Weight (4)	4,237
Engine Installation	636
Auxiliary Power Unit	162
Fuel System	987
Landing Gear	1916
Electrical System	356
Instrumentation/Avionics/Furnishings	3,000
Wing	9,312
Vertical Stabilizer	659
Horizontal Stabilizer	1,901
Trapeze Struts	371
Cargo Handling System	2,000
Tail Boom	835
Tilting Mechanism	1,166
Crew Compartment (structure)	500
Tilt Boom	583
Wing Folding Mechanism	93

Table 3.3: Component weights for heavy-lift, long-range MTR point design.

helicopter [29], a tandem design that also features dual hubs with similarly sized rotors and overall gross weight. The transmission weight is also comparable to the HLH, although it is slightly lower because the more stringent demands placed on a heavy-lift tandem helicopter, which requires heavy torque transmission components distributed across a very large airframe.

Component Weight Sensitivity

The MTR component weight calculations presented in Section 2.4 were carefully developed and validated with the goal to be conservative whenever possible. However, as the MTR program moves forward into the detailed design phase, it is inevitable that some of these component weights will be found to be either optimistic or pessimistic. Over-prediction of weights would actually be beneficial to vehicle size and performance, but any significant under-prediction could lead to size increases or performance degradations. For this reason, the design tools should continue to be refined throughout the design process as new information becomes available.

One component weight that may have been under-predicted in the development of the analysis is the weight of the wing folding mechanism. It was initially sized as 1% of the total wing weight. In further consideration of the kinematics and required loads on the hinge in conversion between flight modes, this weight factor seems optimistic. Therefore, it was decided to do a brief study into the sensitivity of the overall vehicle size to increasing this weight factor to more conservative values.

When sizing wing morphing mechanisms on fighter planes, it is typical to

allow for a weight factor of 20% of the total wing weight [25]. The maneuvering loads on these mechanisms would likely be much higher than those required for the MTR design, but nevertheless this could serve as a point of reference, or an upper bound, on the weight of the MTR wing folding mechanism. Sizing the wing folding mechanism at 10% of total wing wing weight might be a more reasonable choice.

The sensitivity of the overall size of the heavy-lift, long-range MTR point design to increases in wing folding mechanism weight are shown in Figures 3.45 and 3.46, in terms of takeoff weight and rotor diameter respectively. It is shown that the increase in wing folding mechanism weight (as a percentage of wing weight) results in slight linear increases in overall aircraft size. The takeoff weight of the MTR point design is shown to increase by 2% at 10% wing weight, and by 4.5% at 20% wing weight. The rotor diameter is shown to increase by 1% at 10% wing weight, and by 2.2% at 20% wing weight. Furthermore, it was found that the empty weight was increased by 4% at 10% wing weight, and by 8.5% at 20% wing weight. Therefore, the overall size of the MTR point design is shown to be relatively insensitive to reasonable increases in wing folding mechanism weight.

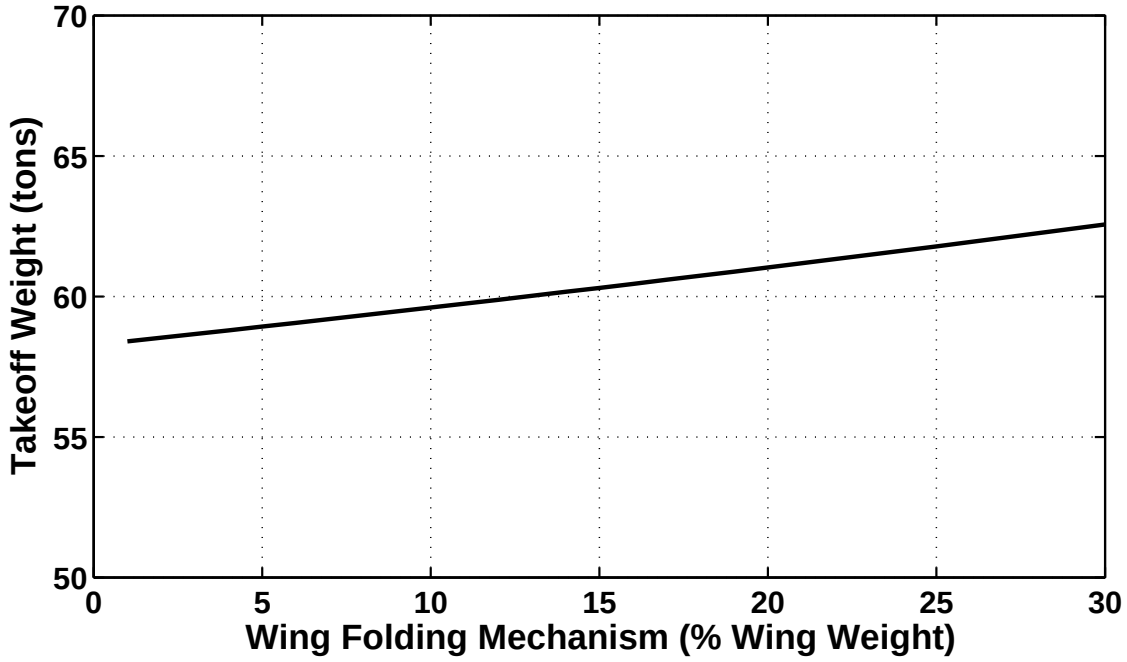

Figure 3.45: Effect of increasing wing folding mechanism weight on takeoff weight for heavy-lift, long-range MTR point design.

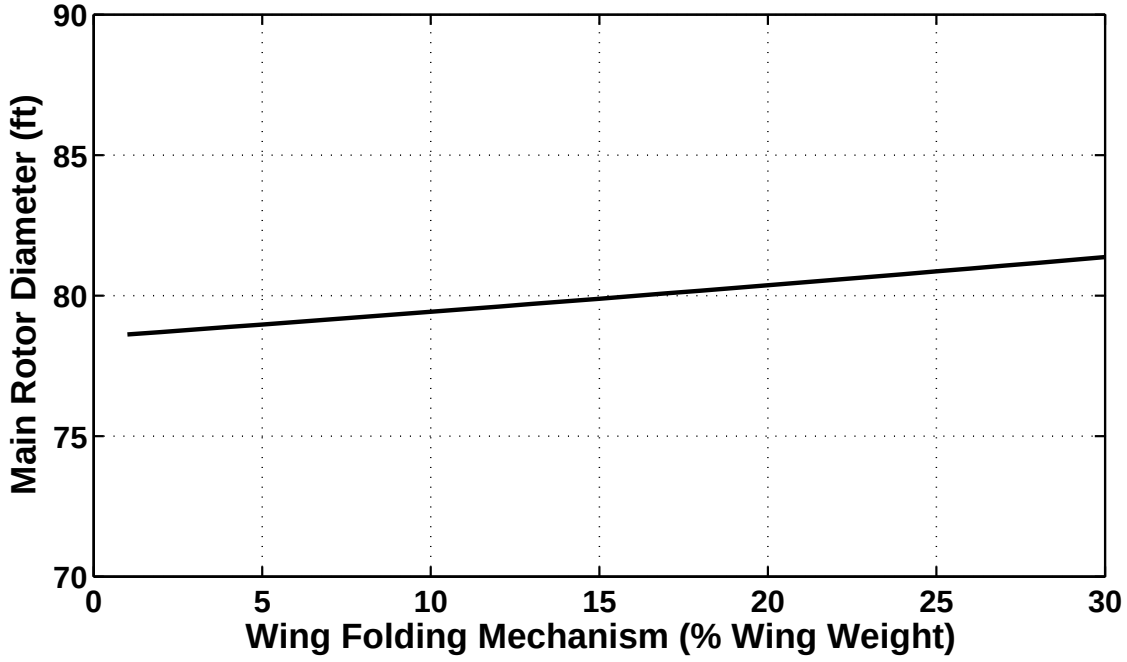

Figure 3.46: Effect of increasing wing folding mechanism weight on rotor size for heavy-lift, long-range MTR point design.

3.3.3 Preliminary Sizing of an MTR Scaled Demonstrator

The following is the preliminary sizing of the MTR-SD, which was designed as a small scale MTR suitable for testing in the NASA Ames 40 x 80 wind tunnel. The goal is for the MTR-SD to prove the feasibility of the MTR design by demonstrating the ability to overcome key engineering problems such as the tilting coaxial rotor system, folding wings and tail structure, as well as the successful integration of all these systems. The purpose of the MTR-SD is also to demonstrate performance capabilities of the MTR concept to create value and initiative for a full-scale MTR. In addition, designing, manufacturing and testing the MTR-SD would give further insight toward overcoming the engineering problems that may be related to realizing the full-scale MTR.

Design Requirements

The initial requirement given for the MTR-SD was to carry a 2-ton payload with a mission radius of action (ROA) of 500 nm (1,000 nm unrefueled range), while keeping within the rotor size constraints to allow testing in the NASA Ames 40 x 80 wind tunnel. This leads to a maximum rotor diameter of approximately 25 ft – similar to that of the XV-15. Therefore, The wing span is limited to no greater than 35 ft to allow sufficient space for the downward folded wings in the hover condition.

A version of the MTR design code was developed specifically for the MTR-SD design, including updated weight factors, to ensure the accurate design predictions at a significantly lower scale. Initial results based on these design requirements

were obtained using the same mission profile as was optimized for the full-scale, 20 ton, 500 nm ROA MTR. These results indicated a significant increase in the fuel requirements, in terms of the fuel fraction ($W_{\text{fuel}}/W_{\text{TO}}$), increasing from 21%, for the full-scale design, to 28% for the MTR-SD to achieve the same range. This loss of fuel efficiency results from a significant degradation in the aerodynamic efficiency, or lift-to-drag ratio (L/D), stemming from performance losses related to geometric scaling, as well as a non-optimized mission profile.

The degradation in L/D for the configuration is, in part, because of the square-cube law. Essentially, the size of the aircraft (frontal area) decreases at a slower rate than the weight of the vehicle when geometrically scaled. Therefore, the equivalent flat plate area of the same design configuration (constant C_{D_0}) will be relatively higher than the ratio at a larger scale. Because of this issue, it was decided to reduce the range requirements of the MTR-SD such that the fuel fraction was reduced to a value consistent with that of the full-scale MTR. A requirement of a 350 nm ROA (700 nm unrefueled range) was found to satisfy this requirement. Additionally, it was decided that the mission profile and design parameters for the MTR-SD be optimized independently of the full-scale MTR design outputs.

Design Drivers & Trade Studies

Several key design drivers were analyzed in trade studies to optimize the design of the MTR-SD, which included disk loading, rotor geometry, wing aspect ratio, design cruise speed, and cruise altitude.

The disk loading of the full-scale MTR design was increased to 12 lb/ft^2, in part, to adjust the design to the excess amount of available power when using the AE1107C engines. At this stage of the preliminary sizing for the MTR-SD, the power plant was considered as a "rubber engine," thus keeping the flexibility to perform key design trades until an actual candidate engine was selected. Typically, smaller helicopters tend to have lower disk loading than larger helicopters. The benefits of a decrease in disk loading typically are increased hover efficiency and weight efficiency, but at the cost of a relatively larger rotor disk area.

With the constant blade loading assumption, it can be shown that decreases in disk loading also lead to a decrease in the required rotor solidity. It was found that when decreasing the disk loading to approximately 11.4 lb/ft^2, the decrease in required solidity to maintain adequate blade loading was enough to allow a decrease in the number of blades from six to five blades per rotor without a significant loss in aerodynamic efficiency. This is desirable because it allows for reduced cost and design complexity for the MTR-SD. Therefore, a disk loading of approximately 11.4 lb/ft^2 was selected to increase hover and weight efficiency, decrease downwash velocity, lower design complexity, and minimize cost. The increase in rotor size for this selection was sufficiently low to stay within the size constraints of the MTR-SD design.

Another key design parameter that was examined was the wing aspect ratio of the MTR-SD. The full-scale MTR design features a wing aspect ratio of 7.5. The benefits in increasing this aspect ratio for the MTR-SD would be an increase in L/D and decreased fuel weight, which are both significant concerns in the MTR design,

as discussed previously. However, increasing the wing aspect ratio also leads to an increase in the wing span, which has a size constraint because of the required wing folding mechanics. Additionally, increasing the wing aspect ratio tends to result in increases in wing and empty weight.

When running a study to test the effects of changes in aspect ratio on the MTR-SD design, it was found that with the exception of wing span, the overall size of the vehicle is surprisingly insensitive. However, it was found that the wing span is much more sensitive to changes in wing aspect ratio. The results were very similar to the wing aspect ratio trade study reported in Section 2.3.3. With the length of the wing span becoming an issue in the design of the MTR-SD, it was decided to reduce the wing aspect ratio to a value of 7. This allowed the design to fit the overall size requirements, but without losing much in terms of aerodynamic efficiency.

The design cruise speed and cruise altitude for the full-scale MTR design were selected as 260 knots and 20,000 ft, respectively. This combination was found to lead to an optimized mission profile that took advantage of flying at both the maximum L/D, and near to the maximum continuous power rating of the power plant. This led to maximized fuel efficiency and an efficient overall design. However, for the MTR-SD, this combination does not lead to an optimum design point. In fact, because of the higher relative drag of the MTR-SD, this combination turns out to require more power in cruise than is required for take-off at maximum gross weight, thereby making it an infeasible design point. Therefore, the optimum combination of cruise speed and altitude was obtained by again examining a range of possible combinations and the resulting power required curves of those designs.

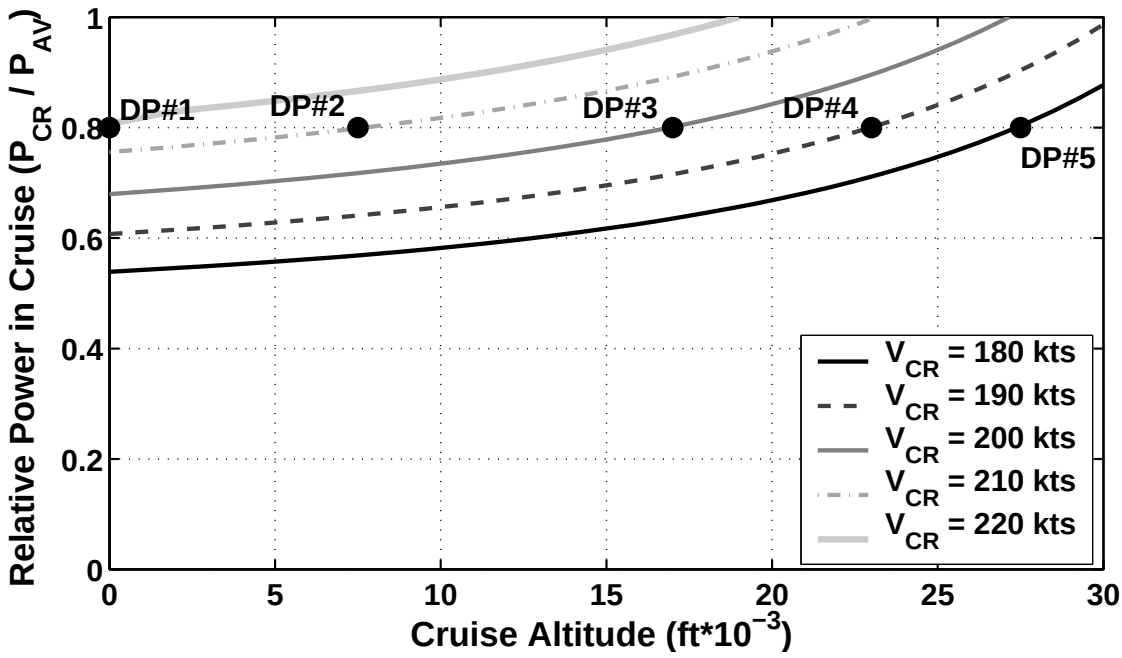

Figure 3.47: MTR-SD relative power in cruise vs. cruise altitude and cruise speed.

Figure 3.47 shows the relative power of a sampling of design points resulting from various combinations of design cruise speed and altitude. A relative power equal to 1 is the maximum power available at altitude and a relative power equal to 0.8 is an estimate of the maximum continuous power available for the "rubber engine." Flying near (but not above) this value will lead to minimized specific fuel consumption. It is shown in Figure 3.47 that to cruise at or below the estimated maximum continuous power rating, lower speeds and/or lower altitudes than that of the full-scale combination must be selected. There are several sample design points that fall near the maximum continuous power that can be selected for further study. These design points are:

$$\begin{aligned}
&\text{DP\#1:} \quad V_{\text{cr}} = 180 \text{ kts}, \quad H_\rho = 27,000 \text{ ft} \\
&\text{DP\#2:} \quad V_{\text{cr}} = 190 \text{ kts}, \quad H_\rho = 23,000 \text{ ft} \\
&\text{DP\#3:} \quad V_{\text{cr}} = 200 \text{ kts}, \quad H_\rho = 17,000 \text{ ft} \\
&\text{DP\#4:} \quad V_{\text{cr}} = 210 \text{ kts}, \quad H_\rho = 7,500 \text{ ft} \\
&\text{DP\#5:} \quad V_{\text{cr}} = 220 \text{ kts}, \quad H_\rho = 0 \text{ ft}
\end{aligned}$$

There are clearly many other possible choices, but these design points serve as a basis to use when studying the behavior of the design characteristics with changes in cruise speed and altitude. Figures 3.48 through 3.50 show the changes in the overall design for various cruise combinations in terms of rotor size, takeoff weight, and wing span respectively.

For each cruise speed depicted in Figures 3.48 and 3.49, rotor size and takeoff weight are shown to initially decrease with increasing cruise altitude. The decrease in rotor size is the result of reductions in the required fuel weight, which stem from improvements in L/D at these higher altitudes. The steady, almost linear, decrease in the fuel requirements with increasing cruise altitude is shown in Figure 3.52. It is also shown in these cases that at some point, both rotor size and takeoff weight reach a trough, and then begin to increase with increasing cruise altitude. This increase in size is a result of the increasing wing area required to maintain the design lift coefficient at higher altitudes. This result is shown in Figure 3.50 in terms of wing span. In addition, the rapid increase in empty weight with cruise altitude because of wing growth is shown in Figure 3.51.

Varying cruise speed is also shown to have a strong effect on the overall design.

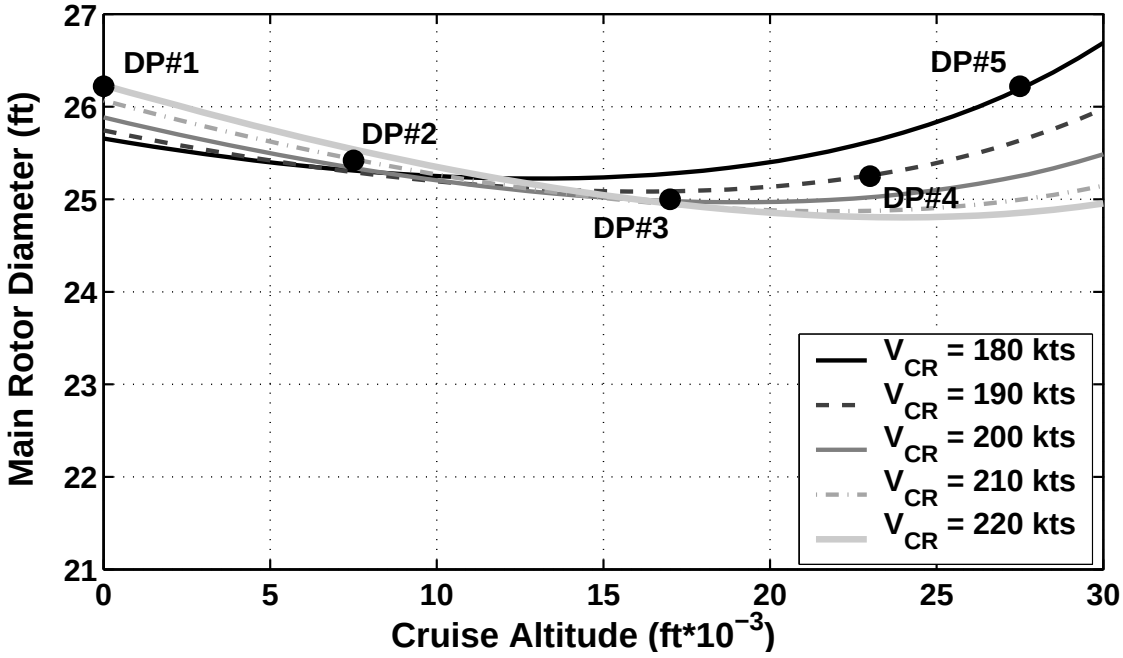

Figure 3.48: MTR-SD rotor diameter vs. cruise altitude and cruise speed.

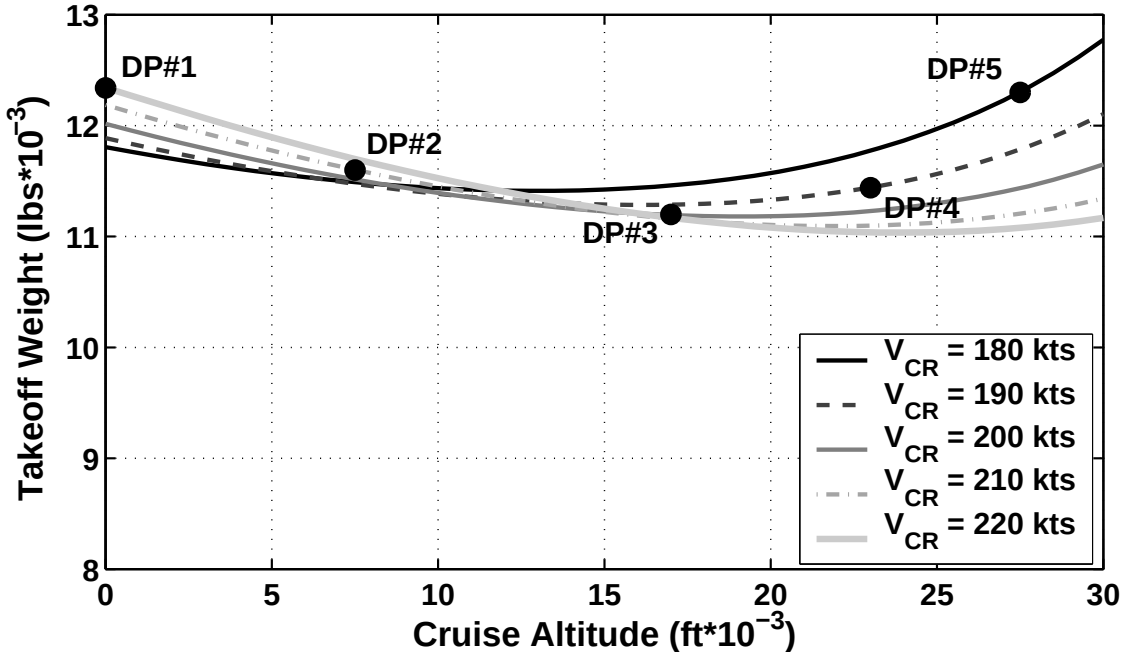

Figure 3.49: MTR-SD maximum takeoff weight vs. cruise altitude and cruise speed.

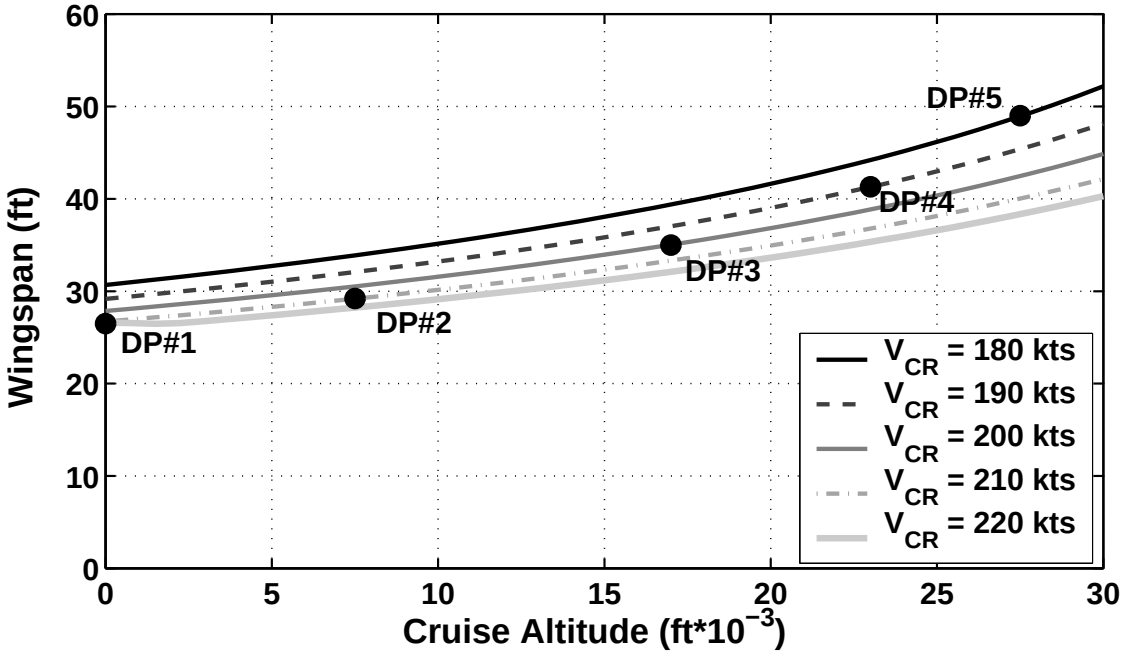

Figure 3.50: MTR-SD wingspan vs. cruise altitude and cruise speed.

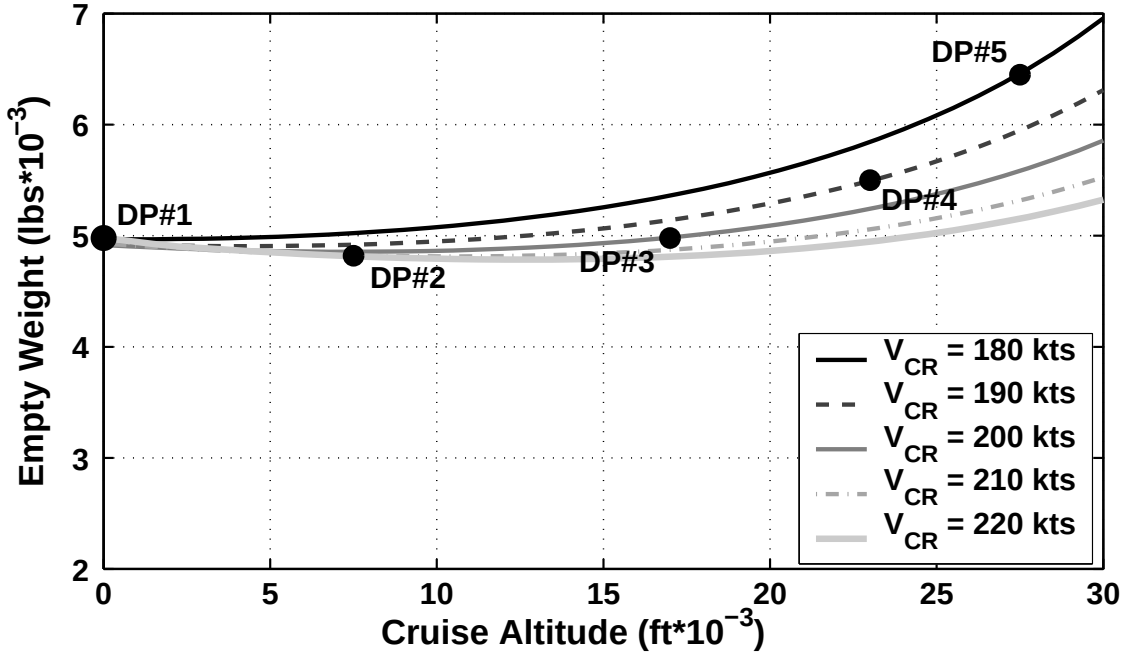

Figure 3.51: MTR-SD empty weight vs. cruise altitude and cruise speed.

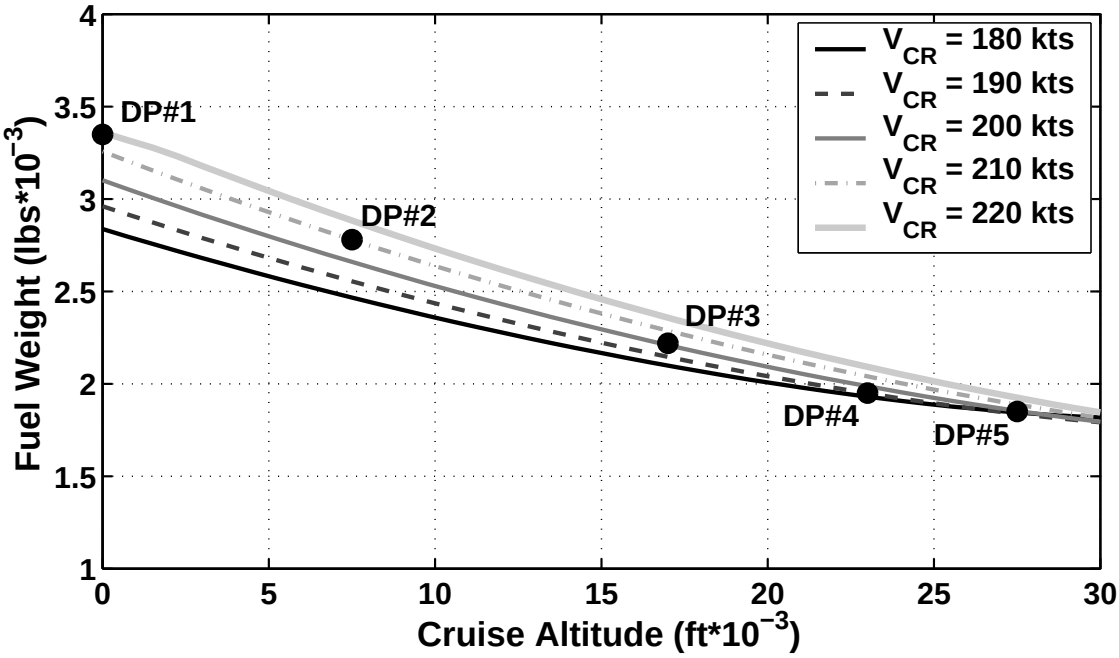

Figure 3.52: MTR-SD required fuel weight vs. cruise altitude and cruise speed.

Figures 3.48 and 3.49 show that the rotor size and takeoff weight increase with increasing cruise speed at lower cruise altitudes. This weight increase is the result of increasing power requirements at higher cruise speeds, which lead to more fuel burned (see Figure 3.52). At higher altitudes, it is shown that increasing cruise speed decreases rotor size and takeoff weight. In this case, the increase in fuel weight is being offset by greatly decreased required wing size and empty weight (see Figures 3.50 and 3.51.

It is shown in Figures 3.48 and 3.49 that design point 3 results in the minimum aircraft size in terms of rotor size and takeoff weight. Design point 3 is also shown to be the only point design compliant with the maximum rotor size of 25 ft. The other four design points are larger because of great increases in either fuel because of lower L/D (high cruise speed, low altitude) or empty weight because of increasing

wing size (low cruise speed, high altitude), as shown in Figures 3.50 through 3.52. While the wing span predicted at design point 3 (35 ft) is significantly larger than those predicted at design points 1 and 2 (28 ft and 30 ft respectively), this value still falls within the wing folding constraints set by the design. This larger wing span is also offset by large reductions in gross weight and fuel, as shown in Figures 3.49 and 3.52. In fact, the fuel requirements of design point 2 are 25% higher than those of design point 3, which would lead to greatly increased operating costs over the course of the service life span of the aircraft. Further reduction in fuel requirements could be obtained by choosing design point 4 or 5, but these design points result in wing spans that are too long for safe wing folding, which is critical to the MTR and MTR-SD design. For these reasons, design point 3 (200 kts, 17,000 ft) was selected as the optimal cruising profile for the MTR-SD.

MTR-SD Sizing Results

The MTR concept was optimized for the MTR-SD by decreasing the rotor disk loading, rotor solidity, and number of rotor blades. This led to improved hover efficiency, better weight efficiency and reductions in design complexity and cost. The wing aspect ratio was also reduced to meet the size constraints of the design. Finally, the mission profile was optimized to yield an MTR-SD design with great overall efficiency in the cruise condition. Table 3.4 lists the mission parameters for the MTR-SD design. Table 3.5 details the predicted sizing specifications of the MTR-SD. This point design meets all of the specified design requirements of

Payload (tons)	2
Radius of Action (nm)	350
Destination Hover (min)	20
Design Cruise Altitude (ft)	17,000
Design Cruise Speed (kts)	200

Table 3.4: Mission profile for MTR Scaled Demonstrator.

Max Takeoff Weight (lbs)	11,194
Empty Weight (lbs)	4,984
Empty Weight Fraction	0.445
Rotor Diameter (ft)	25.0
Rotor Disk Loading (lb/ft^2)	11.4
Number of Blades / Rotor	5
Rotor Solidity	0.123
Installed Power (shp)	2,288
Fuel Weight (lbs)	2,210
Fuel Fraction	0.197
Wingspan (ft)	35.0
Wing Area (ft^2)	175.3
Horizontal Tail Area (ft^2)	63.9
Vertical Tail Area (ft^2)	40.2

Table 3.5: Preliminary sizing for MTR Scaled Demonstrator.

the MTR-SD, while closely resembling the full-scale MTR point design in terms of overall geometry and proportions. Notice the similarities in empty weight fraction and fuel fraction between the MTR-SD and the previously sized heavy-lift, long-range MTR point design. Key differences include: fewer rotor blades, decreased rotor solidity, lower disk loading, a slower design cruise speed, and a reduction in the range capability. The MTR-SD was shown to be approximately 1/10 the size of the full-scale MTR point design (see Table 3.2), which is expected considering that it was required to carry 1/10th of the payload. The predicted component weights for the MTR-SD are given in Table 3.6.

Component	Weight (lb)
Main Rotor Blades (6 x 2)	353
Main Rotor Hub (2)	676
Main Rotor Gear Box	687
Swashplate	51
Control Hydraulics	71
Automatic Flight Control System	33
Engine Weight (2)	454
Engine Installation Weight	68
Auxiliary Power Unit	102
Fuel System	203
Landing Gear	223
Electrical System	91
Instrumentation/Avionics/Furnishings	336
Wing	582
Vertical Stabilizer	107
Horizontal Stabilizer	336
Trapeze Struts	36
Cargo Handling System	400
Tail Boom	36
Tilting Mechanism	112
Crew Compartment (structure)	0
Tilt Boom	56
Wing Folding Mechanism	6

Table 3.6: Predicted component weights for MTR Scaled Demonstrator.

3.4 MTR Performance Studies

This section reports on two comprehensive performance summaries performed for the MTR concept. The first of these studies predicts the performance of the MTR point design developed for the heavy-lift, long-range mission (20 tons, 1,000 nm) in the previous section. The second study predicts the performance of the MTR-SD, which was designed as a sub-scale representation of the previous design sized with reduced mission requirements (2 tons, 700 nm) in the previous section. These performance studies include investigation of power required curves, cruise speed specifications, rate of climb and altitude performance, and payload-range performance.

3.4.1 Performance of a Heavy-Lift Long-Range MTR

The sizing of the heavy-lift, long-range MTR point design was presented in Section 3.3, with the overall sizing results presented in Table 3.2. This study utilizes common aircraft performance methods including the generation and analysis of power required curves and payload-range graphs.

MTR Power Required for Flight Curves

To assess the performance of this particular MTR point design, an important first step is to generate the power required for flight curves with respect to true airspeed. To calculate the power required in helicopter mode, the following equation (presented in Section 2.2) was used.

$$P_{\text{req}_{\text{air}}} = \frac{1}{2\ \eta_{\text{prop}}\ \zeta_{\text{air}}} \rho V_{\text{air}}^3 f_{\text{air}} + \frac{1}{2\ \eta_{\text{prop}}\ \zeta_{\text{air}}} \rho V_{\text{air}}^3 S_{\text{w}} \frac{C_L^2}{\pi\ e_{\text{w}}\ AR_{\text{w}}} \tag{3.2}$$

This is the standard engine power required equation for an airplane including propro-tor efficiency, η_{prop}, mechanical efficiency, ζ_{air}, dynamic pressure and equivalent flat plate area, f_{air}, as developed in Section 2.2. The power requirements in helicopter mode were calculated with the following equation.

$$P_{\text{req}_{\text{hel}}} = \frac{\kappa W_{\text{TO}} \lambda_{\text{i}} (\Omega R)_{\text{MR}}}{\eta_{\text{pr}}\ \zeta_{\text{hel}}} + \frac{\sigma C_{d_0}}{8\ \eta_{\text{pr}}\ \zeta_{\text{hel}}}(1 + 4.65\ \mu^2)\rho A_{\text{MR}}(\Omega R)^3_{\text{MR}} + \frac{1}{2\ \eta_{\text{pr}}\ \zeta_{\text{hel}}}\rho V^3_{\text{hel}} f_{\text{hel}} \tag{3.3}$$

Where the three parts of this equation represent the induced, profile and parasitic components of the power required respectively. In the induced power component, the term λ_i represents the non dimensional inflow velocity through the disk, and is calculated iteratively based on the equation

$$\lambda_i = \mu \tan \alpha_{\text{tpp}} + \frac{C_{\text{T}}}{2\sqrt{\mu^2 + \lambda_i^2}} \tag{3.4}$$

Where α_{tpp} is the angle of attack of the tip path plane and μ is the advance ratio of the helicopter, as described by Leishman [22].

The power required curves for both flight modes at MSL conditions are shown in Figure 3.53. It is apparent that the power required in helicopter mode exceeds the available power at a much lower airspeed than the MTR in airplane mode, which illustrates the clear airspeed advantage that the conventional airplane possesses over the conventional helicopter. It is shown that if the power curves of the two flight modes were to be connected, there would be some conversion corridor (dashed line) over which the rotor tilts 90° forward gradually from a fully vertical orientation to the forward flight orientation. The stall speed of the MTR in airplane mode is shown to be nearly 107 knots for this point design, which would be the minimum

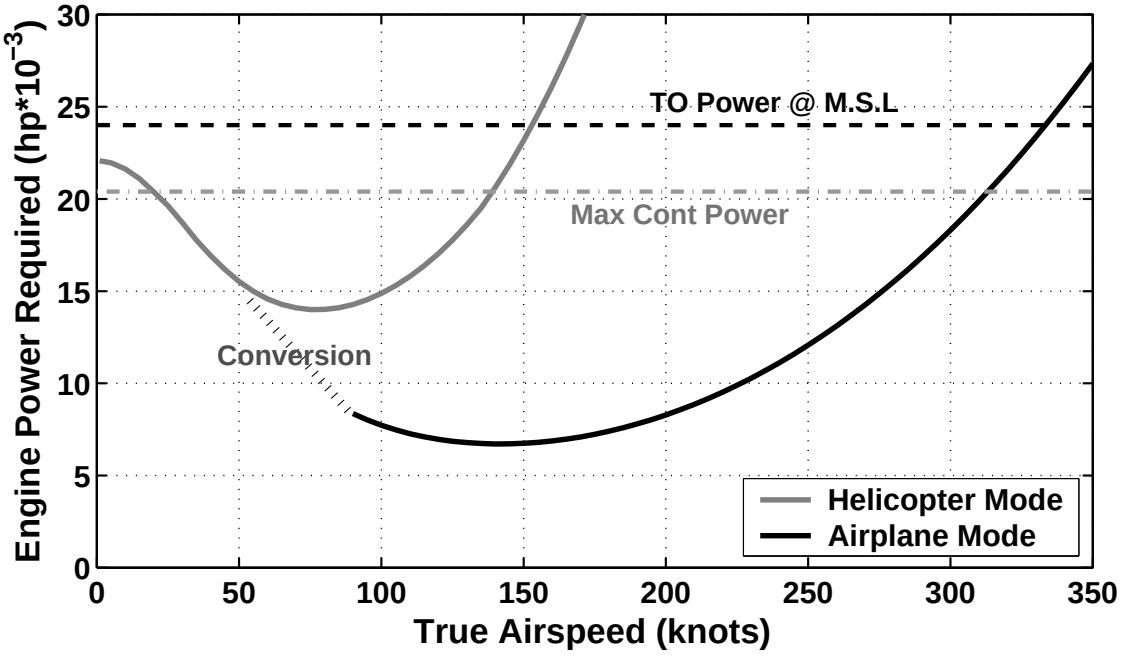

Figure 3.53: MTR engine power required versus airspeed at MSL conditions for both helicopter and airplane flight modes.

airspeed for the complete conversion to axial flight. The conversion could begin in helicopter mode at or near the airspeed for minimum power, which is shown to be approximately 75 knots. The specifics of this conversion corridor will be further defined and constrained by aeroelastic limitations of the rotor, the dermination of which is a matter for further study. It is also shown that maximum speeds in the neighborhood of over 300 knots might be possible in airplane mode at MSL conditions, although it should be noted that this study assumes a constant propulsive efficiency. Propulsive efficiency would likely be reduced at high speeds because of compressibility effects associated with high helicoidal tip Mach number, which measures the combination of the freesteam velocity and tip speed of the proprotor in cruise.

MTR Altitude and Climb Performance

The cruise speed capability as it varies with altitude is detailed in Figure 3.54. The cruise speeds depicted include best endurance speed, best range speed and the maximum continuous power speed. Best endurance speed is defined as the cruise speed at which a minimum fuel flow, or fuel weight per unit time (lb/h), is achieved. The best endurance speed will result in the maximum endurance, or flight time, for a given cruise altitude. Fuel flow is calculated as the product of power required and specific fuel consumption for a given cruise speed and altitude, i.e.,

$$\text{Fuel Flow} = P_{\text{cr}}\, SFC_{\text{cr}} \tag{3.5}$$

A short optimization routine was created to determine the cruise speed for minimum fuel flow (best endurance speed) based on Eqs. 3.2 and 3.5. The best range speed is defined as the cruise speed at which a minimum specific range, or distance per unit fuel weight (nm/lb), is achieved. Cruising at the best range speed will result in the maximum range for a given cruise altitude. Specific range is calculated in terms of the engine power requirements, specific fuel consumption and cruise velocity.

$$\text{Specific Range} = \frac{V_{\text{cr}}}{P_{\text{cr}}\, SFC_{\text{cr}}} \tag{3.6}$$

The cruise speed for minimum specific range (best range speed) was calculated in the same optimization routine as the best endurance speed. The cruise speed for maximum continuous power is simply the cruise speed that is obtained when operating at the maximum continuous power rating of the engine, which was assumed to be 80% of the engine's takeoff power rating. This maximum continuous speed

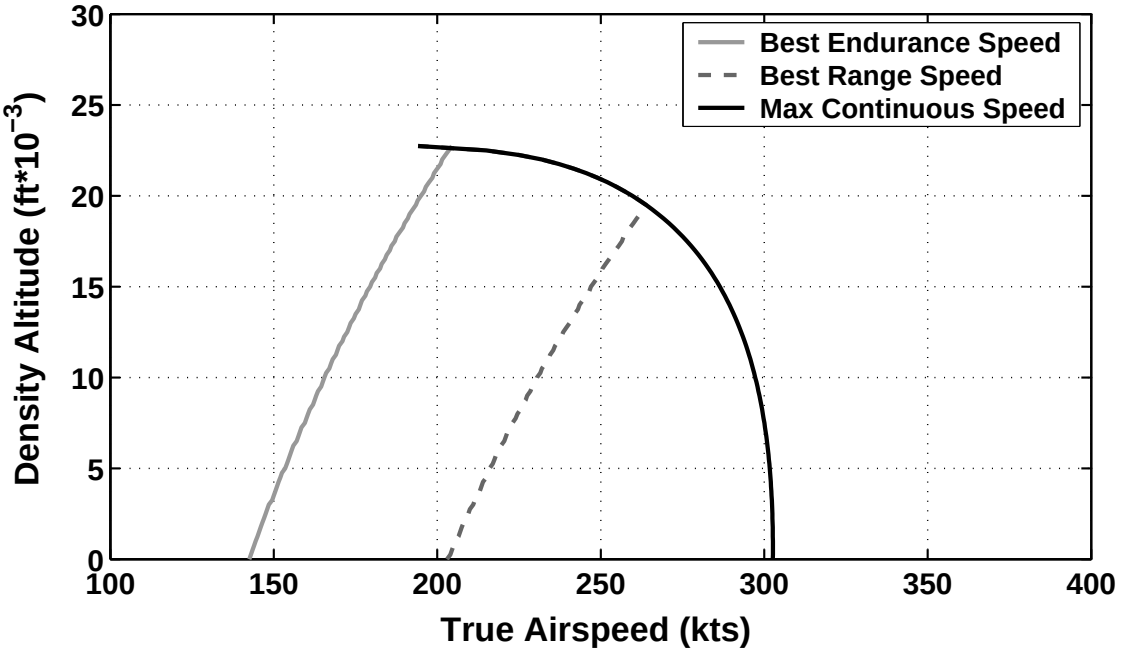

Figure 3.54: MTR best endurance, best range and max continuous power cruise speeds versus density altitude.

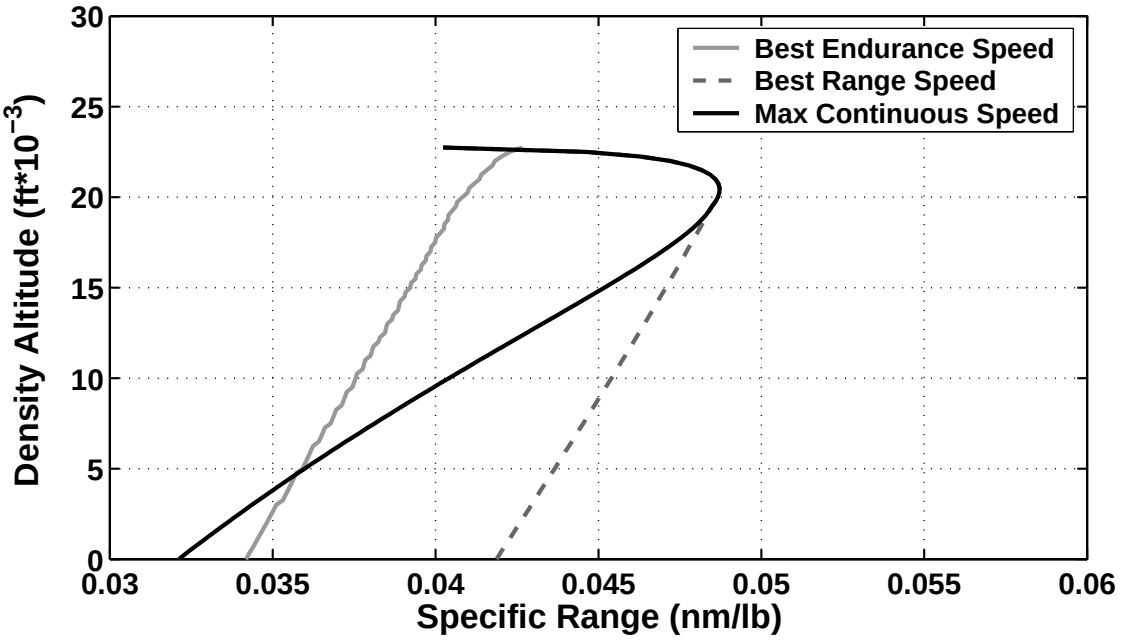

Figure 3.55: MTR specific range for various cruise speeds versus density altitude.

is essentially the fastest cruise speed possible for an indefinite period of time. In Figure 3.54 it is shown that the best endurance and best range speeds increase with increasing density altitude, while the max continuous cruise speed decreases at higher altitudes because of engine lapse. The design cruise speed of 260 knots is shown to be both the best endurance and the maximum continuous speeds at the design cruise altitude of 20,000 ft. For cruising at sea level, the predicted best range cruise speed is much lower at 205 knots. The results for specific range for the three cruise speeds at varying altitudes are shown in Figure 3.55. As expected, the results for the best range speed correspond to the highest specific range values. The design cruise condition (260 knots, 20,000 ft) is shown to be the point at which the maximum specific range is achieved, making it the most efficient cruise condition in terms of range capability. The maximum specific range of approximately 0.048 nm/lb when multiplied by the fuel weight (over 24,000 lb) indicates a range capability of over 1,100 nm after taking into account reserve and unusable fuel, which satisfies the original design requirements.

Another point of interest is the maximum continuous speed at MSL (300 knots), which results in a specific range of only 0.0325 nm/lb. If this cruise speed were achievable given the limits of propulsive efficiency, this would indicate a range capability of approximately 700 nm after accounting for reserve and unusable fuel. While this is a significant reduction from the capability in the design profile, this is still an impressive range for a VTOL aircraft, and the flight time would be significantly reduced in this mission when compared to cruising at the best range speed.

An important parameter in the assessment of aircraft performance is climb

capability, particularly the maximum rate of climb. The rate of climb for either flight mode is characterized by the ratio of the excess power to the aircraft gross weight given by

$$V_{\mathrm{C}} = \frac{P_{\mathrm{AV}} - P_{\mathrm{req}}}{W_{\mathrm{TO}}} \tag{3.7}$$

Vertical drag is also taken into account in cases of very high rate of climb speeds. The rate of climb capability for the MTR versus airspeed is shown in Figure 3.56 for both flight modes at MSL conditions. It is shown that the rate of climb capability for the MTR in airplane mode far exceeds that of the MTR in helicopter mode by over 1,000 ft/min. This is a result of the much lower power requirements in airplane cruise for the same available power (see Figure 3.53). The maximum rate of climb of the MTR in helicopter mode is approximately 2,800 ft/min, which is comparable to that of a Sikorsky CH-53E Super Stallion. The maximum rate of climb in airplane mode is approximately 4,000 ft/min, which is relatively high compared to conventional transport airplanes because of the abundance of available excess power on the MTR.

The effect of altitude on the maximum rate of climb in airplane mode is illustrated in Figure 3.57. The maximum rate of climb is calculated based on the best endurance cruise speed, which varies with density altitude. The altitude at which the maximum rate of climb is equal to zero is known as the absolute ceiling. The results are shown at the engine's maximum continuous power rating. Based on Figure 3.57, the ceiling at maximum continuous power is reached at approximately 22,000 ft. The absolute ceiling for the MTR point design, at maximum rated power, is reached at approximately 25,000 ft. The service ceiling is defined as the altitude

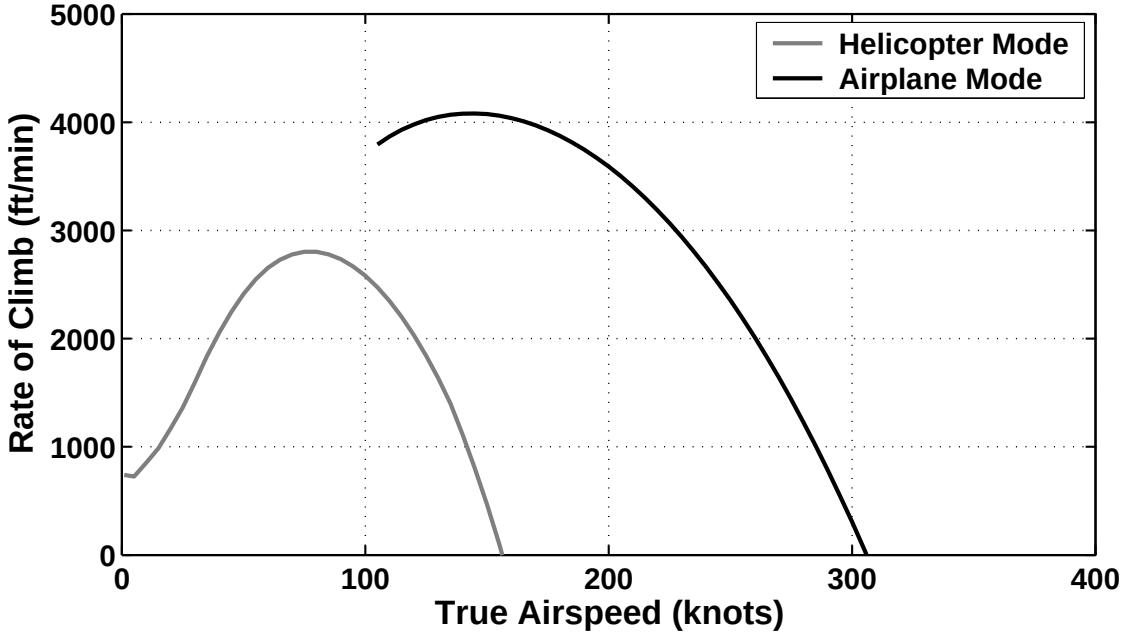

Figure 3.56: MTR rate of climb capability versus airspeed at MSL conditions for both flight modes.

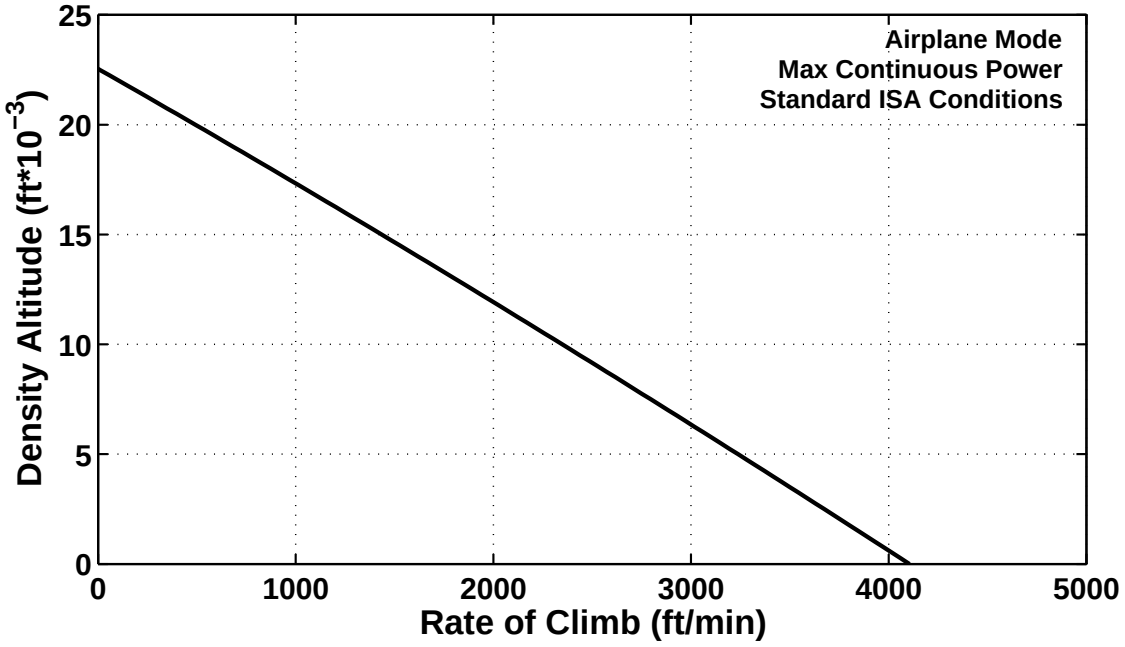

Figure 3.57: MTR maximum rate of climb capability versus density altitude in airplane mode.

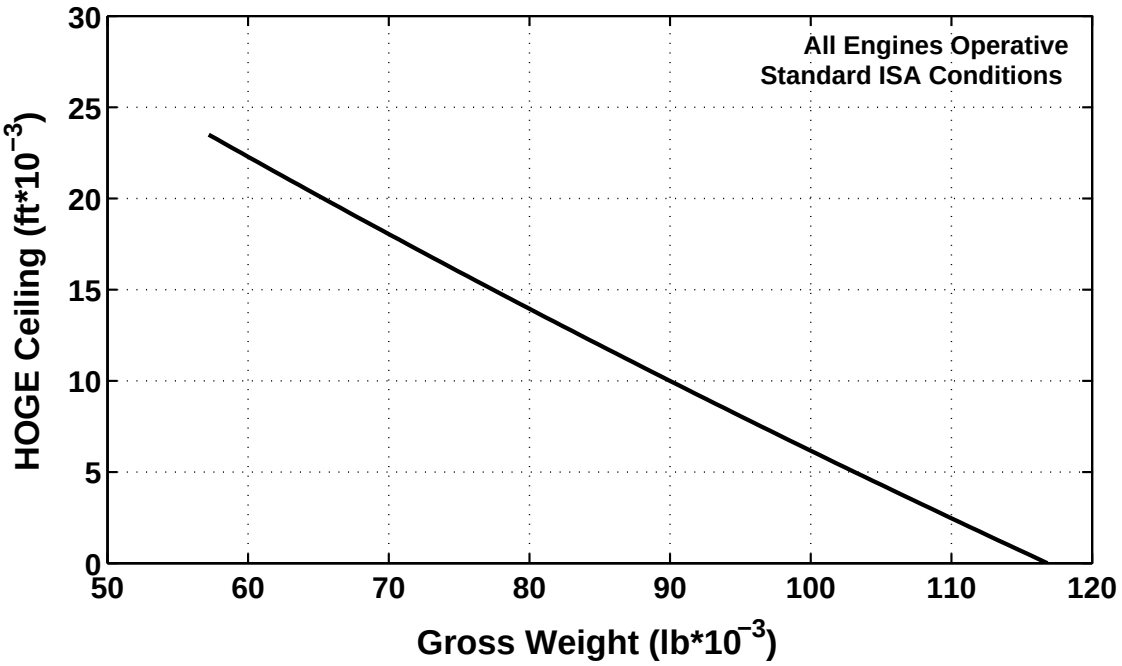

Figure 3.58: MTR hover out of ground effect ceiling versus aircraft gross weight.

at which the maximum rate of climb is 100 ft/min, which occurs for this point design at approximately 24,000 ft at maximum rated power.

The predicted hover out of ground effect (HOGE) ceiling for the heavy-lift, long-range MTR is shown versus aircraft gross weight in Figure 3.58. It is shown that the HOGE ceiling can be increased by decreasing the payload or fuel load of the aircraft with hover ceilings approaching 25,000 ft density altitude as the MTR approaches its empty weight of approximately 52,000 lb. If lightly loaded at 90,000 lb gross weight or less, it is predicted that the MTR hover ceiling would be in excess of 10,000 ft.

MTR Payload-Range Performance

Previously, an estimate of the payload-range performance of a particular MTR design point was shown in comparison to legacy helicopters (see Section 3.2). It was found that even with a non-optimized aircraft and mission profile, that the capability of the MTR was far greater than the heavy-lift rotorcraft currently in production. With the aircraft and mission profile optimized in the heavy-lift, long-range point design, the payload-range performance is increased even further, as shown in Figures 3.59 and 3.60. The payload is plotted versus mission radius for two mission profiles in Figure 3.59. These mission profiles include the design profile, which takes off at MSL conditions and cruises at the best range cruise speed and density altitude (260 knots, 20,000 ft), and a "hot and high" profile which takes off at 4,000 ft pressure altitude with ambient temperature of $95°F$, which also cruises at best range speed and altitude. Both mission profiles are of the radius of action type (Figure 2.3) with a 20 minute fuel reserve, and without any assumed hover time beyond that required to takeoff, convert between flight modes and climb. Additionally, both profiles were used without auxiliary fuel being limited by the maximum capacity of the fuel tank (over 24,000 lbs). The payload capability is seen to decrease sharply after this capacity is reached, because it is no longer possible to trade payload weight for additional fuel weight.

The more stringent "hot and high" takeoff condition is a common military requirement that leads to a significant degradation in the engine performance and power available. This results in reduced maximum takeoff weight of approximately

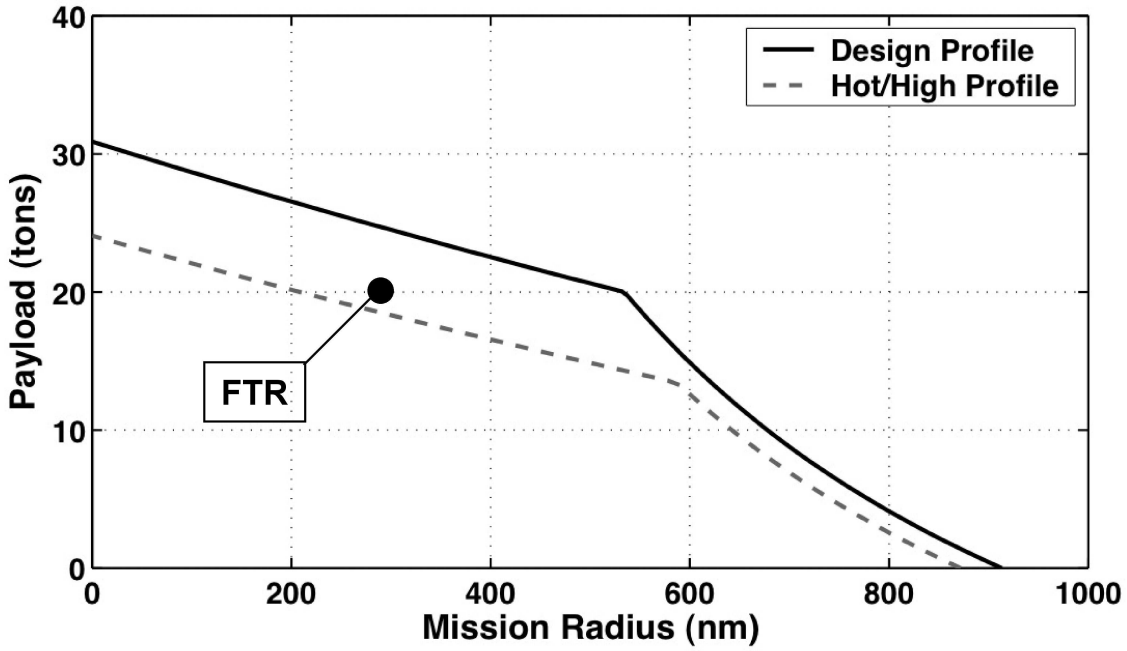

Figure 3.59: Payload versus mission radius for MTR design mission profile and "hot and high" profile

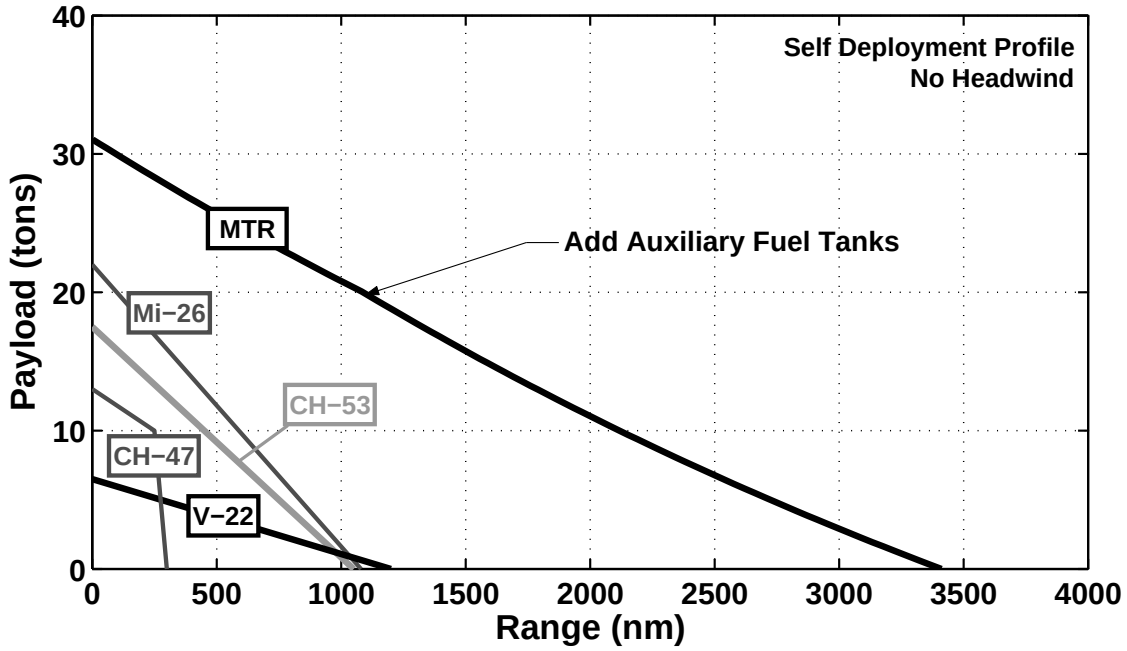

Figure 3.60: Payload versus range for MTR self-deployment profile compared with current rotorcraft.

103,500 lbs, which means that less fuel and payload can be carried to perform the mission. The result, as shown in Figure 3.59, is a dramatic decrease in the payload capability (approximately 6 tons less payload) for a given range. Both profiles show the same slope because of an identical cruise condition. The design requirement of a 20 ton payload being carried over a 500 nm ROA is shown to be exceeded in the design profile because of the reduction in the hover time requirements. The design profile shows the capability to carry a 27 ton payload over a 200 nm ROA or a 8 ton payload over a 700 nm ROA. The "hot and high" profile is predicted to potentially carry a 15 ton payload over a 500 nm ROA or a 20 ton payload over a 210 nm ROA. Despite the reduction in performance for the "hot and high" profile, the heavy-lift, long-range MTR very nearly meets the US Army's FTR requirements [8] shown in Figure 1.1. For larger values of mission radius where the fuel weight is limited by tank capacity, the discrepancy between the payload capability of the two mission profiles is greatly reduced.

The self deployment capability of the MTR design is predicted in Figure 3.60. This self deployment profile is of the singular cruise leg type (Figure 2.2), including a 20 minute fuel reserve, cruise at best range speed and altitude, no significant hover time requirements, and the use of auxiliary fuel tanks, when required. These auxiliary fuel tanks were calculated as simply being 15% of the additional fuel requirements for a given range, which is a conservative value allowing for the additional lines required to transmit fuel from the payload unit up to the engine. The results show that a maximum ferry range, or self deployment without payload, of nearly 3,500 nm is possible with the heavy-lift, long-range MTR design. This is a very

impressive deployment capability that would lead to incredible mission flexibility and set the MTR well apart from current heavy-lift rotorcraft designs. The overall performance summary of the MTR point design shows that if the MTR were to be technically realized as a heavy-lift rotorcraft, it could result in a very versatile aircraft with unprecedented performance potential.

MTR Drag Sensitivity Study

The drag of the heavy-lift, long-range MTR was estimated in the last chapter (see Section 2.2) with the end result of equivalent flat plate area of 37 ft^2 in airplane mode and 116 ft^2 in helicopter mode. While these results were carefully derived, making accurate estimations of drag at the conceptual level can be very difficult. Despite empirical data obtained on streamlining a rectangular box [20], the drag of the cargo handling system (CHS), including the payload unit and suspension struts, remains uncertain. For this reason it was decided to examine the effect of increased flat plate drag on the performance of the aircraft, particularly that of the CHS. The design excursion selected for this study was the case where the drag of the CHS was double that of the predicted value, giving an equivalent flat plate area in airplane mode of approximately 50 ft^2 and nearly 130 ft^2 in helicopter mode. This results in a 35% increase in overall flat plate drag in airplane mode, and a 12% increase in the drag of the helicopter mode configuration.

The effects of increased CHS drag on the MTR lift-to-drag ratio and engine power requirements are shown in Figures 3.61 and 3.62 respectively. The lift-to-drag

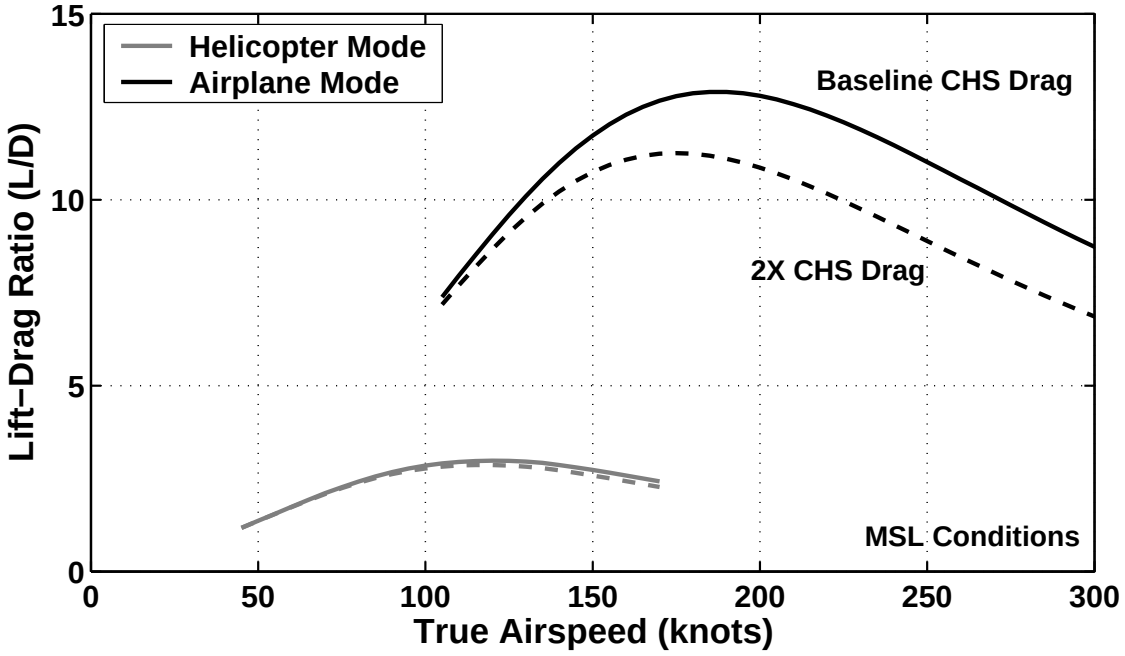

Figure 3.61: Lift-to-drag ratio of MTR with doubled CHS drag in both flight modes at MSL conditions.

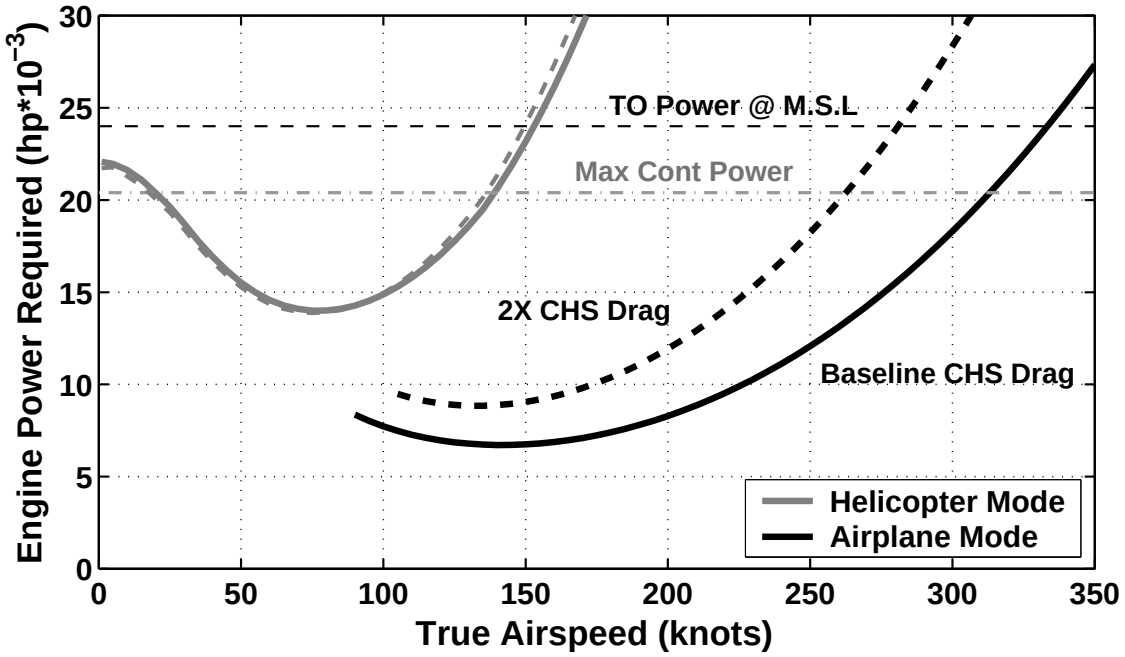

Figure 3.62: Engine power required curves of MTR with doubled CHS drag in both flight modes at MSL conditions.

ratio in airplane mode is shown to be reduced when doubling the CHS drag, from a maximum of nearly 13 down to a maximum L/D of 11 at MSL. Despite this decrease in performance, it still represents an aerodynamically efficient vehicle. The MTR L/D with doubled CHS drag is over twice that of a typical conventional helicopter. The lift-to-drag ratio in helicopter mode is shown to be relatively insensitive to increased CHS drag. This is a result of the already high flat plate area in helicopter mode. The engine power requirements at MSL conditions (Figure 3.62) are shown to significantly increase in airplane mode at higher cruise speeds with the increased CHS drag. For the case of doubled CHS drag, it is shown that the maximum cruise speed capability at MSL conditions is reduced from over 300 kts to 275 kts, which is still a significant forward flight velocity for a VTOL aircraft.

The cruise speed capability with varying altitude is shown for the case of doubled CHS drag along with that of the baseline CHS drag in Figure 3.63. It is shown that the best endurance, best range and max continuous cruise speeds are reduced at every altitude when doubling CHS drag. It is shown that the design cruise condition of the heavy-lift, long-range MTR (260 kts at 20,000 ft) would no longer be achievable with twice the CHS drag. The optimum cruise condition for maximum specific range becomes 235 kts at 17,000 ft. This condition leads to an increase in mission time and a decrease in range capability for the design fuel capacity.

The reduction in range capability for this increased CHS drag is shown in Figure 3.64. Despite the reduced performance, it is shown that the MTR with twice the CHS drag is still capable of carrying 20 tons nearly 1,000 nm without additional

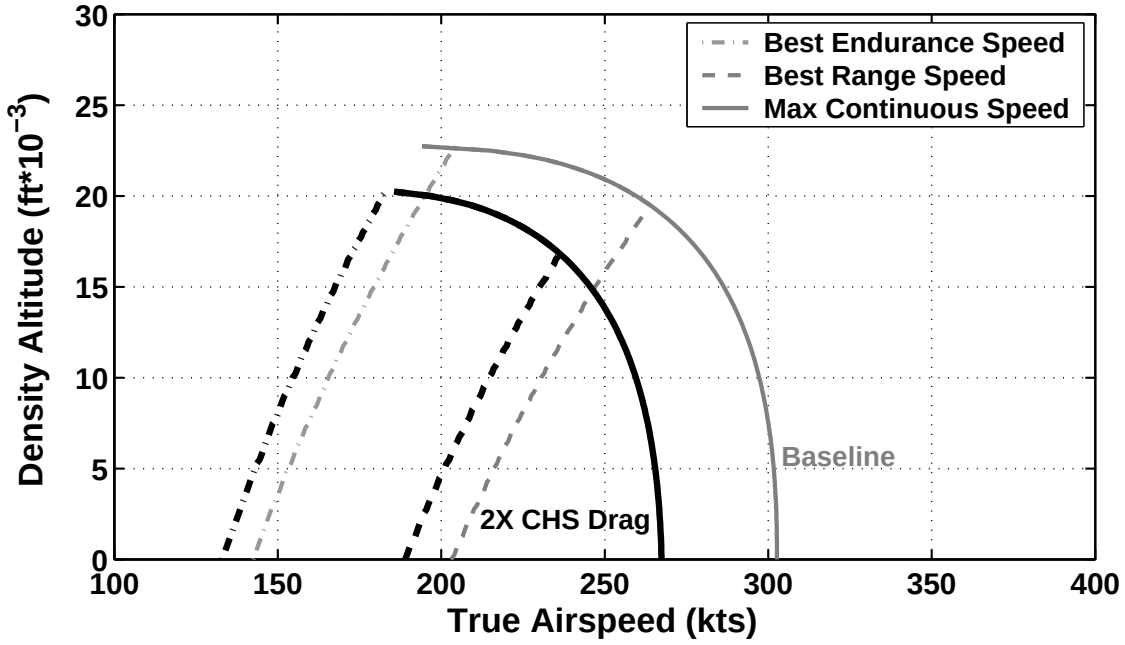

Figure 3.63: MTR best endurance, best range and max continuous power cruise speeds versus density altitude with doubled CHS drag.

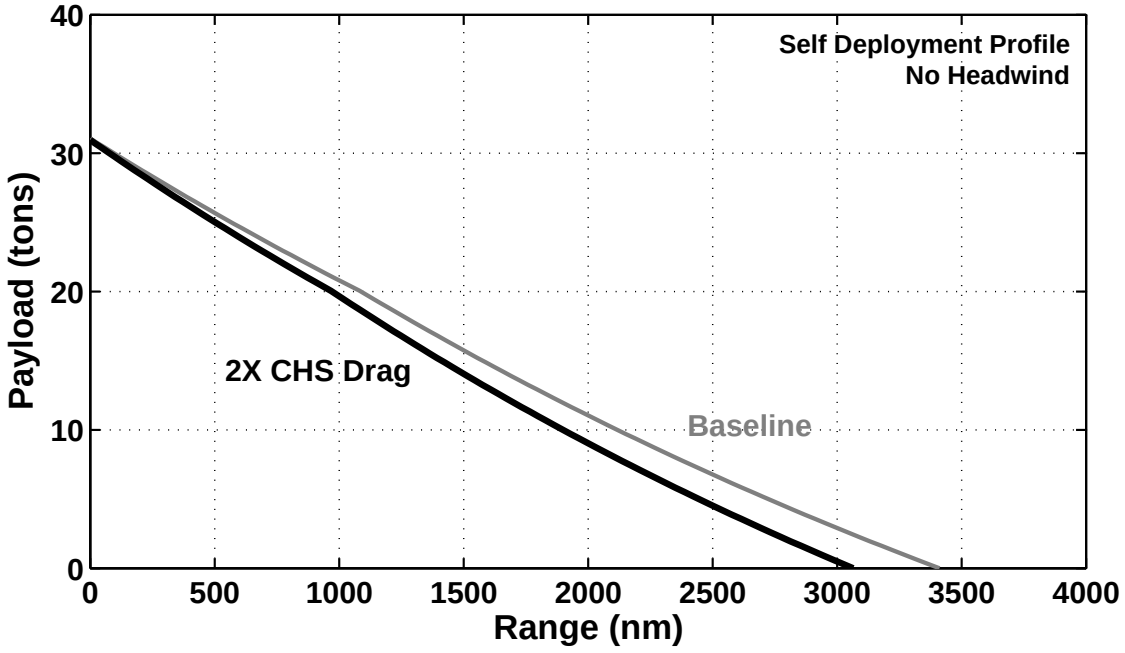

Figure 3.64: Payload versus range for MTR self-deployment profile with doubled CHS drag.

hover time requirements when cruising at 235 kts at 17,000 ft. Overall, the performance of the heavy-lift, long-range MTR is shown to be reduced with increased CHS drag, but the losses are not so significant that the potential performance advantages of the MTR concept are negated.

3.4.2 Performance of an MTR Scaled Demonstrator

A similar performance study was performed to project the performance for the MTR-SD that was sized in Section 3.3.3. Like the performance study for the heavy-lift, long-range MTR point design, the MTR-SD study contains power curves, altitude performance, and payload-range performance.

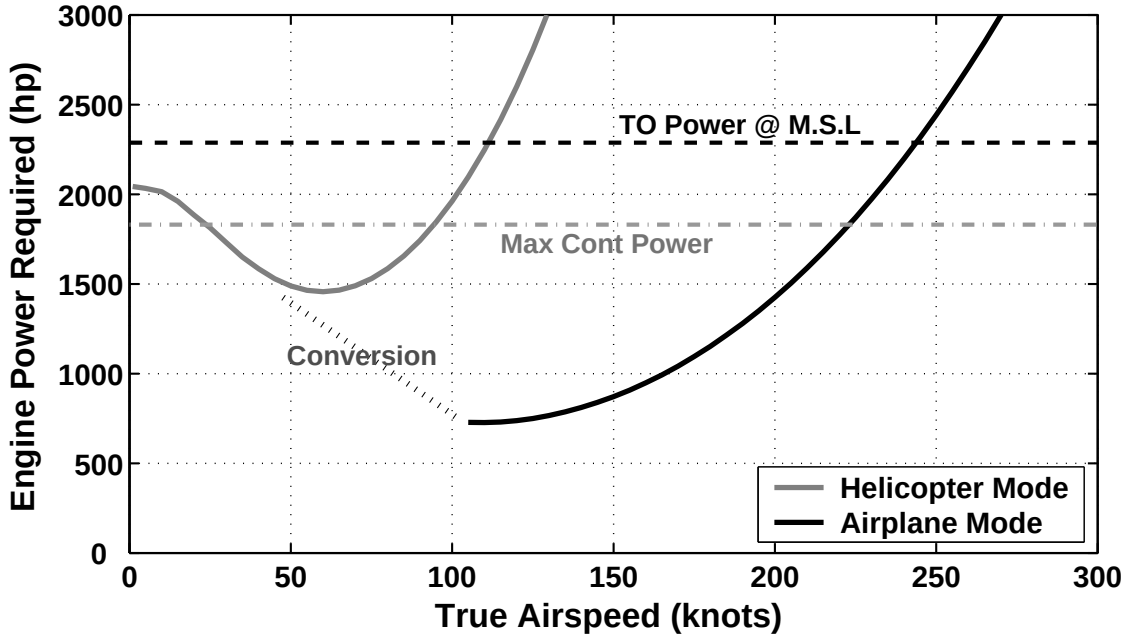

Figure 3.65: Engine power required versus airspeed of the MTR-SD at MSL conditions for both helicopter and airplane flight modes.

MTR-SD Power Required for Flight Curves

The power required curves for the MTR-SD were developed (see Section 3.4 for the methodology) for both flight modes at MSL conditions, as shown in Figure 3.65. The overall behavior was found to be similar to the power curves of the full-scale MTR (Figure 3.53). However, the power required and power available are an order of magnitude smaller for the MTR-SD, and the cruise speed capability in both flight modes is shown to be reduced. The maximum cruise speed using continuous power for the MTR-SD is shown to be in the neighborhood of 220 kts, as compared with the heavy-lift point design at approximately 300 kts.

MTR-SD Altitude and Climb Performance

The reduction in overall cruise speed capability of the MTR-SD is further detailed in Figure 3.66. These results show the change in best endurance, best range, and max continuous cruise speeds with changing cruise density altitude (see Section 3.4 for the methodology). The design cruise speed of 200 knots is shown to be the best range and max continuous speed at the design cruise altitude of 17,000 ft. It is also shown in Figure 3.67 that this combination of design cruise speed and altitude leads to the best specific range, or maximum distance per unit fuel weight. It should be noted that the values of specific range for the MTR-SD are an order of magnitude greater than those of the full-scale design because of the lower power requirements for the much smaller aircraft when carrying far less payload. The specific range value of the design mission profile is shown to be approximately 0.41 nm/lb, which

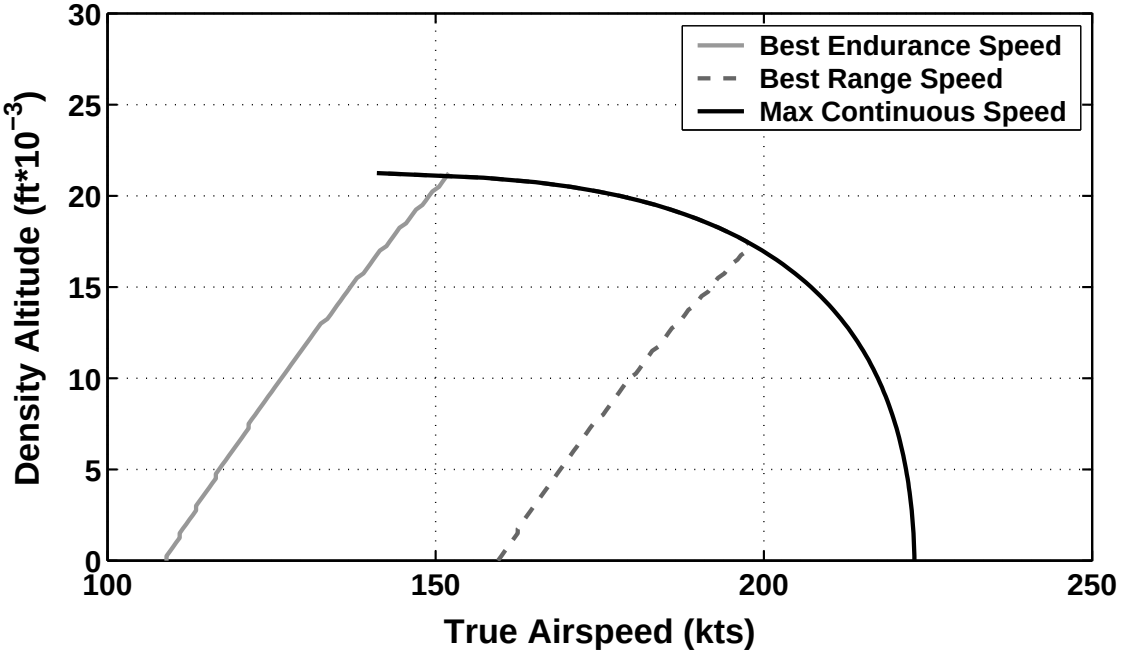

Figure 3.66: MTR-SD best endurance, best range and max continuous power cruise speeds versus density altitude.

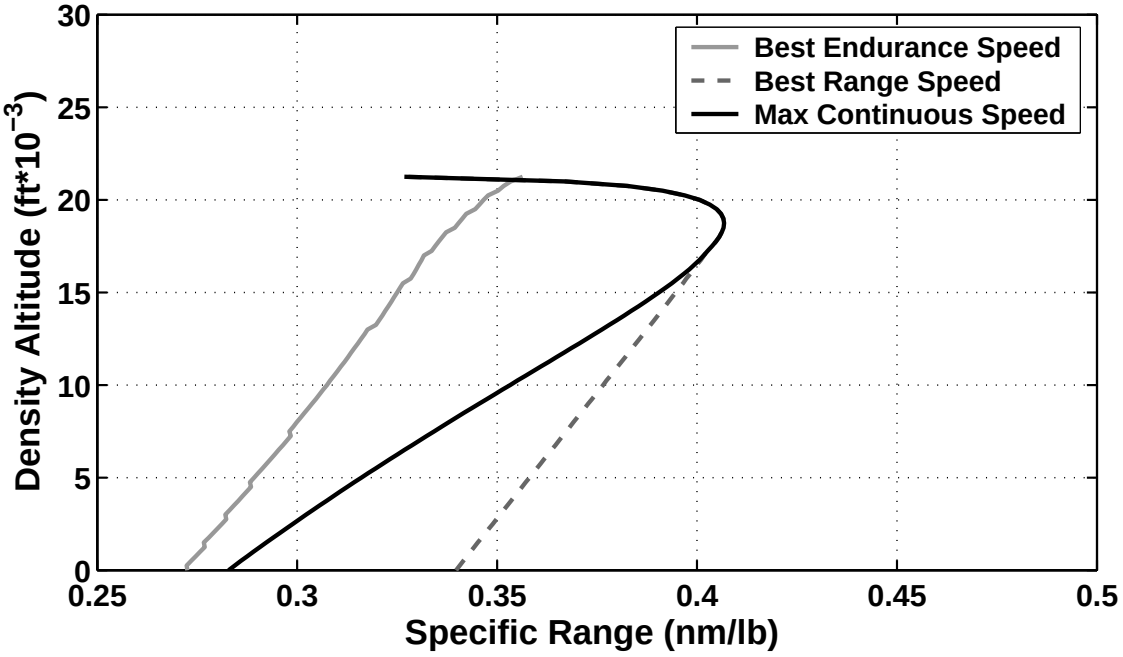

Figure 3.67: MTR-SD specific range for various cruise speeds versus density altitude.

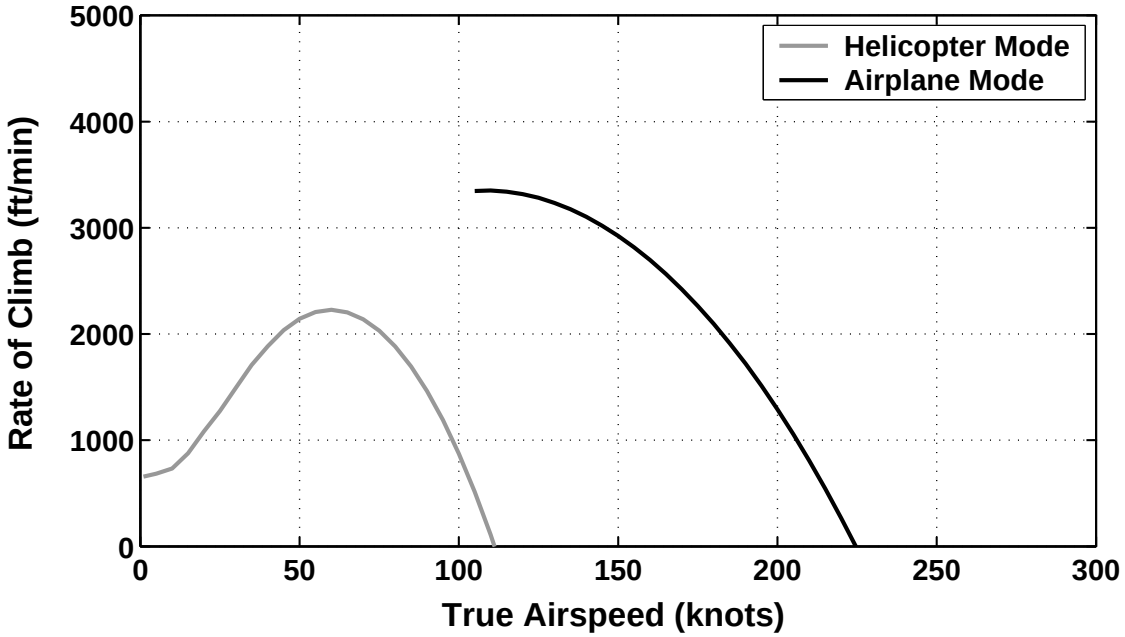

Figure 3.68: MTR-SD rate of climb capability versus airspeed at MSL conditions for both flight modes.

multiplied by the fuel capacity of the MTR-SD (over 2,200 lbs) indicates a range potential of approximately 800 nm when accounting for reserve and unusable fuel. This is in excess of the initial design requirements, which included a destination hover time of 20 minutes. If a mission were to require maximum speed, the MTR-SD is shown to have the capability to fly at 220 knots at MSL conditions. The specific range for this cruise condition is shown to be approximately 0.28 nm/lb, which would result in a reduced range capability of about 500 nm.

The rate of climb capability for the MTR-SD versus airspeed is shown in Figure 3.68 for both flight modes at MSL conditions. It is shown that the rate of climb capability for the MTR in airplane mode far exceeds that of the MTR in helicopter mode by approximately 1,000 ft/min. This is a result of the much lower power requirements in airplane cruise for the same available power (see Figure 3.65).

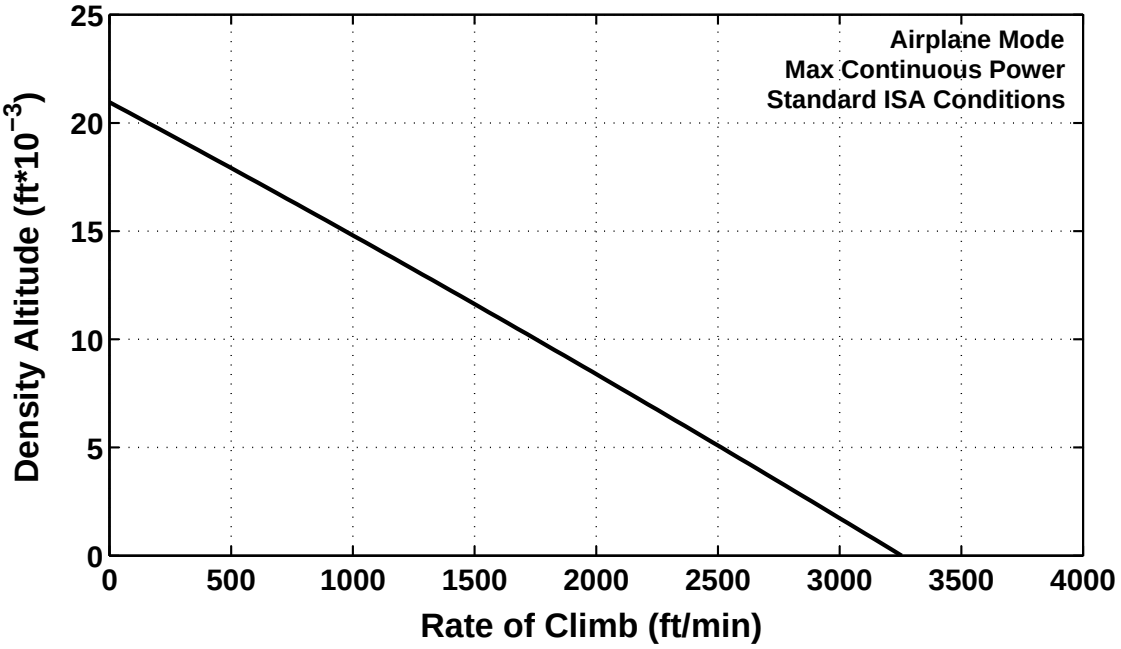

Figure 3.69: MTR-SD maximum rate of climb capability versus density altitude in airplane mode.

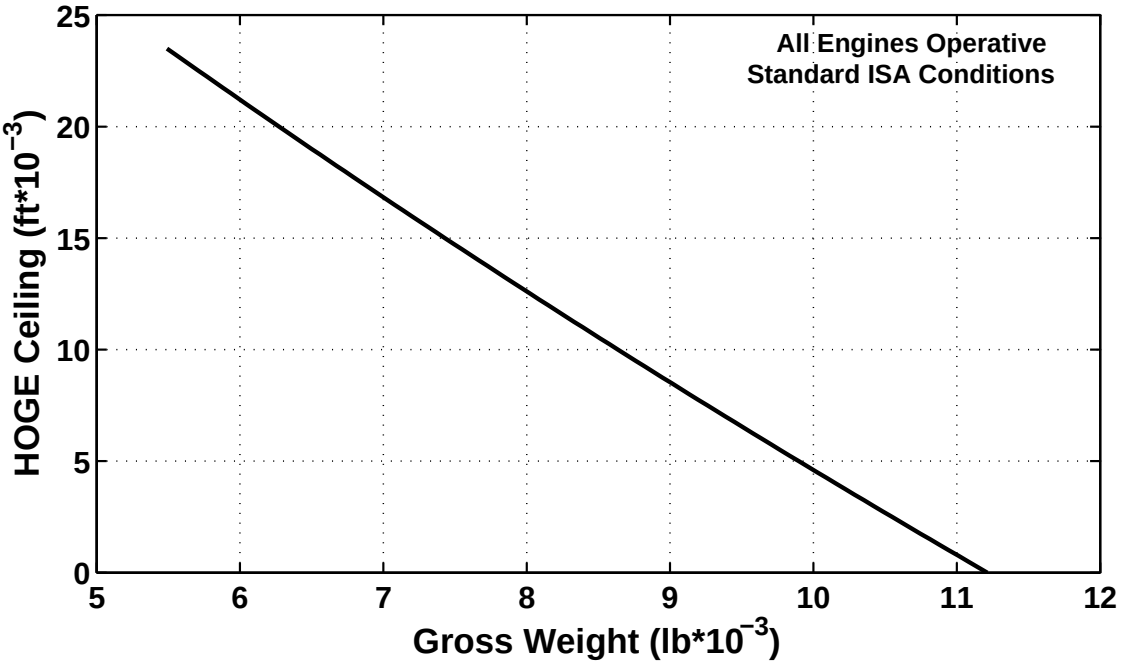

Figure 3.70: MTR-SD hover out of ground effect ceiling versus aircraft gross weight.

The maximum rate of climb of the MTR-SD in helicopter mode of 2,200 ft/min is comparable to that of a typical light, utility helicopter, while the maximum rate of climb in airplane mode of over 3,000 ft/min is comparable to that of the Kamov Ka-32, which is a coaxial helicopter with similar gross weight to the MTR-SD. The climb capability in both flight modes is significantly reduced relative to the full-scale point design (see Figure 3.56).

The effect of altitude on maximum rate of climb for the MTR-SD in airplane mode is depicted in Figure 3.69. The results show that the ceiling of the MTR-SD at maximum continuous power would be over 20,000 ft, as designed. The absolute ceiling at the engine's maximum power rating is reached at approximately 23,000 ft. These ceilings are slightly lower than those of the heavy-lift design point. The HOGE ceiling results are very similar to those of the full-scale MTR, as shown in Figure 3.70. When lightly loaded (8,500 lbs or less), the MTR-SD can achieve hover ceilings in excess of 10,000 ft.

MTR-SD Payload-Range Performance

A similar investigation of payload-range performance as that listed in Section 3.4 was completed for the MTR-SD. Payload is plotted versus mission radius for two mission profiles in Figure 3.71. These mission profiles again include the design profile, which takes off at MSL conditions and cruises at the best range cruise speed and density altitude (200 knots, 17,000 ft), and a "hot and high" profile which takes off at 4,000 ft pressure altitude with ambient temperature of 95°F, which also

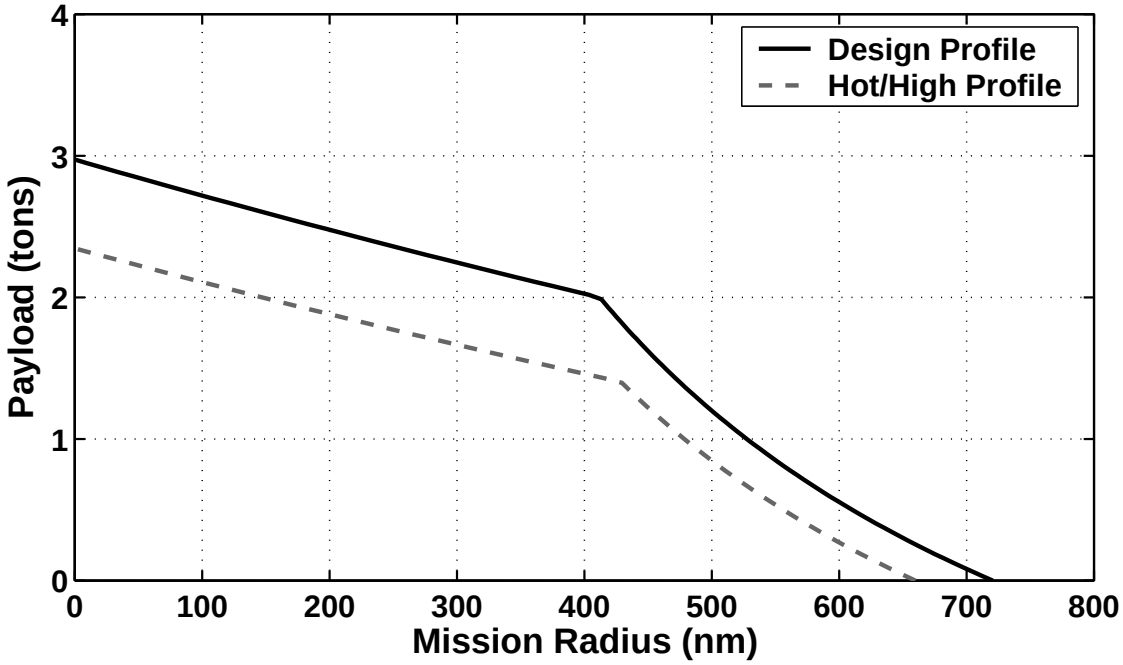

Figure 3.71: Payload versus mission radius for MTR-SD design mission profile and hot and high profile

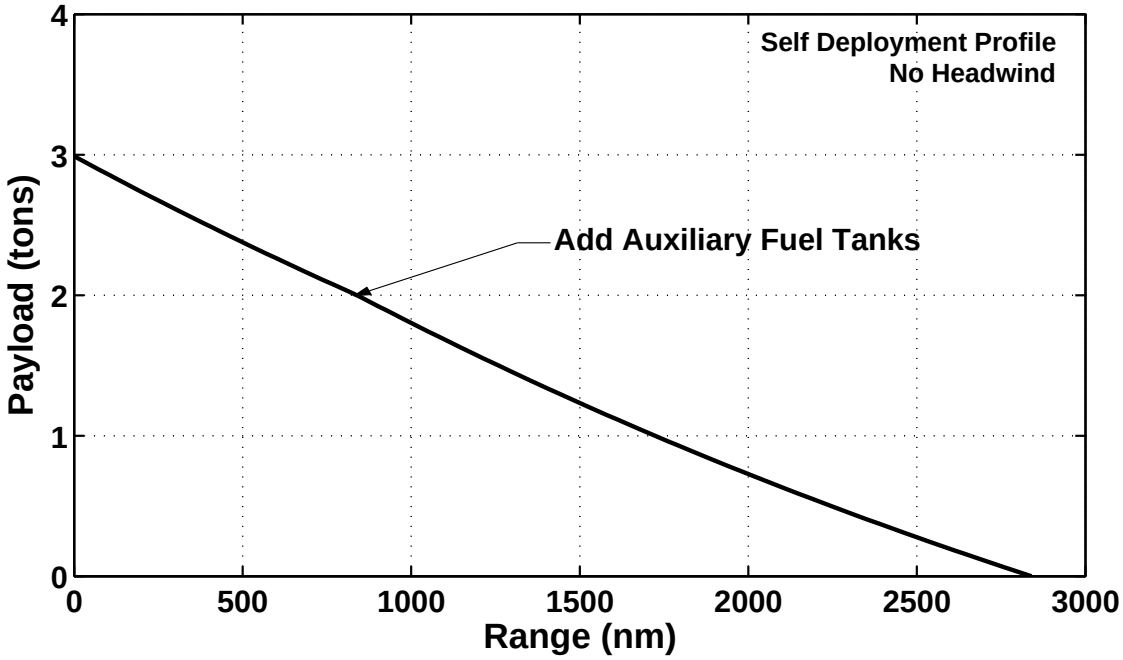

Figure 3.72: Payload versus range for MTR-SD self-deployment profile.

cruises at best range speed and altitude. As before, both mission profiles are of the radius of action type (Figure 2.3) with a 20 minute fuel reserve and without any assumed hover time beyond that required to takeoff, convert between flight modes and climb. Additionally, both profiles were used without auxiliary fuel being limited by the maximum capacity of the fuel tank (over 2,200 lbs). It is shown in Figure 3.71 that the design payload of 2 tons can be carried over a ROA in excess of 400 nm in the design profile, while the "hot and high" profile allows for 2 tons of payload to be carried over only a 150 nm ROA. This degradation in performance in the "hot and high" conditions is mainly a result of lapse in available engine power, which leads to a lower maximum takeoff weight of approximately 10,000 lbs. The predicted capability of the design profile also includes carrying payloads of nearly 3 tons over short distances, and carrying 1,000 lb of payload over a 600 nm ROA without the use of auxiliary fuel tanks. This is significantly better performance potential than is offered by any current similarly sized rotorcraft.

The self deployment profile for the MTR-SD is detailed in Figure 3.72. The mission profile and auxiliary fuel tanks assumed were the same as the self deployment profile for the full-scale MTR (see Section 3.4). It is shown that while the payload capability of the MTR-SD is approximately ten times less than the full-scale MTR, the range capability is not so significantly reduced. The MTR-SD is predicted to have a maximum ferry range capability of 2,800 nm, which is far greater than any helicopter or tiltrotor. While the overall performance predicted for the heavy-lift, long-range MTR is significantly greater than that predicted for the MTR-SD, the sub-scale design still offers impressive performance potential. If it were to be

successfully produced, the MTR-SD should prove to be an excellent platform to prove the great value and performance potential of the MTR concept.

3.5 MTR Cost Estimation

A preliminary cost estimate was performed for the MTR heavy-lift, long-range (20 ton payload, 500 nm ROA) point design, which was sized in Section 3.3. There has been a great deal of work in the rotorcraft and fixed-wing industries regarding cost estimation. While it would eventually possible to develop a cost analysis specifically for the MTR concept, including a detailed component breakdown, for this conceptual study it was decided to use an established rotorcraft technique developed by Harris and Scully [31]. This method estimates the aircraft's base price as a function of the empty weight, engine power requirements, number of blades per rotor, and several other factors according to the following equation.

$$\text{Base Price} = \$267\ H\ W_{\text{EW}}^{0.4638}\ P_{\text{ENG}_{\text{nom}}}^{0.5945}\ N_{\text{B}_{\text{MR}}}^{0.1643} \qquad \text{(1994 US Dollars)} \tag{3.8}$$

Where, H is a factor that takes into account such factors as engine type, number of engines, number of main rotors, country of manufacture and landing gear type.

This method was developed to estimate the price of helicopters, but the results show good correlation with the base price of the V-22 Osprey. For this reason, it was thought that this would serve as a good first approximation of the potential base price of the heavy-lift, long-range MTR. Recall that this MTR point design had an empty weight of 51,500 lb, engine power requirements of 24,600 shp, and six blades per main rotor. Applying these inputs to Equation 3.8, results in a base price of

$55.2 million in 1994 US Dollars, or $70.7 million in 2005 US Dollars for the MTR, adjusted according to the Consumer Price Index. This will likely serve as a lower bound for the MTR potential price because there will be a great deal of research and development costs required to bring this new concept into production, provided that the many technological challenges can be overcome. It should however be noted that according to the results from Section 3.2 and Equation 3.8, the estimated price of a conventional helicopter to carry a 20 ton payload over a 1,000 nm range is $90.6 million in 1994 US Dollars or $116 million in 2005 US Dollars. Therefore, if technically realized the MTR would be up to 40% less expensive than a conventional helicopter designed to meet the same heavy-lift, long-range mission requirements.

Chapter 4

Conclusions

The Mono Tiltrotor (MTR) has been proposed as an innovative VTOL concept that integrates a tilting coaxial rotor, an aerodynamically deployed folding wing, and an efficient cargo handling system. The MTR has been targeted to meet heavy-lift, long-range mission objectives, for which there is a growing need in the military. There are many technological issues that need to be addressed with the MTR, such as the ability to tilt a large coaxial rotor 90° without blade strikes or other failures related to aeroelastics. Other key technical issues include the ability to deploy the wings and tail from a folded position solely through aerodynamic forces, handling qualities issues related to the location of the crew compartment and the ability to build the suspension struts with sufficient strength to compensate for the large moments that may be created through the motion of the suspended load.

A series of conceptual design studies have been presented that were aimed at determining the potential value that this design concept would possess, if it were to be technically realized. A versatile rotorcraft sizing analysis was developed to perform sizing and weight predictions for conventional single rotor and coaxial helicopters and the MTR concept based on key input mission and design requirements. This analysis was based on previous work in the rotorcraft industry by Tishchenko [11] and many others, and was expanded to include the capability for sizing the

unique MTR concept.

This sizing methodology was validated against legacy helicopter sizing and component weights data. The validated analysis was then used to draw comparisons in terms of sizing and potential performance between the MTR concept and conventional and coaxial helicopters sized to perform the same heavy-lift, long range mission. Key mission and design trade studies were performed to study and refine the design concept and analytical methodology. Design point optimization was performed for two key objectives: a full scale, long-range, heavy-lift MTR, and a MTR Scaled Demonstrator. Finally, detailed performance studies were completed for each optimized point design. The following conclusions have been drawn from the conceptual design studies conducted in this thesis:

1. The design analysis developed was validated against historical sizing and weight data for legacy helicopters, including both single rotor conventional and coaxial dual rotor designs. Overall, the design predictions have shown satisfactory levels of correlation when compared to historical data, both for heavy-lift vehicles and otherwise.

2. The proposed ability to morph the MTR architecture to fixed-wing borne flight allows the vehicle to cruise at a substantially better lift-to-drag ratio and cruise speed than could be achieved with a conventional helicopter. This is the key to reducing overall vehicle weight, substantially improving its range, reducing fuel burn, and improving overall operational economics.

3. The coaxial rotor and the relatively lightweight overall design of the MTR

allow a much smaller vehicle with better weight efficiency than a conventional helicopter for any size of payload. This allows the MTR to carry less fuel and more useful payload over a longer flight range. Overall, the results suggest that if the MTR concept were to be technically realized, then it could be up to 50% smaller and up to 65% lighter than a conventional helicopter when carrying the same useful payload over the same distance.

4. It was found that significant increases in mission parameters, such as hover time or takeoff density altitude, result in either a marked increase in the overall aircraft size or notable degradations in the payload or range performance capabilities of the aircraft.

5. Optimizing the mission design for the best cruise speed and altitude lead to a significant reduction in the required fuel, driving down operating costs as well as the overall size and weight of the MTR aircraft. Also tailoring the design of the MTR for the use of modern, off-the-shelf, tiltrotor engine systems lead to significant reductions in the overall size. The size of the main rotor is substantially reduced, which leads to a smaller vertical footprint, perhaps enhancing the ship basing potential of the MTR.

6. When investigating the effects of significant drag increases on the performance of the MTR heavy-lift, long-range point design, the results showed noticeable losses in cruise speed and payload-range capability. However, the losses were not so significant that the potential performance advantages of the MTR concept were negated.

7. The sizing of the proposed MTR Scaled Demonstrator resulted in significant performance losses relative to the heavy-lift, long-range MTR point design. However, the performance predictions of the MTR-SD are sufficient to provide a platform that could demonstrate the potential advantages of the MTR concept.

8. While the resulting MTR point design optimized to carry a 20 ton payload over an unrefueled mission radius of action of 500 nm yields an aircraft that is very large with high potential acquisition costs, the value of having a large transport aircraft with both efficient vertical lift and long-range flight capability may very well outweigh such concerns.

Chapter 5

Future Work

To move forward in the development of the MTR concept, there are many analytical, experimental and design studies that must be performed. In particular, the ability to deploy the wings and tail solely through aerodynamic forces must be investigated. Studies have been initiated by the MTR team toward creating an analytical model to predict the kinematics of the wing and tail and an MTR Parametric Research Model (MTR-PRM) is currently being designed to test the deployment capability in the Glenn L. Martin Wind Tunnel at the University of Maryland.

Another key technical barrier of the MTR concept is the ability to tilt the coaxial proprotor system through a full 90° rotation. Aeroelastic modeling of the proprotor system as it moves through this trajectory will be necessary along with wind tunnel experiments to prove this ability and the fidelity of the modeling tools.

There is ongoing work at the University of Maryland related to the study of the MTR coaxial proprotor efficiency as a lifting rotor and a propellor. The proprotor is being optimized to be efficient in both flight modes, which is a difficult compromise. Once the initial design of the proprotor system is complete, it will be necessary to make accurate predictions of the flight loads and aeroelastics to determine if further changes in the design are necessary.

The sizing analysis developed and validated in this thesis should continue to be used as a resource for predicting the effects of any necessary design changes, and it should continue to be refined whenever new information becomes available in the detailed design process.

The detailed design phase of the MTR Scaled Demonstrator (MTR-SD) must be carefully performed such that the MTR-SD can be manufactured, tested and flown to prove the viability of the MTR concept. If this is successfully accomplished, scaling issues related to the dynamics and aeroelastics of the MTR must be analyzed and overcome before attempting to build a full-scale MTR aircraft.

Appendix A

Helicopter Sizing & Weight Equations

The following is a full list of sizing and weight equations used in this work for sizing conventional and coaxial helicopters. For some parameters, different equations are used depending on whether the helicopter is a conventional single rotor or a dual rotor coaxial design. These equations are marked accordingly. The analysis follows the same structure as described in the methodology section (Fig. 2.1).

TAKEOFF & FUEL WEIGHT

$$W_{\mathrm{TO}} = \frac{W_{\mathrm{PL}} + W_{\mathrm{crew}} + W_{\mathrm{MEP}} + W_{\mathrm{fuel_{hov}}}}{k_{\mathrm{WE}} - k_{\mathrm{FW}} - 0.005} \tag{A.1}$$

$$k_{\mathrm{FW}} = 1 - \exp\left(-\frac{L_{\mathrm{hel}} + V_{\mathrm{hel}}\, t_{\mathrm{RES_{hel}}}}{E_{\mathrm{hel}}}\right) \tag{A.2}$$

$$W_{\mathrm{fuel_{hov}}} = SFC_{\mathrm{hov}} N_{\mathrm{ENG}} P_{\mathrm{ENG}}\, t_{\mathrm{hov}} \tag{A.3}$$

$$W_{\mathrm{fuel}} = W_{\mathrm{TO}} \left(\frac{L_{\mathrm{hel}} + V_{\mathrm{hel}}\, t_{\mathrm{RES_{hel}}}}{E_{\mathrm{hel}}} + 0.005\right) + W_{\mathrm{fuel_{hov}}} \tag{A.4}$$

$$E_{\mathrm{hel}} = \frac{(L/D)_{\mathrm{hel}}\, \eta_{\mathrm{PR}}\, \zeta_{\mathrm{hel}}}{SFC_{\mathrm{hel}}} \tag{A.5}$$

MAIN ROTOR SIZING

$$\sigma_{\mathrm{MR}} = \frac{N_{B_{\mathrm{MR}}}}{\pi AR_{B_{\mathrm{MR}}}} \tag{A.6}$$

$$DL = \left(\frac{C_T}{\sigma}\right)_{\mathrm{MR}} \sigma_{\mathrm{MR}}\, \rho_{\mathrm{HOGE}}\, (\Omega R)^2_{\mathrm{MR}} \tag{A.7}$$

$$D_{\mathrm{MR}} = \sqrt{\frac{4W_{\mathrm{TO}}}{\pi DL}} \quad \text{for a conventional design} \tag{A.8}$$

$$D_{\mathrm{MR}} = \sqrt{\frac{2W_{\mathrm{TO}}}{\pi DL}} \quad \text{for a coaxial design} \tag{A.9}$$

POWER REQUIREMENTS

$$N_{\mathrm{ENG}}P_{\mathrm{ENG}} = \frac{(W_{\mathrm{TO}}\ t_{\mathrm{MR}})^{3/2}}{\sqrt{\pi/2}\ FM_{\mathrm{MR}}\ \zeta_{\mathrm{MR}}D_{\mathrm{MR}}\sqrt{\sigma_p}\sqrt{\rho_0}} \quad \text{(conventional)} \tag{A.10}$$

$$N_{\mathrm{ENG}}P_{\mathrm{ENG}} = \frac{(W_{\mathrm{TO}}\ t_{\mathrm{MR}})^{3/2}}{\sqrt{\pi/2}\ FM_{\mathrm{MR}}\ \zeta_{\mathrm{MR}}D_{\mathrm{MR}}\ \eta_{\mathrm{coax}}\sqrt{\sigma_p}\sqrt{\rho_0}} \quad \text{(coaxial)} \tag{A.11}$$

$$P_{\mathrm{ENG}_{\mathrm{nom}}} = P_{\mathrm{ENG}}C_{\mathrm{pow}} \tag{A.12}$$

$$SFC_{\mathrm{hov}} = C_{e_1} + C_{e_2}\left(\frac{P_{\mathrm{ENG}_{\mathrm{nom}}}}{P_{\mathrm{ENG}}}\right) \tag{A.13}$$

$$Q_{\mathrm{MR}} = \frac{(P_{\mathrm{ENG}}N_{\mathrm{ENG}})R_{\mathrm{MR}}\ \zeta_{\mathrm{MR}}}{(\Omega R)_{\mathrm{MR}}} \tag{A.14}$$

TAIL ROTOR SIZING

$$T_{\mathrm{TR}} = \frac{2Q_{\mathrm{MR}}}{(D_{\mathrm{MR}} + D_{\mathrm{TR}} + D_{\mathrm{off}})} \quad \text{conventional} \tag{A.15}$$

$$P_{\mathrm{TR}} = \frac{(T_{\mathrm{TR}}\ t_{\mathrm{TR}})^{3/2}}{\sqrt{\pi/2}\ FM_{\mathrm{TR}}\ \zeta_{\mathrm{TR}}D_{\mathrm{TR}}\sqrt{\sigma_p}\sqrt{\rho_0}} \quad \text{conventional} \tag{A.16}$$

$$Q_{\mathrm{TR}} = \frac{P_{\mathrm{TR}}R_{\mathrm{TR}}\zeta_{\mathrm{TR}}}{(\Omega R)_{\mathrm{TR}}} \quad \text{conventional} \tag{A.17}$$

$$Q_{\mathrm{TR}_{\mathrm{SH}}} = \frac{P_{\mathrm{TR}}f_{\mathrm{SH}}}{n_{\mathrm{SH}}} \quad \text{conventional} \tag{A.18}$$

$$\sigma_{\mathrm{TR}} = \frac{T_{\mathrm{TR}}}{(C_T/\sigma)_{\mathrm{TR}}\ \rho_0 A_{\mathrm{TR}}\ (\Omega R)^2_{\mathrm{TR}}} \quad \text{conventional} \tag{A.19}$$

$$c_{\mathrm{TR}} = \frac{\pi R_{\mathrm{TR}}\sigma_{\mathrm{TR}}}{N_{B_{\mathrm{TR}}}} \quad \text{conventional} \tag{A.20}$$

$$AR_{B_{\mathrm{TR}}} = \frac{R_{\mathrm{TR}}}{c_{\mathrm{TR}}} \quad \text{conventional} \tag{A.21}$$

CRUISE REQUIREMENTS

$$P_{\mathrm{cr_{hel}}} = \frac{W_{\mathrm{TO}} V_{\mathrm{hel}}}{(L/D)_{\mathrm{hel}}\ \eta_{\mathrm{pr}}\ \zeta_{\mathrm{cr}}} \quad \text{(conventional)} \tag{A.22}$$

$$P_{\mathrm{cr_{hel}}} = \frac{W_{\mathrm{TO}} V_{\mathrm{hel}}}{(L/D)_{\mathrm{hel}}\ \eta_{\mathrm{pr}}\ \eta_{\mathrm{coax}}\zeta_{\mathrm{cr}}} \quad \text{(coaxial)} \tag{A.23}$$

$$SFC_{\mathrm{cr}} = C_{e_1} + C_{e_2}\left(\frac{P_{\mathrm{ENG_{nom}}} N_{\mathrm{ENG}}}{P_{\mathrm{cr_{hel}}}}\right) \tag{A.24}$$

MAIN ROTOR WEIGHTS

$$W_{\mathrm{B_{MR}}} = k_{\mathrm{B_{MR}}}\left(\frac{\sigma_{\mathrm{MR}} R_{\mathrm{MR}}^{2.7}}{\bar{AR}^{0.7}}\right) \tag{A.25}$$

$$\bar{AR} = \frac{AR_{\mathrm{B_{MR}}}}{18} \tag{A.26}$$

$$W_{\mathrm{HUB_{MR}}} = k_{\mathrm{HUB_{MR}}} N_{\mathrm{B_{MR}}} f_{Z_{\mathrm{MR}}} \left(10^{-4} F_{CF_{\mathrm{MR}}}\right)^{N_{\mathrm{HUB}}} \quad \text{(for conventional)} \tag{A.27}$$

$$W_{\mathrm{HUB_{MR}}} = 2.25 k_{\mathrm{HUB_{MR}}} N_{\mathrm{B_{MR}}} f_{Z_{\mathrm{MR}}} \left(10^{-4} F_{CF_{\mathrm{MR}}}\right)^{N_{\mathrm{HUB}}} \quad \text{(for coaxial)} \tag{A.28}$$

$$N_{\mathrm{HUB}} = \begin{cases} 1.35 & \text{if } W_{\mathrm{PL}} \leq 6 \text{ tons} \\ 1.5 & \text{if } W_{\mathrm{PL}} > 6 \text{ tons} \end{cases} \tag{A.29}$$

$$f_{Z_{\mathrm{MR}}} = \begin{cases} 1 & \text{if } N_{\mathrm{B_{MR}}} \leq 4 \\ 1 + 0.05(N_{\mathrm{B_{MR}}} - 4) & \text{if } N_{\mathrm{B_{MR}}} > 4 \end{cases} \tag{A.30}$$

$$F_{CF_{\mathrm{MR}}} = \left(\frac{W_{\mathrm{B_{MR}}}}{N_{\mathrm{B_{MR}}}}\right)\left(\frac{(\Omega R)_{\mathrm{MR}}}{R_{\mathrm{MR}}}\right)^2 \frac{R_{\mathrm{MR}}}{2g} \tag{A.31}$$

TAIL ROTOR WEIGHTS

$$W_{\mathrm{B_{TR}}} = k_{\mathrm{B_{TR}}}\left(\frac{\sigma_{\mathrm{TR}} R_{\mathrm{TR}}^{2.7}}{\bar{AR}_{\mathrm{TR}}^{0.7}}\right) \tag{A.32}$$

$$\bar{AR}_{\mathrm{TR}} = \frac{AR_{\mathrm{B_{TR}}}}{18} \tag{A.33}$$

$$W_{\mathrm{HUB_{TR}}} = k_{\mathrm{HUB_{TR}}} N_{\mathrm{B_{TR}}} f_{Z_{\mathrm{TR}}} \left(10^{-4} F_{CF_{\mathrm{TR}}}\right)^{1.35} \tag{A.34}$$

$$f_{Z_{\mathrm{TR}}} \begin{cases} 1 & \text{if } N_{\mathrm{B_{TR}}} \leq 4 \\ 1 + 0.05(N_{\mathrm{B_{TR}}} - 4) & \text{if } N_{\mathrm{B_{TR}}} > 4 \end{cases} \tag{A.35}$$

$$F_{CF_{\mathrm{TR}}} = \left(\frac{W_{\mathrm{B_{TR}}}}{N_{\mathrm{B_{TR}}}}\right) \left(\frac{(\Omega R)_{\mathrm{TR}}}{R_{\mathrm{TR}}}\right)^2 \frac{R_{\mathrm{TR}}}{2} \tag{A.36}$$

TRANSMISSION WEIGHTS

$$W_{\mathrm{GB_{MR}}} = k_{\mathrm{GB_{MR}}} (Q_{\mathrm{MR}})^{0.8} \quad \text{(for conventional)} \tag{A.37}$$

$$W_{\mathrm{GB_{MR}}} = 1.3 k_{\mathrm{GB_{MR}}} (Q_{\mathrm{MR}})^{0.8} \quad \text{(for coaxial)} \tag{A.38}$$

$$W_{\mathrm{IGB}} = k_{\mathrm{IGB}} (Q_{\mathrm{TR_{SH}}})^{0.8} \tag{A.39}$$

$$W_{\mathrm{GB_{TR}}} = k_{\mathrm{GB_{TR}}} (Q_{\mathrm{TR}})^{0.8} \tag{A.40}$$

$$W_{\mathrm{SH}} = k_{\mathrm{SH}} C_{\mathrm{SH_G}} Q_{\mathrm{TR_{SH}}}^{0.8} l_{\mathrm{SH}} \tag{A.41}$$

$$l_{\mathrm{SH}} = \frac{(D_{\mathrm{MR}} + D_{\mathrm{TR}} + D_{\mathrm{off}})}{2} \tag{A.42}$$

ROTOR CONTROL WEIGHTS

$$W_{\mathrm{SP}} = k_{\mathrm{SP_1}} c^2 R_{\mathrm{MR}}\, \mu + k_{\mathrm{SP_2}} \tag{A.43}$$

$$\mu = \frac{V_{\mathrm{hel}} \cos \alpha_{\mathrm{TPP}}}{(\Omega R)_{\mathrm{MR}}} \tag{A.44}$$

$$W_{\mathrm{SP}} = 1.75 \left(k_{\mathrm{SP_1}} c^2 R_{\mathrm{MR}}\, \mu + k_{\mathrm{SP_2}}\right) \tag{A.45}$$

$$W_{\mathrm{BCS}} = k_{\mathrm{BCS_1}} c^2 R_{\mathrm{MR}} \mu + k_{\mathrm{BCS_2}} \tag{A.46}$$

$$W_{\text{AFCS}} \begin{cases} 165 \text{ lb} & \text{if } W_{\text{PL}} \leq 6 \text{ tons} \\ \\ 330 \text{ lb} & \text{if } W_{\text{PL}} > 6 \text{ tons} \end{cases} \tag{A.47}$$

AIRFRAME WEIGHTS

$$W_{\text{FUS}} = k_{\text{FUS}_1} W_{\text{TO}} + k_{\text{FUS}_2} W_{\text{PL}} + k_{\text{FUS}_3} \left(D_{\text{MR}} - D_{\text{ref}} \right) \tag{A.48}$$

$$W_{\text{INST}} = 0.075 W_{\text{PL}} \tag{A.49}$$

EMPENNAGE WEIGHT

$$W_{\text{EMP}} = k_{\text{EMP}} \, A_{\text{EMP}} = 0.005\pi \, k_{\text{EMP}} \, D_{\text{MR}}^2 \quad \text{(for conventional)} \tag{A.50}$$

$$W_{\text{EMP}} = k_{\text{EMP}} A_{\text{EMP}} = 0.015\pi \, k_{\text{EMP}} D_{\text{MR}}^2 \quad \text{(for conventional)} \tag{A.51}$$

POWERPLANT & FUEL SYSTEM WEIGHT

$$W_{\text{ENG}} = N_{\text{ENG}} \left(k_{\text{ENG}_1} P_{\text{ENG}} + k_{\text{ENG}_2} \right) \tag{A.52}$$

$$W_{\text{PIS}} = k_{\text{PIS}} W_{\text{ENG}} \tag{A.53}$$

$$W_{\text{FS}} = k_{\text{FS}} W_{\text{FUEL}} \tag{A.54}$$

$$W_{\text{APU}} = k_{\text{APU}_1} P_{\text{ENG}} + k_{\text{APU}_2} \tag{A.55}$$

ELECTRICAL SYSTEM WEIGHT

$$W_{\text{ES}} = k_{\text{ES}} \left(1 + 0.08 N_{B_{\text{MR}}} c_{\text{MR}} R_{\text{MR}} \right) \tag{A.56}$$

$$W_{\mathrm{LG}} = k_{\mathrm{LG}} W_{\mathrm{TO}} \tag{A.57}$$

$$W_{\mathrm{GHE}} = k_{\mathrm{GHE}} W_{\mathrm{PL}} \tag{A.58}$$

Appendix B
Correlation Coefficients and Weight Factors

AR_{HT}	4	
AR_{VT}	1.7	
C_{e_1}	0.386	lb/hp/hr
C_{e_2}	0.053	lb/hp/hr
C_{HT}	0.7	
C_{pow}	1.1	
C_{VT}	0.09	
$C_{L_{\mathrm{des}}}$	0.8	
$C_{\mathrm{SH_G}}$	1.1	
$(C_T/\sigma)_{\mathrm{MR}}$	0.075	
$(C_T/\sigma)_{\mathrm{MR}}$	0.075	
$(C_T/\sigma)_{\mathrm{TR}}$	0.08	
FM_{MR}	0.72	
FM_{TR}	0.67	
f_{SH}	1.80	
g	32.2	ft/s^2
$(L/D)_{\mathrm{hel}}$	4.60	
$(L/D)_{\mathrm{coax}}$	4.20	
n_{MTR}	5	

n_{SH}	4000	rpm
N_{ENG}	4	
N_{ult}	6	
P_{DC}	150	hp
t_{RES}	0.33	hr
t_{hov}	0.33	hr
t_{MR}	1.02	
t_{TR}	1.06	
$(t/c)_{\mathrm{w}}$	0.12	
$(t/c)_{\mathrm{HT}}$	0.12	
$(t/c)_{\mathrm{VT}}$	0.12	
V_{hel}	124	kts
V_{air}	260	kts
η_{pr}	0.98	
η_{coax}	0.85	
η_{prop}	0.60	
Λ_{w}	10	deg
Λ_{HT}	0	deg
Λ_{VT}	0	deg
ρ_0	.002377	slugs/ft^3
$(\Omega R)_{\mathrm{MR}}$	722	ft/s
$(\Omega R)_{\mathrm{TR}}$	722	ft/s

ζ_{cr}	0.88
ζ_{MGB}	0.96
ζ_{MR}	0.94
ζ_{TR}	0.975
ζ_{air}	0.92
k_{APU_1}	0.013
k_{APU_2}	88.2
$k_{\mathrm{B}_{\mathrm{MR}}}$	0.94
$k_{\mathrm{B}_{\mathrm{TR}}}$	1.25
k_{BCS_1}	1.56
k_{BCS_2}	66.2
k_{CHS}	0.05
k_{EMP}	2.46
k_{ENG_1}	0.16
k_{ENG_2}	176.4
k_{ES}	0.026
k_{FS}	0.04
k_{FUS_1}	0.095
k_{FUS_2}	0.09
k_{FUS_3}	0.013
$k_{\mathrm{GB}_{\mathrm{MR}}}$	0.172
$k_{\mathrm{GB}_{\mathrm{TR}}}$	0.226

k_{GHE}	0.05
$k_{\mathrm{HUB_{MR}}}$	16.6
$k_{\mathrm{HUB_{TR}}}$	8.27
k_{IGB}	0.272
k_{LG}	0.025
k_{PIS}	0.15
k_{SH}	0.0069
$k_{\mathrm{SP_1}}$	2.87
$k_{\mathrm{SP_2}}$	119
$k_{\mathrm{SS_1}}$	104
$k_{\mathrm{SS_2}}$	240646
$k_{\mathrm{SS_3}}$	2494.4
k_{TB}	0.005
k_{TM}	0.01
k_{WFM}	0.01
W_{crew}	440
W_{MEP}	0

Appendix C

Sample MTR Sizing Code (MATLAB)

MTR SIZING CODE – MAIN ROUTINE

```
% This is the main routine for the latest MTR design methodology. It establishes
the important initial values and calls various study based subroutines that call the
main calculation loops for a design output

clear; % clear workspace
clc;

% Unit Conversions / Constants
N_lb=4.44822161525; % N to lbs (divide)
W_hp=745.699871582; % W to hp (divide)
nm_m=1852; % nm to m (multiply)
kt_ms=1.94384449244; % knots to m/s (divide)
N_Wsec_lb_hphr=603504; % N/W.sec to lb/hp.hr (divide)
N_m2_lb_ft2=47.8802589802; % N/mˆ2 to lb/ftˆ2 (divide)
m_ft=3.28083989502; % m to ft (multiply)
kmh_ms = 1/3.6; % km/h to m/s (multiply)
rpm_rads = pi/30; % RPM to rad/s (multiply)
g = 9.80665; % Acceleration due to gravity [m/sˆ2]
rho_0 = 1.22554; % Air density at sea level [kg/mˆ3.g]

% Initial Data for Performance Calculations
% Main Rotor
Ct_sig_mr = 0.075; % Ct/sigma ratio for main rotor
FM_mr = 0.72; % Figure of Merit for main rotor
V_tip_mr = 220; % Main rotor tip speed [m/s]
t_mr = 1.02; % Thrust loss of main rotor
eta_pr = 0.98; % Main rotor propulsive efficiency
k_int = 1.18;
```

```
eta_coax = 1/k_int;
zeta_cr_1 = 0.88; % Main rotor cruise power conversion efficiency (1 Main Rotor)
zeta_cr_2 = 0.94; % Main rotor cruise power conversion efficiency (2 Main Rotors)
zeta_mgb = 0.96; % Main transmission efficiency
zeta_mr_1 = 0.82; % Main rotor hover power conversion efficiency (1 Main Rotor)
zeta_mr_2 = 0.94; % Main rotor hover power conversion efficiency (2 Main Rotors)
eta_prop = 0.60; % Propellor efficiency of coax rotor system
zeta_air = 0.92; % Transmission efficiency in forward flight

% Tail Rotor
Ct_sig_tr = 0.08; % Ct/sigma ratio for tail rotor
FM_tr = 0.67; % Figure of Merit for tail rotor
V_tip_tr = 220; % Tail rotor tip speed [m/s]
n_mtr = 5; % Ratio of main rotor diameter to tail rotor diamter
f_sh = 1.80; % Transmission shaft torque overload factor
omega = 4000; % Shaft rotational velocity [RPM]
t_tr = 1.06; % Thrust loss of tail rotor
zeta_tr = 0.975; % Tail rotor hover power conversion efficiency

% Power Plant
N_eng = 4; % Number of engines
Ce_1 = 0.175; % Specific fuel consumption coefficient [kg/hp.h]
Ce_2 = 0.024; % Specific fuel consumption coefficient [kg/hp.h]
C_pow = 1.1; % Nominal engine power factor
P_dc = 150; % Power consumption of pump, generator, other devices [hp]

% Mission Data for Performance Calculations
N_crew = 2; % Number of crew members
W1_crew = 100; % Weight of average crew member
W_crew = N_crew*W1_crew; % Total Crew weight
K = 4.60; % Initial Helicopter Lift to Drag Ratio
K_air = 10; % Initial Lift-drag ratio of airplane0
V_cr = 230; % Helicopter cruise velocity [km/h]
V_air = 445; % Cruise speed in airplane mode [km/h]

% Initial Data for Sizing Calculations
v_stall = 120/kt_ms; % Stall Velocity for Airplane Mode (m/s)
cl_max = 2.5; % Wing Max Lift Coefficient
```

```
AR_w = 7.5; % Wing Aspect Ratio
e_w = 0.9; % Wing Oswald Efficiency Factor
N_ult = 6; % Ultimate load factor
t_c_w = 0.12; % Average thickness-chord ratio for wing
lambda_w = 7/12; % Wing taper ratio (tip/root)
gam_w = 10*pi/180; % Wing sweep angle (rad)
Cvt = 0.09; % Volume coefficient for vertical tail
Cht = 1; % Volume coefficient for horizontal tail
gam_h = 0; % Horiz tail sweep angle (rad)
gam_v = 0; % Vert tail sweep (rad)
AR_h = 4; % Horiz tail aspect ratio
AR_v = 1.7; % Vert tail aspect ratio
N_strut = 2; % Number of trapeze struts

% Initial Data for Component Weight Calculations
k_growth=1; % Empty weight growth factor
k_mrb = 10.5; % Weight coefficient of main rotor blades
k_mrb_s = 14; % Weight coefficient of main rotor blades (smaller payloads)
k_trb = 14; % Weight coefficient of tail rotor blades
k_trb_s = 23; % Weight coefficient of tail rotor blades (smaller payloads)
k1_apu = 0.006; % Weight coefficients of auxilary power unit
k2_apu = 40;
k1_bcs = 25; % Weight coefficients of booster control system
k2_bcs = 30;
k1_eng = 0.072; % Weight coefficients of engine
k2_eng = 80;
k_eng_s = 1.13; % Weight coefficients of engine (smaller payloads)
k1_fus_1 = 0.095; % First Weight coefficient of fuselage (1 Main Rotor)
k1_fus_2 = 0.120; % First Weight coefficient of fuselage (2 Main Rotors)
k2_fus = 0.09; % Weight coefficients of fuselage
k3_fus = 0.02;
k1_fus_s = .115; % Weight coefficients of fuselage (smaller payloads)
k2_fus_s = 0.065;
k1_sp = 46; % Weight coefficients of swashplate
k2_sp = 54;
k_sp_s = 8; % Weight coefficients of swashplate (smaller payloads)
k_elsys = 1.9; % Weight coefficient of electrical system
k_empen = 12; % Weight coefficient of empennage
```

```
k_fs = 0.04; % Weight coefficient of fuel system
k_fs_s = 0.092; % Weight coefficient of fuel system (smaller payloads)
k_igb = 0.6; % Weight coefficient of intermediate gear box
k_igb_s = 0.7; % Weight coefficient of intermediate gear box (smaller payloads)
k_lg = 0.025; % Weight coefficient of landing gear
k_lg_s = 0.031; % Weight coefficient of landing gear (smaller payloads)
k_mgb = 0.38; % Weight coefficient of main rotor gear box
k_mgb_s = 0.5; % Weight coefficient of main rotor gear box (smaller payloads)
k_mrhub = 0.8; % Weight coefficient of main rotor hub
k_mrhub_s = 0.8; % Weight coefficient of main rotor hub (smaller payloads)
k_pis = 0.15; % Weight coefficient of powerplant installation system
k_sh_1 = 0.05; % Weight coefficient of shaft (1 Main Rotor)
k_sh_2 = 0.02; % Weight coefficient of shaft (2 Main Rotors)
k_sh_s = 0.1; % Weight coefficient of shaft (smaller payloads)
k_ghe = 0.05; % Weight coefficient of ground handling equipment
k_tgb = 0.5; % Weight coefficient of tail rotor gear box
k_tgb_s = 0.85; % Weight coefficient of tail rotor gear box (smaller payloads)
k_trhub = 0.5; % Weight coefficient of tail rotor hub
k_trhub_s = 0.85; % Weight coefficient of tail rotor hub (smaller payloads)
k1_strut = 1174705; % Coefficient for calculating strut surface area
k2_strut = 1131.23; % Coefficient for calculating strut surface area
rho_strut = 0.06*12^3/g*N_lb*m_ft^3; % Density of strut material epoxy/graphite
[kg/m^3]
k_plh = 0.05; % Weight coefficient for payload handling group (smaller payloads)

% Size MTR point designs (one at a time)
mtr(k_growth, t_c_w, eta_coax, rpm_rads, kmh_ms, N_lb, W_hp, nm_m, kt_ms, N_Wsec_lb_hphr,
N_m2_lb_ft2, m_ft, g, Ce_1, Ce_2, Ct_sig_mr, C_pow, FM_mr, K, P_dc, t_mr, N_eng,
eta_pr, rho_0, V_tip_mr, zeta_cr_1, zeta_cr_2, zeta_mgb, zeta_mr_1, zeta_mr_2, zeta_tr,
W_crew, k_mrb, k1_apu, k2_apu, k1_bcs, k2_bcs, k1_eng, k2_eng, k1_sp, k2_sp, k_elsys,
k_fs, k_lg, k_mgb, k_mrhub, k_pis, v_stall, cl_max, AR_w, e_w, N_ult, lambda_w,
gam_w, Cvt, Cht, gam_h, gam_v, AR_h, AR_v, N_strut, eta_prop, zeta_air, K_air,
k1_strut, k2_strut, rho_strut, k_plh)

% Study influence of number of blades, solidity on design
blades_m(k_growth, t_c_w, eta_coax, rpm_rads, kmh_ms, N_lb, W_hp, nm_m, kt_ms,
N_Wsec_lb_hphr, N_m2_lb_ft2, m_ft, g, Ce_1, Ce_2, Ct_sig_mr, C_pow, FM_mr, K,
P_dc, t_mr, N_eng, eta_pr, rho_0, V_tip_mr, zeta_cr_1, zeta_cr_2, zeta_mgb, zeta_mr_1,
```

zeta_mr_2, zeta_tr, W_crew, k_mrb, k1_apu, k2_apu, k1_bcs, k2_bcs, k1_eng, k2_eng, k1_sp, k2_sp, k_elsys, k_fs, k_lg, k_mgb, k_mrhub, k_pis, v_stall, cl_max, AR_w, e_w, N_ult, lambda_w, gam_w, Cvt, Cht, gam_h, gam_v, AR_h, AR_v, N_strut, eta_prop, zeta_air, K_air, k1_strut, k2_strut, rho_strut, k_plh)

% Mission trade studies
sizing_m(k_growth, t_c_w, eta_coax, rpm_rads, kmh_ms, N_lb, W_hp, nm_m, kt_ms, N_Wsec_lb_hphr, N_m2_lb_ft2, m_ft, g, Ce_1, Ce_2, Ct_sig_mr, C_pow, FM_mr, K, P_dc, t_mr, N_eng, eta_pr, rho_0, V_tip_mr, zeta_cr_1, zeta_cr_2, zeta_mgb, zeta_mr_1, zeta_mr_2, zeta_tr, W_crew, k_mrb, k1_apu, k2_apu, k1_bcs, k2_bcs, k1_eng, k2_eng, k1_sp, k2_sp, k_elsys, k_fs, k_lg, k_mgb, k_mrhub, k_pis, v_stall, cl_max, AR_w, e_w, N_ult, lambda_w, gam_w, Cvt, Cht, gam_h, gam_v, AR_h, AR_v, N_strut, eta_prop, zeta_air, K_air, k1_strut, k2_strut, rho_strut, k_plh)

% Cruise optimization studies
cruise_m(k_growth, t_c_w, eta_coax, rpm_rads, kmh_ms, N_lb, W_hp, nm_m, kt_ms, N_Wsec_lb_hphr, N_m2_lb_ft2, m_ft, g, Ce_1, Ce_2, Ct_sig_mr, C_pow, FM_mr, K, P_dc, t_mr, N_eng, eta_pr, rho_0, V_tip_mr, zeta_cr_1, zeta_cr_2, zeta_mgb, zeta_mr_1, zeta_mr_2, zeta_tr, W_crew, k_mrb, k1_apu, k2_apu, k1_bcs, k2_bcs, k1_eng, k2_eng, k1_sp, k2_sp, k_elsys, k_fs, k_lg, k_mgb, k_mrhub, k_pis, v_stall, cl_max, AR_w, e_w, N_ult, lambda_w, gam_w, Cvt, Cht, gam_h, gam_v, AR_h, AR_v, N_strut, eta_prop, zeta_air, K_air, k1_strut, k2_strut, rho_strut, k_plh)

% MTR performance studies
MTR_Performance(k_growth, t_c_w, eta_coax, rpm_rads, kmh_ms, N_lb, W_hp, nm_m, kt_ms, N_Wsec_lb_hphr, N_m2_lb_ft2, m_ft, g, Ce_1, Ce_2, Ct_sig_mr, C_pow, FM_mr, K, P_dc, t_mr, N_eng, eta_pr, rho_0, V_tip_mr, zeta_cr_1, zeta_cr_2, zeta_mgb, zeta_mr_1, zeta_mr_2 , zeta_tr, W_crew, k_mrb, k1_apu, k2_apu, k1_bcs, k2_bcs, k1_eng, k2_eng, k1_sp, k2_sp, k_elsys, k_fs, k_lg, k_mgb, k_mrhub, k_pis, v_stall, cl_max, AR_w, e_w, N_ult, lambda_w, gam_w, Cvt, Cht, gam_h, gam_v, AR_h, AR_v, N_strut, eta_prop, zeta_air, K_air, k1_strut, k2_strut, rho_strut, k_plh)

MTR SIZING CODE - POINT DESIGN ROUTINE

% This subroutine is called by the main design routine and establishes the mission and design inputs for a particular point design MTR, prints sizing outputs and calls routines that calculate performance.

function mtr(k_growth, t_c_w, eta_coax, rpm_rads, kmh_ms, N_lb, W_hp, nm_m, kt_ms, N_Wsec_lb_hphr, N_m2_lb_ft2, m_ft, g, Ce_1, Ce_2, Ct_sig_mr, C_pow, FM_mr, K, P_dc, t_mr, N_eng, eta_pr, rho_0, V_tip_mr, zeta_cr_1, zeta_cr_2, zeta_mgb, zeta_mr_1, zeta_mr_2, zeta_tr, W_crew, k_mrb, k1_apu, k2_apu, k1_bcs, k2_bcs, k1_eng, k2_eng, k1_sp, k2_sp, k_elsys, k_fs, k_lg, k_mgb, k_mrhub, k_pis, v_stall, cl_max, AR_w, e_w, N_ult, lambda_w, gam_w, Cvt, Cht, gam_h, gam_v, AR_h, AR_v, N_strut, eta_prop, zeta_air, K_air, k1_strut, k2_strut, rho_strut, k_plh)

% Design Inputs
config = 3; % Aircraft Configuration (1 = Conventional Helicopter, 2 = Coaxial Helicopter, 3 = MTR)
N_eng = 4; % Number of engines
N_mrb = 6; % Number of Main Rotor Blades (Per Rotor)
lambda_mrb = 14.75; % Main Rotor Blade Aspect Ratio
k_tran = 0.001; % Fuel Fraction for Transition
k_climb = 0.004; % Fuel Fraction for TOL, Climb and Descent

% Mission Inputs
mission = 2; % Mission Type (1 = Long Range Haul, 2 = Radius of Action, 3 = Helicopter Pickup)
W_pl_1 = 40000*N_lb/g; % Design Payload 1 [kg]
W_pl_2 = 40000*N_lb/g; % Design Payload 2 (If Applicable) [kg]
T_res = 0.33; % Time Reserve in Cruise [h]
Hp_1 = 0; % Pressure Altitude, Mission 1-3, Leg 1 [m]
Hp_2 = 20000/m_ft; % Pressure Altitude, Mission 1-3, Leg 2 [m]
Hp_3 = 0/m_ft; % Pressure Altitude, Mission 1-3, Leg 3 [m]
Hp_4 = 20000/m_ft; % Pressure Altitude, Mission 2-3, Leg 4 [m]
Hp_5 = 0; % Pressure Altitude, Mission 2-3, Leg 5 [m]
dT_1 = 0; % Change in Air Temperature Above MSL, Mission 1-3, Leg 1 [C]
dT_2 = 0; % Change in Air Temperature Above MSL, Mission 1-3, Leg 2 [C]
dT_3 = 0; % Change in Air Temperature Above MSL, Mission 1-3, Leg 3 [C]
dT_4 = 0; % Change in Air Temperature Above MSL, Mission 2-3, Leg 4 [C]

```
dT_5 = 0; % Change in Air Temperature Above MSL, Mission 2-3, Leg 5 [C]
L_2 = 926; % Range, Mission 1-3, Leg 2 [km]
L_4 = 926; % Range, Mission 2-3, Leg 4 [km]
V_hel = 220; % Helicopter Cruise Velocity, Mission 3, Leg 2 [km/h]
V_2 = 260*1.852; % Airplane Mode Cruise Velocity, Mission 1-2, Leg 2 [km/h]
V_4 = 260*1.852; % Airplane Mode Cruise Velocity, Mission 2, Leg 4 [km/h]
t_1 = 0; % Hover Time, Mission 1-3, Leg 1 [h]
t_3 = 0.33; % Hover Time, Mission 1-3, Leg 3 [h]
t_5 = 0; % Hover Time, Mission 2-3, Leg 5 [h]

% Run Main calculation loop
[k_we, DL, D_mr, W_to, W_empty, W_mrb, W_mrhub, W_mgb, W_eng, P_eng,
W_fuel, W_wing, W_hor, W_ver, W_boom, W_strut, W_plh, W_fs, W_cc, W_tb,
W_tm, b_w, S_w, sig_mr, lambda_mrb, Cl_4, K_4, P_2, P_eng_nom, Pa_2, E_2] =
calcs_m(mission, k_growth, t_c_w, eta_coax, L_2, L_4, W_pl_1, W_pl_2, lambda_mrb,
N_mrb, rpm_rads, kmh_ms, N_lb, W_hp, nm_m, kt_ms, N_Wsec_lb_hphr, N_m2_lb_ft2,
m_ft, g, config, Ce_1, Ce_2, Ct_sig_mr, C_pow, FM_mr, t_mr, N_eng, eta_pr, T_res,
rho_0, Hp_1, Hp_2, Hp_3, Hp_4, Hp_5, dT_1, dT_2, dT_3, dT_4, dT_5, t_1, t_3,
t_5, V_tip_mr, zeta_cr_1, zeta_cr_2, zeta_mgb, zeta_mr_1, zeta_mr_2, W_crew, k_mrb,
k1_apu, k2_apu, k1_bcs, k2_bcs, k1_eng, k2_eng, k1_sp, k2_sp, k_elsys, k_fs, k_lg,
k_mgb, k_mrhub, k_pis, V_2, V_4, V_hel, k_climb, k_tran, v_stall, cl_max, AR_w, e_w,
N_ult, lambda_w, gam_w, Cvt, Cht, gam_h, gam_v, AR_h, AR_v, N_strut, eta_prop,
zeta_air, K_air, k1_strut, k2_strut, rho_strut, k_plh);

% Print Design Outputs (english units)
W_to = W_to*g/N_lb
W_empty = W_empty*g/N_lb
D_mr = D_mr*m_ft
P_tot = P_eng*N_eng*1.1
W_fuel = W_fuel*g/N_lb
W_mrb = W_mrb*g/N_lb
W_mrhub = W_mrhub*g/N_lb
W_fs = W_fs*g/N_lb
W_mgb = W_mgb*g/N_lb
W_eng = W_eng *g/N_lb
W_wing=W_wing*g/N_lb
W_hor=W_hor*g/N_lb
W_ver=W_ver*g/N_lb
```

```
W_boom=W_boom*g/N_lb
W_strut=W_strut*g/N_lb
W_plh=W_plh*g/N_lb
W_cc=W_cc*g/N_lb
W_tb=W_tb*g/N_lb
W_tm=W_tm*g/N_lb

sig_mr
DL = DL*g/(N_lb*m_ft^2)
AR_w
S_w = S_w*m_ft^2
b_w = b_w*m_ft
EWF = W_empty/W_to
FF = W_fuel/W_to
Range = (L_2 + L_4)/1.852
% Plot power curves for point design
% power_curves(W_to, D_mr, S_w, P_eng, AR_w, sig_mr)
% Plot payload-range performance
% payload_range(L, E_2, T_res, W_crew, k_we, W_to*N_lb/g, V_2, g, N_lb)
```

MTR SIZING CODE - MAIN CALCULATION ROUTINE

% This subroutine is fed initial values and design parameters and runs the main sizing and weight calculation loop which calls the individual mission specific subroutines

function [k_we, DL, D_mr, W_to, W_empty, W_mrb, W_mrhub, W_mgb, W_eng, P_eng, W_fuel, W_wing, W_hor, W_ver, W_boom, W_strut, W_plh, W_fs, W_cc, W_tb, W_tm, b_w, S_w, sig_mr, lambda_mrb, Cl_4, K_4, P_2, P_eng_nom, Pa_2, E_2, c_mr, c_w, l_sep, S_h, S_v, l_strut] = calcs_m(mission, k_growth, t_c_w, eta_coax, L_2, L_4, W_pl_1, W_pl_2, lambda_mrb, N_mrb, rpm_rads, kmh_ms, N_lb, W_hp, nm_m, kt_ms, N_Wsec_lb_hphr, N_m2_lb_ft2, m_ft, g, config, Ce_1, Ce_2, Ct_sig_mr, C_pow, FM_mr, t_mr, N_eng, eta_pr, T_res, rho_0, Hp_1, Hp_2, Hp_3, Hp_4, Hp_5, dT_1, dT_2, dT_3, dT_4, dT_5, t_1, t_3, t_5, V_tip_mr, zeta_cr_1, zeta_cr_2, zeta_mgb, zeta_mr_1, zeta_mr_2, W_crew, k_mrb, k1_apu, k2_apu, k1_bcs, k2_bcs, k1_eng, k2_eng, k1_sp, k2_sp, k_elsys, k_fs, k_lg, k_mgb, k_mrhub, k_pis, V_2, V_4, V_hel, k_climb, k_tran, v_stall, cl_max, AR_w, e_w, N_ult, lambda_w, gam_w, Cvt, Cht, gam_h, gam_v, AR_h, AR_v, N_strut, eta_prop, zeta_air, K_air, k1_strut, k2_strut, rho_strut, k_plh)

% Calculate Density for Each Mission Leg
rho_1 = 1.22554*(1-0.0000225694*Hp_1)^4.2553 * 288/(288+dT_1);
rho_2 = 1.22554*(1-0.0000225694*Hp_2)^4.2553 * 288/(288+dT_2);
rho_3 = 1.22554*(1-0.0000225694*Hp_3)^4.2553 * 288/(288+dT_3);
rho_4 = 1.22554*(1-0.0000225694*Hp_4)^4.2553 * 288/(288+dT_4);
rho_5 = 1.22554*(1-0.0000225694*Hp_5)^4.2553 * 288/(288+dT_5);

% Calculate Density Ratio for Each Mission Leg
sigma_1 = rho_1/rho_0;
sigma_2 = rho_2/rho_0;
sigma_3 = rho_3/rho_0;
sigma_4 = rho_4/rho_0;
sigma_5 = rho_5/rho_0;

% Calculate Engine Losses for Each Mission leg
kh_1 = 1 / ((1-0.00007*Hp_1) * (1-0.00667*dT_1));
kh_2 = 1 / ((1-0.00007*Hp_2) * (1-0.00667*dT_2));
kh_3 = 1 / ((1-0.00007*Hp_3) * (1-0.00667*dT_3));

kh_4 = 1 / ((1-0.00007*Hp_4) * (1-0.00667*dT_4));
kh_5 = 1 / ((1-0.00007*Hp_5) * (1-0.00667*dT_5));

% Initial Values - first calculation of takeoff & empty weights
k_we = 0.59; % weight efficiency first estimate
er_kwe = 1; % weight efficiency error for while loop
Ce = Ce_1+Ce_2/.8; % SFC first estimate
L_tot = L_2 + L_4; % combined range
E_air = K_air*eta_prop*zeta_air/Ce * W_hp/(kmh_ms*g); % Vehicle Energy Efficiency
% estimate takeoff and empty weight
W_to = (W_pl_1 + W_crew) / (k_we - (1 - 1/exp((L_tot + T_res*V_2)/E_air)) - 0.005);
W_empty = (1-k_we)*W_to;
% Initial Rotor Sizing (Based on N_b and AR_b)
sig_mr = N_mrb/(pi*lambda_mrb); % Main Rotor Solidity
DL = Ct_sig_mr*sig_mr*rho_0*V_tip_mrˆ2/g; % TO Disk loading of Main Rotor
D_mr = sqrt(2*W_to/(pi*DL)); % Diamter of Main Rotor (Coaxial)
% Initial Wing Sizing S_w = W_to*g / (0.5*rho_1*(v_stall)ˆ2*cl_max);

% Main calculation Loop - iterates until design output achieved based on convergence of weight efficiency.
while (er_kwe 0.0000005)

% Performance / Fuel Burn Loop
% Long-range haul
if (mission==1) [P_eng, M_mr, W_fuel, W_to, D_mr, S_w] = m1(W_to, W_empty, W_crew, D_mr, S_w, DL, N_eng, W_pl_1, T_res, rho_0, rho_1, rho_2, V_2, L_2, sigma_1, sigma_3, kh_1, kh_2, kh_3, t_1, t_3, v_stall, cl_max, AR_w, e_w, k_tran, k_climb, t_mr, C_pow, FM_mr, eta_coax, eta_prop, zeta_air, zeta_mr_1, Ce_1, Ce_2, V_tip_mr, E_air, W_hp, g, kmh_ms);

% Radius of action
elseif (mission==2) [P_eng, M_mr, W_fuel, W_to, D_mr, S_w, Cl_4, K_4, P_2, P_eng_nom, Pa_2, E_2] = m2(W_to, W_empty, W_crew, D_mr, S_w, DL, N_eng, W_pl_1, W_pl_2, T_res, rho_0, rho_1, rho_2, rho_4, V_2, V_4, L_2, L_4, sigma_1, sigma_3, sigma_5, kh_1, kh_2, kh_3, kh_4, kh_5, t_1, t_3, t_5, v_stall, cl_max, AR_w, e_w, k_tran, k_climb, t_mr, C_pow, FM_mr, eta_coax, eta_prop, zeta_air, zeta_mr_1, Ce_1, Ce_2, V_tip_mr,

```
W_hp, g, kmh_ms); end

% MTR Sizing Calculations
R_mr = D_mr/2; % Radius of main rotor [m]
c_mr = R_mr/lambda_mrb; % Chord of main rotor blade at 0.7R [m]
b_w = sqrt(AR_w*S_w); % Wingspan [m]
b_w_e = b_w*m_ft; % Wingspan [ft]
S_w_e = S_w*m_ft^2; % Wing area [ft^2]
c_w = S_w / b_w; % Wing mean aerodynamic chord [m]
c_w_e = c_w*m_ft; % Wing mean aerodynamic chord [ft]

% tail group
l_sep = 1.07*R_mr; % Tail separation distance [m]
l_sep_e = l_sep*m_ft; % Tail separation distance [ft]
S_h = Cht*c_w*S_w / l_sep; % Horiz tail area [m^2]
S_h_e = S_h*m_ft^2; % Horiz tail area [ft^2]
S_v = Cvt*b_w*S_w / l_sep; % Vert tail area [m^2]
S_v_e = S_v*m_ft^2; % Vert tail area [m^2]
b_h = sqrt(AR_h*S_h); % Span of horiz tail [m]
b_h_e = b_h*m_ft; % Span of horiz tail [ft]
b_v = sqrt(AR_v*S_v); % Span of vert tail [m]
b_v_e = b_v*m_ft; % Span of vert tail [ft]
l_boom = 1.35*R_mr; % Length of tail boom [m]
l_boom_e = l_boom*m_ft; % Length of tail boom [ft]
D_boom = 0.03*R_mr; % Diamter of tail boom [m]
D_boom_e = D_boom*m_ft; % Diameter of tail boom [ft]
W_to_e = W_to*g/N_lb; % Takeoff weight [lbs]
W_fuel_e = W_fuel*g/N_lb; % Fuel weight [lbs]

% suspension group
l_strut = 1.35*R_mr; % Length of trapeze strut [m]
l_strut_e = l_strut*m_ft; % Length of trapeze strut [ft]
P_crit = W_to / 11; % Critical load [kg]
P_crit_e = P_crit*g/N_lb; % Critical load [lbs]

% MTR Component Weight Calculations
mu = V_hel/(3.6*V_tip_mr); % Advance Ratio of Helicopter
lam_mr = lambda_mrb/18; % Relative Aspect Ratio for Main Rotor blades
```

```
W_mrb = k_mrb*sig_mr*R_mr^2.7/lam_mr^0.7; % Weight of Main Rotor Blades
[kg] (11)
% Factor for number of MR blades - hub weight
if (N_mrb   4)
f_zmrb = 1 + 0.05*(N_mrb-4);
else
f_zmrb = 1;
end
F_cf_mrb = R_mr*(W_mrb/N_mrb)*(V_tip_mr/R_mr)^2/(2); % Centrifugal Force
of Main Rotor Blade [kg]
W_mrhub = 1.125*k_mrhub*N_mrb*f_zmrb*(F_cf_mrb*10^-4)^1.5; % Hub weight
[kg]
W_mgb = 1.3*k_mgb*(M_mr)^0.8; % 30% penalty in MGB weight for coaxial
W_sp = k1_sp*R_mr*c_mr^2*mu + k2_sp; % Weight of Swashplate [kg]
W_bcs = k1_bcs*R_mr*c_mr^2*mu + k2_bcs; % Weight of Booster Control System
[kg]
W_pbs = 150; % Weight of automatic flight control system [kg]
W_eng = N_eng * (k1_eng*P_eng + k2_eng); % Weight of Engines [kg]
W_pis = k_pis*W_eng; % Weight of Powerplant Installation System [kg]
W_apu = k1_apu*P_eng + k2_apu; % Weight of Auxilary Power Unit [kg]
W_fs = k_fs*W_fuel; % Weight of Fuel System [kg]
W_lg = k_lg*(W_to-W_pl_1); % Weight of Landing Gear [kg]
W_elsys = k_elsys * (15+1.2*N_mrb*c_mr*R_mr); % Weight of Electrical System
[kg]
% Weight of Wings [lb]
W_wing_e = .0051*((W_to_e-0.5*W_fuel_e)*N_ult)^0.557*S_w_e^0.649*AR_w^0.5*t_c_w^-
0.4*(1+lambda_w)^0.1*cos(gam_w)^-1*(.09*S_w_e)^0.1;
W_wing = W_wing_e*N_lb/g; % Weight of Wings [kg]
W_hor_e = 5.25*S_h_e + 0.8*10^-6 * N_ult*b_h_e^3*W_to*c_w_e*sqrt(S_h_e) / (t_c_w
*cos(gam_h)^2 *l_sep_e*S_w_e^1.5); % Weight of horiz tail [lb]
W_hor = W_hor_e*N_lb/g; % Weight of horiz tail [kg]
W_ver_e = 2.65*S_v_e + 0.8*10^-6 * N_ult*b_v_e^3*(8+0.44*(W_to_e/S_w_e)) / (t_c_w
*cos(gam_v)^2); % Weight of vert tail [lb]
W_ver = W_ver_e*N_lb/g; % Weight of vert tail [kg]
W_boom_e = 0.998*(W_to_e-0.5*W_fuel_e)^0.35*N_ult^0.25*l_boom_e^0.5*D_boom_e^1.534;
% Weight of tail boom [lb]
W_boom = W_boom_e*N_lb/g; % Weight of tail boom [kg]
```

```
W_strut = N_strut*rho_strut*l_strut * (P_crit-k2_strut)/k1_strut ; % Weight of both
struts [kg]
W_tm = 0.01*W_to; % Weight of tilt mechanism [kg]
W_cc = 500*N_lb/g; % Weight of crew compartment [kg]
W_tb = 0.005*W_to; % Weight of tilt boom [kg]
W_wfm = 0.01*W_wing; % Weight of wing folding mechanism [kg]
W_empen = W_ver + W_hor; % Weight of empennage [kg]
W_plh = k_plh*W_pl_1; % Weight of payload handling group [kg]
W_furn = 0.075.*W_pl_1; % Weight of Furnishings [kg]

% Sum component weights for new estimate of empty weight
W_mrb = 2*W_mrb;
W_mrhub = 2*W_mrhub;
W_sp = 1.75*W_sp;

W_empty = k_growth*(W_wfm + W_furn + W_mrb + W_mrhub + W_mgb + W_sp
+ W_bcs + W_pbs + W_eng + W_pis + W_apu + W_fs + W_lg + W_elsys + W_wing
+ W_ver + W_hor + W_strut + W_plh + W_boom + W_tm + W_cc + W_tb);

k_we_new = (W_to-W_empty)/W_to; % Adjusted Weight Efficiency Coefficient

% Relaxation for better convergence
if (k_we_new   1.05*k_we)
k_we_new = 1.05*k_we;
elseif (k_we_new   0.95k_we)
k_we_new = 0.95*k_we;
end

er_kwe = abs(k_we_new-k_we)/k_we; % Calculate error
k_we = k_we_new;

end

% Save weights value to file "weights" in working directory
save('weights', 'W_to', 'W_empty', 'W_fuel', 'W_mrb', 'W_mrhub', 'W_mgb', 'W_sp',
'W_bcs', 'W_pbs', 'W_eng', 'W_pis', 'W_apu', 'W_fs', 'W_lg', 'W_elsys', 'W_furn',
'W_wing', 'W_ver', 'W_hor', 'W_strut', 'W_plh', 'W_boom', 'W_tm', 'W_cc', 'W_cc',
'W_tb', 'W_wtm', '-ASCII')
```

MTR SIZING CODE - MISSION PROFILE 1 (LONG-RANGE HAUL)

% This mission profile subroutine runs the calculations for the long range haul mission based on design and mission inputs as well as initial estimates of aircraft size from the main calculation loop. The routine iterates until converging on the fuel requirements and size of the MTR for the input conditions.

function [P_eng, M_mr, Wf_tot, W_to, D_mr, S_w] = m1(W_to, W_empty, W_crew, D_mr, S_w, DL, N_eng, W_pl_1, T_res, rho_0, rho_1, rho_2, V_2, L_2, sigma_1, sigma_3, kh_1, kh_2, kh_3, t_1, t_3, v_stall, cl_max, AR_w, e_w, k_tran, k_climb, t_mr, C_pow, FM_mr, eta_coax, eta_prop, zeta_air, zeta_mr_1, Ce_1, Ce_2, V_tip_mr, E_air, W_hp, g, kmh_ms);

er_wto = 1; % error for while loop

% Fuel burn calculation loop - fuel weight and aircraft size are calculated iteratively until they are sufficiently consistent (W_to converges)
while (er_wto 0.00005)

% Leg 1: TO Hover
P_1 = (W_to*t_mr)^1.5 / (33.25*FM_mr*eta_coax*zeta_mr_1*D_mr*sqrt(2)*sqrt(sigma_1));
% Engine Power Required to Hover [shp]
P_eng = P_1*kh_1/(N_eng); % Single Engine Power Required to Hover [shp]
P_eng_nom = P_eng*C_pow; % Nominal Engine Power [shp]
M_mr = 0.5*P_eng*N_eng*D_mr*zeta_mr_1/V_tip_mr * W_hp/g; % Shaft Torque of Main Rotor [kg.m]
SFC_1 = Ce_1 + Ce_2/(P_1/(P_eng_nom*N_eng)); % Specific Fuel Consumption [kg/shp.h]
Wf_1 = P_1*SFC_1*t_1; % Fuel weight rfor first mission leg [kg]

% Leg 2: Long Range Cruise
W_2 = W_to - Wf_1; % Updated weight for leg 2 [kg]
Cl_2 = W_2*g / (0.5*rho_2*(V_2*kmh_ms)^2*S_w); % Cruise lift coefficient
Cdi_2 = Cl_2^2 / (pi*AR_w*e_w); % Induced drag in cruise
f_air = 0.004906*(W_to*g)^0.5; % Equivalent flat plate area [m^2]
P_2 = 0.5*rho_2*(V_2*kmh_ms)^3 * (f_air + S_w*Cdi_2) / (eta_prop*zeta_air) /W_hp;
% Power required in cruise [shp]
Pa_2 = P_eng_nom*N_eng/kh_2;; % Power available in cruise [shp]
SFC_2 = Ce_1 + Ce_2/(P_2/(Pa_2)); % Specific Fuel Consumption [kg/shp.h]

```
K_2 = W_2*V_2 / (P_2*zeta_air*eta_prop) * g*kmh_ms/W_hp; % L/D in cruise
E_2 = K_2*eta_prop*zeta_air/SFC_2 * W_hp/(kmh_ms*g); % Vehicle energy efficiency in cruise
Wf_2 = W_2 * [1 - 1/exp(L_2/E_2)]; % Fuel weight for second mission leg [kg]

% Leg 3: Destination Hover
W_3 = W_2 - Wf_2; % updated weight for
P_3 = (W_3*t_mr)^1.5 / (33.25*FM_mr*eta_coax*zeta_mr_1*D_mr*sqrt(2)*sqrt(sigma_3));
% Engine Power Required to Hover [shp]
Pa_3 = P_eng_nom*N_eng/kh_3; % Power available at landing site [shp]
SFC_3 = Ce_1 + Ce_2/(P_3/Pa_3); % Specific Fuel Consumption [kg/shp.h]
Wf_3 = P_3*SFC_3*t_3; % Fuel weight for third mission leg [kg]

% Total Fuel Weight
Wf_res = SFC_2*P_2*T_res; % Weight of fuel reserve [kg]
k_f = 2*k_tran + k_climb; % Transition, climb factor
Wf_tot = (1+k_f) * (Wf_1 + Wf_2 + Wf_3 + Wf_res); % Total fuel weight [kg]

% Iterate Sizing
W_to_new = W_empty + W_pl_1 + Wf_tot + W_crew; % Update takeoff weight [kg]
er_wto = abs(W_to_new - W_to)/W_to;
W_to = W_to_new;
D_mr = sqrt(2*W_to/(pi*DL)); % Update rotor diameter [m]
S_w_1 = W_to*g / (0.5*rho_1*(v_stall)^2*cl_max); % Update wing area [m^2]
S_w_2 = W_to*g / (0.5*rho_2*(V_2*kmh_ms)^2*0.8);
S_w = max(S_w_1, S_w_2); % Wing area is maximum limiter

end
```

BIBLIOGRAPHY

[1] Baldwin, G. D., "Rapid Vertical Deployment Systems," Baldwin Technology Company, LLC. Available from: http://www.baldwintechnology.com. Sept. 2003.

[2] Baldwin, G. D., "Logical Development of the Scalable MTR Aircraft Architecture," Baldwin Technology Company, LLC. Available from: http://www.baldwintechnology.com. Oct. 2003.

[3] Gillmore, K. B., Schneider, J. J., "Design Considerations of the Heavy Lift Helicopter," *Journal of the American Helicopter Society*, Vol. 8, No. 1, 1963, pp. 31–37.

[4] Wax, C. M. and Torci, R. C., "Study of the Heavy-Lift Helicopter Rotor Configuration," USAAVLABS Technical Report 66-61, Nov. 1966.

[5] Schneider, J. J., "The Influence of Propulsion Systems on Extremely Large Helicopter Design," Paper No. 334, Proceedings of the 25th Annual National Forum of the American Helicopter Society, Washington DC, May 16—18, 1969. See also the *Journal of the American Helicopter Society*, Vol. 15, No. 1, Jan. 1970.

[6] Schneider, J. J., "The Developing Technology and Economics of Large Helicopters," Paper No. 3, Proceedings of the Sixth European Rotorcraft and Powered Lift Aircraft Forum, Bristol, England, Sept. 16–18, 1980.

[7] Schrage, D.P., Costello, M. F., Mittlevden, D. N., "Design Concepts for an Advanced Cargo Rotorcraft," Paper AIAA-88-4496, Proceedings of the AIAA/AHS/ASEE Aircraft Design, Systems and Operations Meeting, Atlanta, Georgia, Sept. 1988.

[8] Grossman, J. G., Rubenson, D., Sollfrey, W., Steele, B., "Vertical Envelopment and the Future Transport Rotorcraft: Operational Considerations for the Objective Force", Santa Monica, CA: RAND, MR-1713, 2003.

[9] Tishchenko, M. N., "Simplified Performance Determination Method – Helicopter Design Lecture Notes," University of Maryland, College Park, 1998.

[10] Tishchenko, M. N., "Helicopter Parameters Optimization at Preliminary Designing – Helicopter Design Lecture Notes," University of Maryland, College Park, 2002.

[11] Tishchenko, M. N., Nagaraj, V. T., and Chopra, I., "Preliminary Design of Transport Helicopters," *Journal of the American Helicopter Society*, Vol. 48, No. 2, April 2003, pp. 71–79.

[12] "Chesapeake Civil Transport Rotorcraft," AHS Student Design Competition Report, University of Maryland, College Park, May 1998. Available on-line from: http://www.enae.umd.edu/AGRC/Design98/chesapeake.html

[13] "CalVert High-Speed Personal V/STOL Personal Transport," AHS Student Design Competition Report, University of Maryland, College Park, June 1999. Available on-line from: http://www.enae.umd.edu/AGRC/Design99/Calvert.html.

[14] "The Martian Autonomous Rotary-Wing Vehicle (MARV)," AHS Student Design Competition Report, University of Maryland, College Park, June 2000. Available on-line from: http://www.enae.umd.edu/AGRC/Design00/MARV.html.

[15] "Raven SAR Rotorcraft Advanced Rotor Control Concept," AHS Student Design Competition Report, University of Maryland, College Park, June 2001. Available on-line from: http://www.enae.umd.edu/AHS/Raven_Design_Proposal.pdf.

[16] "406-UM TerpRanger Light Helicopter Upgrade Program," AHS Student Design Competition Report, University of Maryland, College Park, June 2002. Available on-line from: http://www.glue.umd.edu/~shreyas/ahsdesign2003/TerpRanger.pdf.

[17] "UM-911 Aeneas - The Urban Disaster Response System," AHS Student Design Competition Report, University of Maryland, College Park, June 2003. Available on-line from: http://www.glue.umd.edu/~shreyas/ahsdesign2003/Aeneas.pdf.

[18] "UM-Condor Mountain Rescue Helicopter," AHS Student Design Competition Report, University of Maryland, College Park, June 2004. Available on-line from: http://www.enae.umd.edu/AHS/design/reports/2004_condor.pdf.

[19] Schoen, A.H., Rosenstein, H., Stanzione, K. A., and Wisniewski, J. S., "User's Manual for VASCOMP II: The V/STOL Aircraft Sizing and Performance Computer Program," Prepared by Boeing Vertol Company, Philadelphia, PA for NASA Ames Research Center, May 1980.

[20] Hoerner, S., *Fluid Dynamic Drag*, Hoerner Fluid Dynamics, Vancouver, WA, 1965.

[21] Prouty, R., *Helicopter Performance, Stability and Control*, PWS Engineering Publishing, Boston, MA, 1986.

[22] Leishman, J. G, *Principles of Helicopter Aerodynamics*, Cambridge University Press, New York, NY, 2000.

[23] Anderson, J. D., *Aircraft Performance and Design*, The McGraw-Hill Companies, Boston, MA, 1999.

[24] Dingeldein, R. C. 1954. "Wind Tunnel Studies of the Performance of Multirotor Configurations," NACA Technical Note 3236.

[25] Raymer, D. P., and Przemieniecki, J. S., *Aircraft Design: A Conceptual Approach*, AIAA Education Series, 3rd edition, 1999.

[26] Kroo, I. *Aircraft Design: Synthesis and Analysis*, http://adg.stanford.edu/ aa241/ AircraftDesign.html

[27] Boeing Vertol Company, "Heavy Lift Helicopter – Prototype Technical Summary," USAAVRADCOM-TR-80-D-11, April 1980.

[28] Mack, J. C., "Large Rotorcraft Transmission Technology Development Program," NASA-CR-168120, 1983.

[29] Fries, G. H. and Schneider, J. J., "HLH and Beyond," SAE Paper No. 791086, Presented at the SAE Aerospace Meeting, Los Angeles, CA, Dec. 1979.

[30] Farrell, M. K., "Aerodynamic Design of the V-22 Proprotor," Proceedings of the 45th Annual Forum of the American Helicopter Society, Boston, MA, May 22–24, 1989.

[31] Harris, F. D., Scully, M. P., "Rotorcraft Cost Too Much," *Journal of the American Helicopter Society*, Vol. 43, No. 1, January 1998.

[32] Coleman, C.P., "A Survey of Theoretical and Experimental Coaxial Rotor Aerodynamic Research," Proceedings of the 19th European Rotorcraft Forum, Cernobbio (Como), Italy, Sept. 14-16, 1993.